



**Functional Characterization of the Cation Diffusion
Facilitator AtMTP10 in *Arabidopsis thaliana***

Dissertation

zur Erlangung des

Doktorgrades der Agrarwissenschaften (Dr. agr.)

der

Naturwissenschaftlichen Fakultät III
Agrar- und Ernährungswissenschaften,
Geowissenschaften und Informatik

der Martin-Luther-Universität Halle-Wittenberg

vorgelegt von

Herrn Dipl.-Ing. agr. Bastian Meier
geb. am 26.01.1984 in 33100 Paderborn

Halle (Saale), 25.02.2019

Gutachter:

1. Professor Dr. Edgar Peiter
2. Maitre de Conference Dr. Damien Blaudez

Table of contents

List of Abbreviations.....	ii-vi
1 Introduction.....	1
1.1 Manganese in plants.....	1
1.2 Uptake and translocation of manganese.....	5
1.3 Mn homeostasis on cellular level.....	7
1.3.1 Import of manganese into the cytosol.....	8
1.3.2 Export of manganese out of the cytosol.....	10
1.3.3 The CDF (cation diffusion facilitator) family.....	12
1.4 Submergence and the molecular and metabolic changes under limiting oxygen availability.....	16
1.5 Objectives of this work.....	19
2 Material and Methods.....	20
2.1 Plasmids and Constructs.....	20
2.2 Plant material.....	23
2.2.1 Complementation lines: <i>mtp10-1::gMTP10</i>	23
2.2.2 Overexpressor lines: <i>CaMV35S-MTP10</i>	24
2.2.3 Promoter GUS lines: <i>PrMTP10-GUS</i>	25
2.3 Plant cultivation.....	25
2.3.1 Cultivation on sterile agar plates.....	25
2.3.2 Cultivation in liquid media.....	26
2.3.3 Cultivation on soil.....	26
2.4 Examination of Mn toxicity effects on agar plates.....	27
2.5 Examination of Mn deficiency effects in liquid culture media.....	27
2.6 Determination of metal concentrations.....	27
2.7 Promoter-GUS studies.....	28
2.7.1 Visualization of the Casparian strip.....	28
2.8 Yeast complementation assays.....	28
2.8.1 Determination of metal concentration in yeast.....	29
2.8.2 Yeast microsomal vesicle transport assays.....	29
2.9 Quantitative real time RT-PCR.....	30
2.10 Subcellular localization in mesophyll protoplasts.....	31
2.11 Subcellular localization in tobacco.....	32
2.12 Growth experiments under oxygen-deficient conditions.....	33

2.12.1	Submergence of soil-grown plants	33
2.12.2	Anoxic conditions on agar plates	33
2.13	Analysis of xylem exudates	34
3	Results.....	35
3.1	Plant material.....	35
3.1.1	Genotypical analysis of <i>AtMTP10</i> insertional mutants.....	35
3.1.2	Generation of <i>AtMTP10</i> -overexpressing lines	36
3.1.3	Generation of <i>AtMTP10</i> complementation lines.....	37
3.2	Functional characterization of <i>AtMTP10</i>	38
3.2.1	Experiments on the model yeast <i>Saccharomyces cerevisiae</i>	38
3.2.1.1	Yeast complementation assays	38
3.2.1.2	Localization of <i>AtMTP10</i> in <i>S. cerevisiae</i>	39
3.2.1.3	Mn contents in yeast cells	39
3.2.1.4	ATP-dependent $^{54}\text{Mn}^{2+}$ uptake by yeast microsomal vesicles	40
3.2.2	Promoter-GUS studies for localization of <i>AtMTP10</i> expression <i>in planta</i>	41
3.2.3	Subcellular localization of <i>AtMTP10</i> in transiently transformed Arabidopsis mesophyll protoplasts.....	44
3.2.4	Subcellular localization of <i>AtMTP10</i> in tobacco cells.....	46
3.3	Phenotypes of <i>mtp10</i> mutant plants.....	49
3.3.1	Growth of <i>mtp10-1</i> , <i>mtp10-4</i> , and <i>mtp10-1::gMTP10</i> under Mn toxicity	49
3.3.2	Growth of <i>mtp10-1</i> under Mn-deficient conditions	53
3.3.3	Metal contents in xylem exudates	54
3.3.4	Diurnal rhythm of xylem exudation	55
3.3.5	Diurnal rhythm of <i>AtMTP10</i> expression.....	59
3.3.6	The involvement of <i>AtMTP10</i> in submergence tolerance of Arabidopsis.....	60
3.3.6.1	Regulation of <i>AtMTP10</i> under oxygen deprivation.....	60
3.3.6.2	Submergence of <i>mtp</i> mutant lines.....	62
3.3.7	Growth of seedlings on ½ MS agar plates under anoxic conditions triggered by N ₂ aeration	64
3.3.8	Growth of plants in liquid culture media under anoxic conditions of the root zone triggered by N ₂ aeration	66
3.3.9	Xylem exudation of plants after anoxia conditions in the root zone.....	68
3.3.10	Xylem exudates of <i>mtp10-1::gMTP10.2</i> after anoxia conditions in the root zone	70
3.4	The possible involvement of alanine in the <i>AtMTP10</i> -dependent submergence tolerance	71

4	Discussion	73
4.1	AtMTP10 is a Mn and Fe transporter expressed in the vascular system and localized in intracellular compartments	73
4.2	AtMTP10 is a negative factor of Mn tolerance, improves growth at low Mn availability, and contributes to xylem loading of Mn	79
4.3	AtMTP10 is important to overcome post-anoxia conditions	83
4.4	Function of AtMTP10 during post-anoxic conditions	87
4.5	AtMTP10 - a novel factor of Mn homeostasis in plants	97
5	Summary.....	100
6	Appendix.....	I
6.1	List of primers	I
6.2	List of chemicals.....	II
6.3	List of enzymes.....	IV
6.4	List of figures and tables	V
6.5	Reference list	VIII
7	Publications	XXXII
7.1	Peer-reviewed papers.....	XXXII
7.2	Poster presentations.....	XXXII
7.3	Oral presentations	XXXIV
8	Curriculum vitae	XXXV
9	Acknowledgments	XXXVII
10	Declaration under Oath.....	XXXIX

List of Abbreviations

List of Abbreviations

µg	Microgram
µM	Micromolar
µmol	Micromole
½ MS	Half-strength Murashige & Skoog medium
A	Alanine
ACC	Aminocyclopropane carboxylate
ACO	Aminocyclopropane carboxylate oxidase
ACS	Aminocyclopropane carboxylate synthase
Acetyl CoA	Acetyl coenzyme A
ADH	Alcohol dehydrogenase
Al	Aluminium
AlaAT	Alanine aminotransferase
ALDH	Aldehyde dehydrogenase
amp	Ampicillin
Arabidopsis	<i>Arabidopsis thaliana</i> L. Heyn
ATP	Adenosine triphosphate
<i>A. tumefaciens</i>	<i>Agrobacterium tumefaciens</i>
B	Boron
BOR1	Boron transporter 1
BASTA	Glufosinate (Bayer crop science, Germany)
BSA	Bovine serum albumin
BTP	Bis-Tris propane
C-terminus	Carboxy terminus
Ca	Calcium
CAT	Catalase
CAX	Calcium exchanger
CCC	Calcium sensitive cross complementer
CCX	Calcium cation exchanger
Cd	Cadmium
CDF	Cation diffusion facilitator
cDNA	Complementary DNA

List of Abbreviations

CFP	Cyan fluorescent protein
Co	Cobalt
CO ₂	Carbon dioxide
COT1	Cobalt Toxicity 1
Cu	Copper
CUP2	Copper-binding protein 2
d	Day
D	Aspartic acid
Δ	Greek capital letter Delta (≜ deletion)
DMSO	Dimethyl sulfoxide
DNA	Desoxyribonucleic acid
DW	Dry weight
DTT	Dithiothreitol
E	Glutamic acid
ECA	ER-type calcium ATPase
<i>E. coli</i>	<i>Escherichia coli</i>
EE	Early endosomes
ERF	Ethylene response factor
EDTA	Ethylene diamine tetraacetic acid
EGFP	Enhanced green fluorescent protein
EGTA	Ethylenglycol diamine tetraacetic acid
EIN2;3	Ethylene insensitive 2;3
EIL	Ethylene insensitive 3- like
ER	Endoplasmic reticulum
EYFP	Enhanced yellow fluorescent protein
F	Phenylalanine
Fe	Iron
FW	Fresh weight
g	Gram
G	Glycine
GDH	Glutamate dehydrogenase
gDNA	Genomic DNA

List of Abbreviations

GOGAT	Glutamine oxoglutarate aminotransferase
GUS	β-glucuronidase activity
GS	Glutamine Synthetase
GSH	Glutathione synthetase
h	Hour
H	Histidine
H ⁺	Proton
H ₂ O ₂	Hydrogen peroxide
HRE1	Hypoxia responsive transcription factor 1
I	Isoleucine
IAA	Indole-3-acetic acid
ICDH	Isocitrate dehydrogenase
ICP-MS	Inductively coupled plasma - mass spectroscopy
ICP-OES	Inductively coupled plasma - optical emission spectroscopy
IRT	Iron-regulated transporter
K	Potassium
kan	Kanamycin
kb	Kilo base pairs
kg	Kilogram
M	Molar
ME	Malic enzyme
MES	2-(N-morpholino) ethanesulfonic acid
Mg	Magnesium
mg	Milligram
min	Minute
MIP	Major Intrinsic Protein
mM	Milimolar
Mn	Manganese
mRNA	Messenger RNA
MTP	Metal Tolerance Protein
N	Nitrogen

List of Abbreviations

N	Asparagine
NAD	Nicotinamide adenine dinucleotide
NADP	Nicotinamide adenine dinucleotide phosphate
NADPH	Reduced form of nicotinamide adenine dinucleotide phosphate
N-terminus	Amino terminus
N ₂	Atmospheric nitrogen
NBT	Nitro tetrazolium blue
NCX	Sodium/calcium exchanger
ng	Nanogram
Ni	Nickel
nM	Nanomolar
nmol	Nanomole
NRAMP	Natural Resistance Associated Macrophage Protein
O ₂	Oxygen
OPT	Oligopeptide Transporter
P	Phosphorus
Pb	Lead
PCR	Polymerase chain reaction
PDC	Pyruvate decarboxylase
PGK	3-Phosphoglycerate kinase
pH	Negative decade logarithm of proton activity
PHO1	Phosphate transporter 1
PIP	Plasma membrane Intrinsic Protein
PM	Plasma membrane
PMR1	Plasma Membrane ATPase Related 1
Pr	Promoter
PS	Photosynthesis
PSII	Photosystem II
rH	Relative humidity
RNA	Ribonucleic acid
ROS	Reactive oxygen species

List of Abbreviations

s	Second
<i>S. cerevisiae</i>	<i>Saccharomyces cerevisiae</i>
SC	Synthetic complete
SK	SNORKEL
SKOR	Stelar K ⁺ outward rectifying channel
SMF	Suppressor of Mitochondria import Function
SOD	Superoxide dismutase
SUB1A	Submergence 1A
SUS	Sucrose Synthase
T	Threonine
TCA	Citric acid cycle
TGN	<i>Trans</i> -Golgi network
TMD	Transmembrane domain
TYR A23	Tyrphostin A23
U	Unit
UTR	Untranslated region
V	Valine
VIT	Vacuolar Iron Transporter
VTC	Vitamin C (GDP-L-galactose phosphorylase)
x-Gluc	5-Bromo-4-chloro-3-indolyl- β -D-glucuronic acid
YSL	Yellow Stripe-Like
ZIP	Zinc-regulated, Iron-regulated Transporter-like protein
Zn	Zinc
ZRC1	Zinc Resistance Conferring 1
ZRT	Zinc Regulated Transporter
ZnT	β -Cell-specific Zinc Transporter

1 Introduction

Plant growth does not only depend on water, carbon dioxide, and sunlight, it also requires a large number of inorganic nutrients. Compared to the macronutrients (nitrogen, phosphorus, potassium, sulphur, calcium, and magnesium) that are known to be required in large amounts, the demand on micronutrients (boron, copper, iron, manganese, molybdenum, nickel, and zinc) is much lower. However, all of those nutrients have to be acquired from the rhizosphere. To maintain an optimal supply, the acquisition and distribution of nutrients has to be regulated. One of the most important mechanisms to regulate this acquisition of elements from the soil is their uptake by specific transporters. Once the nutrients have entered the root, they have to be distributed within the plant. One of the main pathways for the translocation of nutrients is the xylem, where the transpiration stream is the driving force. To ensure nutrient translocation and homeostasis, the regulation of the xylem loading mechanisms is essential. In this thesis the function of a putative manganese transporter that appears to be involved in xylem loading mechanisms was examined.

1.1 Manganese in plants

Manganese is an important mineral micronutrient of plants. As a co-factor or activator, it participates in a multitude of enzymatic processes. Next to the most notable involvement in water oxidation in the photosystem II (PSII), it functions as a co-factor of the Mn-dependent superoxide dismutase (MnSOD), which is found in mitochondria and peroxisomes (Marschner, 1995). Due to the ability of manganese to change its oxidation state, the Mn_4CaO_5 cluster in PSII acts as a store of free electrons provided by the splitting reaction of two water molecules. The electron gap in PSII is restocked by the release of these electrons (Rutherford, 1989, Zouni *et al.*, 2001). This function of Mn is the reason for its importance in the evolution of atmospheric oxygen by plants. In addition, Mn is involved in the detoxification of reactive oxygen species (ROS) because of its function as a co-factor of the MnSOD. SODs catalyze the dismutation of two superoxide radicals to hydrogen peroxide and molecular oxygen. Hydrogen peroxide is further catalysed rapidly by catalases (Morgan *et al.*, 2008). Next to the mitochondrial MnSOD, there are further

I Introduction

SODs containing Cu/Zn or Fe as a co-factor (Alscher *et al.*, 2002, Abreu & Cabelli, 2010). The Arabidopsis genome harbours three Cu/ZnSODs, three FeSODs and one MnSOD. The mitochondrial MnSOD was shown to be important for the maintenance of the redox homeostasis in mitochondria (Morgan *et al.*, 2008). Transgenic *MnSOD* antisense plants showed a decreased root growth under control conditions, but especially under oxidative stress mediated by methyl viologen. The redox state of the mitochondria was shifted to the more oxidizing status, and the fluxes of the citric acid cycle were diminished in the mutant plants. The authors concluded that the inhibited growth of the mutant was more likely a consequence of an altered redox signalling than of oxidative damage of the mitochondria itself (Morgan *et al.*, 2008).

Next to the involvement of Mn in the water-splitting system of PSII and the MnSOD, there is a third enzyme class that is Mn-dependent, the Mn-containing acid phosphatases. An isoform in sweet potato was shown to contain one Mn atom per polypeptide (Sugiura *et al.*, 1981). In Arabidopsis, *AtPAP15* encodes for a purple acid phosphatase involved in phytate breakdown and indirectly in abiotic stress tolerance via an involvement in ascorbate metabolism (Zhang *et al.*, 2008). The enzyme hydrolyses *myo*-inositol hexakisphosphate to free phosphate and *myo*-inositol which is known to be a precursor for ascorbate (Zhang *et al.*, 2008).

Mn is also involved in respiration, in the biosynthesis of amino acids, lignin, and chlorophyll, as well as in the hormonal balance of plants (Marschner, 1995, Lidon *et al.*, 2004, Millaleo *et al.*, 2010). The involvement of Mn in respiration lies in the activation of dehydrogenases, transferases, hydroxylases, and decarboxylases. Dehydrogenases, like NAD/NADP-dependent malic enzymes (EC 1.1.1.39/EC 1.1.1.40) are involved in carbon fixation by providing pyruvate, whereas NAD/NADP-dependent isocitrate dehydrogenases (EC 1.1.1.41/EC 1.1.1.42) provide ketoglutarate for the tricarboxylic acid cycle (Lemaitre & Hodges, 2006, Tronconi *et al.*, 2008). One example for the involvement of Mn in amino acid catabolism is the activation of glutamine synthetases (EC 6.3.1.2). This enzyme is responsible for the formation of glutamine from glutamate and ammonium and is activated either by Mg or by Mn (Burnell, 1988, O'Neal & Joy, 1974). The important function of Mn as activator of enzymes is also essential for photosynthesis: Mevalonate kinase (EC 2.7.1.36) utilizes Mn for the formation of precursors of chloroplast pigments.

I Introduction

Additionally, an enzyme that is essential for the formation of β -carotene, phytoene synthase (EC 2.5.1.32), requires Mn, whereas Mg shows an inhibitory effect (Wilkinson & Ohki, 1988).

Even though Mn is required for such important cellular processes, the demand by the plant is relatively low. Most crop species necessitate a concentration of only c. 20-40 mg Mn kg⁻¹ dry weight (Marschner, 1995, He *et al.*, 2005). In many plants, the accumulated amount of Mn is much higher, which indicates that Mn uptake is not strictly regulated (Marschner, 1995). The availability of Mn depends on its oxidation state. In soils, Mn is present in the oxidation states 0, II, III, IV, VI, and VII, but only the divalent cation Mn²⁺ is plant-available (Ducic & Polle, 2005, Yang *et al.*, 2008, Millaleo *et al.*, 2010). Soils of low pH and/or poor aeration contain elevated levels of Mn in the divalent form, while in soils with high pH, the manganic forms (Mn^{3+,4+,5+,6+,7+}) predominate (Ducic & Polle, 2005). Due to these changes in the oxidation states, Mn oxides exhibit amphoteric behaviour and are thus able to interact with cations as also with anions. They can be found in multi-crystalline or pseudocrystalline states and are able to interact with iron oxides that precipitate. A high pH also promotes the adsorption of Mn by clay minerals, which leads to a decreased availability (Bradl, 2004). There are many other factors that have an impact on the availability of Mn²⁺ in the rhizosphere. Mn²⁺ forms complexes with organic ligands like organic acids, amino acids, sugar acids, hydroxamate siderophores, phenols, and other compounds (Stevenson, 1994). Furthermore, in calcareous soils the precipitation of MnCO₃ is a consequence of chemisorption of Mn onto CaCO₃ (Bradl, 2004, Fageria *et al.*, 2002). On the other hand the availability of Mn²⁺ increases with decreasing pH values. Fertilizers that promote soil acidification, like ammonium-based ones, and cation leaching by rainfall increase the acidification of the soil, which in turn results in an increase of plant-available Mn²⁺ (Mora *et al.*, 2006, Millaleo *et al.*, 2010). In addition, the release of protons from plants leads to a local acidification and therefore to an increased Mn²⁺ concentration in the rhizosphere (Rengel & Marschner, 2005). Furthermore, Mn-oxidizing or -reducing soil microorganisms were also shown to have an impact on the amount of the availability of Mn²⁺. The most abundant species in soils, e.g. *Arthrobacter*, *Bacillus*, *Pseudomonas* and *Hyphomicrobium* are considered to be involved in the oxidizing processes of Mn²⁺ (Ghiorse, 1988). Reducing Mn by soil microorganisms

I Introduction

was shown to be either indirect by producing H_2S , H_2O_2 , organic acids or other metabolic products that are able to reduce Mn, or directly by organisms that have enzymatic pathways for the reducing processes. *Bacillus*, but also *Pseudomonas*, *Clostridium Micrococcus*, *Arthrobacter*, and *Acinetobacter* have been studied under this point of view (Ghiorse, 1988).

If Mn availability is excessive, plants can encounter Mn toxicity, which results in interveinal chlorosis or/and tissue necrosis and subsequently in a decreased biomass accumulation (Marschner, 1995). Brown spots on mature leaves and deformation of younger leaves are also indicative of Mn toxicity (Wissemeier & Horst, 1992). Physiologically, Mn toxicity leads to a decrease of the photosynthetic rate either by chlorophyll degradation or by secondary Fe deficiency. Excess Mn also induces a deficiency of calcium and, at higher severity, of magnesium. These deficiencies are more prevalent than induced iron deficiency (Leskova *et al.*, 2017). A toxic accumulation of Mn in the cytosol additionally leads to the production of reactive oxygen species (ROS) either by electron transfer involving metal cations or by a metal-induced inhibition of metabolic processes (Hauck *et al.*, 2003, Millaleo *et al.*, 2010). Another reaction leading to Mn toxicity is the oxidation of Mn II to Mn III in the apoplast that in turn acts as an oxidant for proteins and lipids (Fecht-Christoffers *et al.*, 2003b, Fecht-Christoffers *et al.*, 2003a). However, the most prominent consequence of Mn toxicity is probably, as mentioned before, the induced deficiency of other nutrients like Ca, Mg, P, Fe, or Zn. These secondary induced deficiencies are often a consequence of identical ways to enter the root by transporters or channels with a broad specificity (Pittman, 2005). In the case of phosphorous that is taken up as an anion, it was shown that the high affinity uptake transporter PHO84 was also able to transport $MnHPO_4$ in yeast. Although higher plants like *Arabidopsis* possess many P transporters with a high similarity to PHO84, there is no evidence for a comparable mechanism (Luk *et al.*, 2003).

On the other hand, plants need to prevent a deficiency of manganese. As described above, due to an interrupted chlorophyll synthesis, Mn deficiency leads to chlorosis in leaves. But the first occurring effect of Mn deficiency, even without visible symptoms, is the decreased efficiency of PSII due to a change in the ultrastructure of chloroplasts (Simpson & Robinson, 1984, Papadakis *et al.*, 2007). A reduced loading of Mn

to the PSII complex leads to a loss of the luminal protection proteins of the oxygen evolving complex, which in turn leads to a destabilization of the PSII core and oxidative damage (Schmidt *et al.*, 2016). Studies in the photosynthetically active alga *Chlamydomonas reinhardtii* showed that under Mn-deficient conditions the function of PSII is preferentially sustained compared to the activity of MnSOD (Allen *et al.*, 2007). Furthermore, in barley it was found that Mn deficient plants showed no visual symptoms but a dramatic decrease in PSII efficiency and a higher transpiration rate (Hebberner *et al.*, 2009). This increase in transpiration was shown to be a consequence of a decreased epicuticular wax layer due to a suspected involvement of Mn in fatty acid metabolism.

1.2 Uptake and translocation of manganese

The uptake of manganese depends on the availability of Mn^{2+} in the soil solution. Some plant species have the capability to increase the amount of Mn^{2+} in the rhizosphere by releasing root exudates like phytases or organic anions (George *et al.*, 2014). As mentioned above, soil microorganisms have also an impact on the availability of divalent Mn for plants. Kothari and co-workers found that maize plants showed an increase in Mn uptake when grown on soil that was inoculated with microorganisms compared to sterile soil. This went along with an increased amount of exchangeable Mn in the rhizosphere of soils inoculated with the microorganisms (Kothari *et al.*, 1991). Another pathway for the increase in exchangeable Mn by microorganisms which leads to an increased uptake of Mn has been explored in barley and is based on the capability of microorganisms to produce 2-ketogluconic acid that dissolves minerals and in turn releases trace elements. Such compounds serve also as chelators to keep these micronutrients in solution (Barber & Lee, 1974).

The uptake of Mn may be mediated by plasma membrane Ca^{2+} channels, which are permeable to Mn^{2+} (Wymer *et al.*, 1997, White *et al.*, 2002). In addition, active Mn^{2+} uptake may be accomplished by the cation transporter IRT1 (iron regulated transporter1), a member of the ZIP (zinc-regulated transporter, iron-regulated transporter-like protein) family (Korshunova *et al.*, 1999, Yang *et al.*, 2008) that is mainly considered as the major Fe uptake transporter of dicots. IRT1 of *Arabidopsis thaliana* is not strongly selective for

I Introduction

Fe^{2+} , but also transports Zn^{2+} , Cu^{2+} , Co^{2+} , Ni^{2+} , and Mn^{2+} (Korshunova *et al.*, 1999). Interestingly, in barley, IRT1 has been demonstrated to mediate primarily Mn, but not Fe uptake (Pedas *et al.*, 2008). Furthermore, transporters of the NRAMP (natural resistance associated macrophage protein) family were described to be involved in the transport of the divalent ions Fe^{2+} and Mn^{2+} into the cytosol (Thomine *et al.*, 2000). Under Mn-deficient conditions, the gene encoding the plasma membrane-located AtNRAMP1 is up-regulated, and *nramp1* knockout mutants accumulate less Mn in the shoots under Mn deficiency, which points to a function of this protein in the uptake of Mn^{2+} under conditions of low Mn availability (Cailliatte *et al.*, 2010). In rice, OsNRAMP5 was shown to contribute to the Mn uptake and translocation. *OsNRAMP5* RNAi lines showed next to decreased Mn concentrations in the roots and shoots, also a decrease in Fe concentrations in both tissues (Ishimaru *et al.*, 2012). Further investigations showed that the Mn uptake and translocation works in conjunction with another transporter next to OsNRAMP5, namely OsMTP9 (Ueno *et al.*, 2015). OsNRAMP5, localized to the plasma membranes of the distal side of the exo- and endodermis was shown to be responsible for the transport of Mn from the soil solution and OsMTP9, localized to the plasma membranes of the proximal side of these cell layers mediates the transport of Mn into the stele (Ishimaru *et al.*, 2012, Ueno *et al.*, 2015).

Once Mn^{2+} has been absorbed by the roots, it is translocated to the shoot via the xylem, albeit the molecular basis of xylem loading of Mn is still obscure. The mobility of Mn in the phloem is supposed to be low (Marschner, 1995), but there is evidence that a small amount of Mn may be recycled via the phloem by transporter of the YSL (yellow stripe like) family. It was shown that Mn concentrations in the fifth and sixth leaf of an Arabidopsis wild type Col-0 decreased during senescence, which was not the case in a *ysl1ysl3* double mutant (Waters *et al.*, 2006). Another study in rice showed that *OsYSL2* mediated the translocation of Mn-nicotianamine complexes into the seeds (Ishimaru *et al.*, 2010). Experiments with the positron emitting tracer imaging method also showed a translocation of Mn via the phloem. ^{52}Mn was applied to a cut leaf of a barley plant cultivated under Mn-sufficient conditions. After 27 minutes radioactivity was detectable in the discrimination centre of the shoot, in other leaves, as also in the root tips. It was

suggested that Mn was transported by unknown transporters with a low specificity (Tsukamoto *et al.*, 2006).

1.3 Mn homeostasis on cellular level

Metal transporters are classified into importers and exporters. Importers translocate metals into the cytosol from the extracellular space or from internal compartments, whereas exporters are responsible for the exclusion of metals out of the cytosol into intracellular compartments or into the apoplast. On cellular level, Mn is present in all compartments, including the vacuole, ER, Golgi apparatus, chloroplasts, but also in the cell wall (Wu *et al.*, 2002, Pittman, 2005). Consequently, cells contain a multitude of transporters that are responsible for the import of Mn into or the export from the cytosol, as well as for the allocation of Mn to cellular compartments for storage or for the adequate supply of Mn-dependent targets. Figure 1 shows a schematic cell with an overview of Mn transporters previously described. These transporters will be described in more detail below.

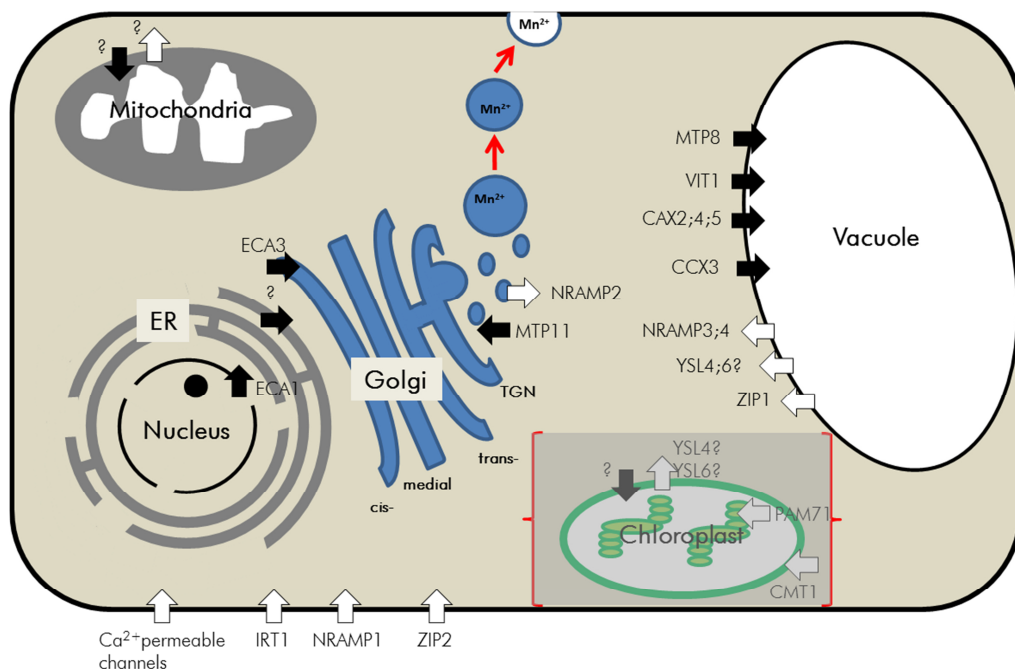


Fig. 1: Schematic representation of an *Arabidopsis thaliana* cell including previously described Mn transporters. White arrows: importers (transport direction into the cytosol). Black arrows: exporters (transport direction out of the cytosol).

1.3.1 Import of manganese into the cytosol

As mentioned before, transporters of the NRAMP family are predicted to be involved in Mn uptake and homeostasis in many organisms, including plants. Members of the NRAMPs have 10 conserved transmembrane domains (TMD) and either one or two non-conserved ones. Next to Mn, they are able to transport Fe, Zn, Cd, Cu, Ni, Co, and Al (Nevo & Nelson, 2006). In the baker's yeast *Saccharomyces cerevisiae*, the uptake of Mn is mediated by the NRAMP member SMF1. SMF1 is located in the plasma membrane, and next to Mn, other metals like Cu, Fe, Zn, and Cd are also transported by SMF1 (Culotta *et al.*, 2005). SMF1 is not the sole uptake transporter for Mn in yeast; the authors found that activities of Mn-dependent enzymes, like superoxide dismutase 2 (SOD2) or glycosyl transferases in the Golgi apparatus, were still active in the deletion mutant *smf1* Δ (Culotta *et al.*, 2005). SMF2, another member of this family, is described to be located to the Golgi apparatus. In contrast to SMF1, SMF2 is very important for the activity of the mitochondrial SOD2 in yeast. Luk and co-workers found that the SOD2 activity was strongly decreased in *smf2* Δ cells, suggesting that this transporter is necessary for the trafficking of Mn to the mitochondria via the Golgi (Luk & Culotta, 2001). The genome of Arabidopsis contains six genes encoding NRAMP transporters, whereby NRAMP1, NRAMP2, NRAMP3, and NRAMP4 have been characterized until now. As mentioned above, NRAMP1 is located to the plasma membrane and up-regulated under Mn deficiency, but also under Fe deficiency (Curie *et al.*, 2000, Cailliatte *et al.*, 2010). NRAMP2 is located to the *trans*-Golgi network and was shown to be able to complement the Mn uptake-defective yeast strain *smf1* Δ . In Arabidopsis NRAMP2 was shown to be involved in the intracellular allocation of Mn. Knockout mutants showed a hypersensitivity to Mn deficiency and a reduction in chlorophyll content with an accompanying reduction in PSII activity under those conditions. The promoter of *NRAMP2* showed an activity in the vasculature of roots and shoots and additionally in the trichomes (Alejandro *et al.*, 2017, Gao *et al.*, 2018). In contrast to NRAMP1 and NRAMP2, NRAMP3 and NRAMP4 are localized to the tonoplast (Thomine *et al.*, 2003, Lanquar *et al.*, 2005). Both were also able to complement yeast cells deficient in Mn uptake, and additionally cells defective in iron uptake (*fet3* Δ *fet4* Δ). Both proteins were shown to be responsible for the retrieval of Mn from the vacuoles in mesophyll cells. The vacuoles of the mesophyll cells of an *nramp3nramp4* double mutant thus showed a strong

I Introduction

overaccumulation of Mn. Under Mn deficiency the double mutant showed a decreased growth which was correlated with a reduced number of active PSII complexes. It was concluded that this decrease in PSII activity was a consequence of a shortage of Mn for the formation of the tetra-Mn cluster (Thomine *et al.*, 2000, Thomine *et al.*, 2003, Oomen *et al.*, 2009).

Members of the ZIP family have also been shown to be transport proteins with a broad substance range and are predicted to be involved in Fe, Zn, Cd, Co, and also Mn transport. They have 8 TMD with extracellular N- and C-termini and a cytosolic histidine-rich loop (Korshunova *et al.*, 1999, Guerinot, 2000). In yeast, two members of this family, ZRT1 and ZRT2, mediate the uptake of Zn (Zhao & Eide, 1996). These transporters show a high similarity to IRT1 (Eide *et al.*, 1996), which was described above. The Arabidopsis genome harbours in total 16 ZIP proteins, but only seven of them were able to complement the yeast strain *smf1Δ* that is deficient in Mn uptake (AtZIP1, AtZIP2, AtZIP5, AtZIP6, AtZIP7, AtZIP9, and AtIRT1) (Maser *et al.*, 2001, Milner *et al.*, 2013, Korshunova *et al.*, 1999). *AtZIP1* and *AtZIP2* are expressed in the root stele, whereas *AtZIP1* also showed promoter activity in the leaf vasculature (Milner *et al.*, 2013). On subcellular level, *AtZIP1* is localized to the vacuole and supposed to be responsible for the remobilization of Mn from the vacuole in cells of the root stele, whereas *AtZIP2* is located to the plasma membrane and may mediate Mn uptake by these cells. Both transporters are predicted to be involved in the transport of Mn and/or Zn into cells of the xylem parenchyma and in turn for the root to shoot transport of those metals (Milner *et al.*, 2013). Interestingly, *AtZIP2* expression decreased under Mn-deficient conditions, which makes it unlikely that this is a primary transporter for Mn translocation (Socha & Guerinot, 2014).

Members of the YSL (yellow stripe-like) family are predicted to transport chelated Mn, Zn, Cu, Ni, Cd, and Fe, but many of them are poorly characterized. They are related to the OPT (oligopeptide transporter) family and mediate the uptake of metal complexes with, e.g., nicotianamine or phytosiderophores (Yen *et al.*, 2001, Schaaf *et al.*, 2004). The first characterized member was YS1 in maize that is located to the plasma membrane of roots under Fe-deficient conditions and whose loss of function leads to interveinal chlorosis due to a defect in the uptake of Fe-phytosiderophores (von Wiren *et al.*, 1994,

I Introduction

Curie *et al.*, 2001). The resulting yellow stripes on the maize leaves were the eponym for this family. Schaaf and co-workers as also Haydon and Cobbett suggested that phytosiderophores and nicotianamines are also ligands for Mn (Schaaf *et al.*, 2004, Haydon & Cobbett, 2007). The Arabidopsis genome contains eight YSL proteins based on the similarity to ZmYS1 (Curie *et al.*, 2001). Expression of Arabidopsis YSL genes is most abundant in the vasculature, pollen grains, and seeds. For *AtYSL1* and *AtYSL3* an additional expression was determined in senescent leaves, suggesting a role in metal remobilization. Single knock-out mutants of those genes showed no phenotype, while the double mutant showed symptoms of Fe deficiency, such as interveinal chlorosis. Furthermore, the translocation rate of Zn, Cu, and, as discussed above, of Mn from senescent leaves was also less in the double mutant compared to the wild type (Waters *et al.*, 2006, Curie *et al.*, 2009).

1.3.2 Export of manganese out of the cytosol

For cellular Mn homeostasis not only the influx but also the efflux of Mn is very important. This efflux is mediated by transporters that move Mn from the cytosol to internal compartments or to the extracellular space. Members of the CAX (cation exchanger) family, that were originally predicted to be $\text{Ca}^{2+}/\text{H}^{+}$ antiporters, mediate the flux of not only Ca^{2+} , but also Mn^{2+} ions into the vacuole (Pittman *et al.*, 2004). Yeast cells expressing *AtCAX2* showed an increased tolerance to Mn toxicity and an increased sensitivity to hydrogen peroxide, pointing to a decreased cytosolic Mn availability (Schaaf *et al.*, 2002). *AtCAX4* and *AtCAX5*, which are located to the tonoplast and up-regulated under Mn toxicity, may also play a role in Mn homeostasis (Cheng *et al.*, 2002, Edmond *et al.*, 2009).

Members of the CCX family were previously described as transporters of the CAX family. However, because they are phylogenetically closer to the mammalian plasma membrane K^{+} -dependent $\text{Na}^{+}/\text{Ca}^{2+}$ exchangers (NCXs), this gene family, which has five members in Arabidopsis (CCX1-5), was re-classified (Socha & Guerinot, 2014). The expression of *AtCCX3* was induced in roots and flowers after a treatment with Mn, and in yeast the expression of *AtCCX3* complemented yeast strains defective in the export

I Introduction

mechanisms of Mn via the plasma membrane or the tonoplast for detoxification. These yeast cells, as also tobacco cells expressing *AtCCX3*, showed enhanced Mn levels, suggesting an ability of *AtCCX3* to transport Mn (Morris *et al.*, 2008).

P-type ATPases are another protein family that contains Mn exporters. In *S. cerevisiae*, PMR1 is a Golgi-localized $\text{Ca}^{2+}/\text{Mn}^{2+}$ -ATPase whose loss of function leads to a lack of Mn removal from the cells and in turn an accumulation of lethal Mn concentrations under conditions of high Mn availability (Maeda *et al.*, 2004). The Arabidopsis genome encodes for 15 P-type ATPases, of which the $\text{P}_{2\text{B}}$ -type, or ECA (ER-type calcium ATPase), subfamily members transport Mn. *AtECA1* is localized to the ER and functions as a pump for Ca and Mn (Wu *et al.*, 2002). Knockout plants of *AtECA1* showed no phenotype when grown under sufficient nutrition, whereas a Ca deprivation as also an excess of Mn lead to an impaired growth. It was shown that under excess Mn, the root hair elongation was inhibited to a larger extend in the mutant compared to the wild type (Wu *et al.*, 2002). *AtECA3* was shown to be localized to the Golgi apparatus (Mills *et al.*, 2008) and in subpopulations of endosomes/pre-vacuolar compartments (Li *et al.*, 2008). Its promoter was primarily active in the vasculature of roots and true leaves of two-week-old seedlings but not in cotyledons, the shoot apex, or the hypocotyl of three-day-old seedlings. This transporter was able to complement a yeast strain defective in its endogenous Ca^{2+} pumps under high supply of Mn as also under Ca depletion (Li *et al.*, 2008). In plants an *eca3* knockout mutant was shown to be sensitive to Mn deficiency and also to Mn toxicity. Taken together, it was concluded that *AtECA3* is responsible for the transport of Mn into Golgi-related compartments for growth and, under Mn excess, for the loading of Mn into post-Golgi compartments for detoxification (Li *et al.*, 2008, Mills *et al.*, 2008).

Members of the CCC1-like (Ca²⁺-sensitive cross complementer 1) family were firstly described in yeast, where they transport Fe and Mn into the vacuole (Li *et al.*, 2001). Arabidopsis has six orthologous of CCC1, called VITs (vacuolar iron transporters). Of them, *AtVIT1* is the best-characterized one. It confers the translocation of Fe into vacuoles of the vascular system in developing embryos, but is also able to transport Mn. Yeast cells deleted in *CCC1* showed elevated levels of Mn in vacuoles upon expression of *AtVIT1* (Kim *et al.*, 2006).

I Introduction

The transport of manganese into the chloroplast is mediated by a member of the uncharacterized protein family 16 (UPF0016) that shows a homology to the GDT1 (GCR1 dependent translation factor 1) family in *Saccharomyces cerevisiae*. This transporter, CMT1 (chloroplast manganese transporter 1) is located in the chloroplast envelope and was shown to be able to complement the Mn-sensitive yeast strain *pmr1Δ*. Arabidopsis mutants for this gene showed a diminished growth which was concluded to be the result of the reduced Mn concentration in the chloroplasts and thus of a decrease in PSII activity (Eisenhut *et al.*, 2018, Zhang *et al.*, 2018). The closest paralog of this transporter is PAM71 (photosynthesis affected mutant 71), which was shown to be localized to the thylakoid membranes of chloroplasts. Its ability to transport manganese was shown by complementation assays with the yeast strain *pmr1Δ*, and knockout mutants showed a decreased Mn binding in PSII (Schneider *et al.*, 2016). Interestingly, a recent study of Frank and co-workers, has demonstrated that CMT1 and PAM71, like their yeast homolog GDT1, also transport Ca and that knockout mutants display altered stromal Ca signals (Frank *et al.*, 2018). To reflect their wider roles, CMT1 and PAM71 were newly denominated as BICAT1 (bivalent cation transporter 1) and BICAT2, respectively (Frank *et al.*, 2018).

Another protein family that has been shown to be involved in Mn export is the CDF (cation diffusion facilitator) family, called MTP (metal tolerance protein) family in plants. The transporter on which this thesis is focussed, AtMTP10, belongs to the CDF family. For this reason, this family will be described in more detail in the following section.

1.3.3 The CDF (cation diffusion facilitator) family

The CDF (cation diffusion facilitator) family has members in all kingdoms of life and was first characterized by Nies and Silver (Nies & Silver, 1995). Most CDFs are $\text{Me}^{2+}/\text{H}^+(\text{K}^+)$ antiporters of substrates with ionic radii between 72 (Zn^{2+}) and 97 (Cd^{2+}). They mediate the efflux of Zn^{2+} , Co^{2+} , Fe^{2+} , Cd^{2+} , Ni^{2+} , or Mn^{2+} . Most of them have 6 TMDs with histidine-rich regions at their cytosolic N- and/or C-terminus and additionally between the 4th and 5th TMD. The TMDs I, II, V, and VI are highly conserved and have been proposed to be

I Introduction

involved in metal transfer (Maser *et al.*, 2001, Haney *et al.*, 2005, Montanini *et al.*, 2007). To examine the importance of conserved residues, site-directed mutagenesis has been performed in several studies. For instance, a H260D (H = histidine; D = aspartic acid) substitution caused a dramatic decrease of the ability of PtdMTP1 from the hybrid poplar *Populus trichocarpa* x *Populus deltoids* (Blaudez *et al.*, 2003) to complement the Zn-sensitive yeast strain *zrc1* Δ (Montanini *et al.*, 2007). For AtMTP1, it was shown that a five residue stretch (VTVTT; V = valine; T = threonine) in the histidine-rich loop is essential for the selectivity of the transporter for zinc. It was also shown that a single substitution of one amino acid in TMD3 of AtMTP1 (V130A, I135F, G140A, E145G, or E145N; A = alanine; I = isoleucine; F = phenylalanine; G = glycine; E = glutamic acid; N = asparagine) led to a complementation of the Mn-sensitive yeast strain *pmr1* Δ that was not apparent in the wild type allele (Podar *et al.*, 2012).

One of the first characterized CDFs was *FieF* (*YiiP*) in *E. coli*. Expression of this gene decreased the cellular Fe accumulation, which makes it possibly the first Fe efflux system that had been described (Haney *et al.*, 2005). Based on phylogenetic relationships, the CDF family can be classified into three major subgroups that correspond with the principally-transported metal. Zinc transporters were classified into the first subgroup while transporters of the second major subgroup are able to transport iron and zinc. The third group of CDFs has been proposed to contain Mn transporters (Montanini *et al.*, 2007). Typical examples for transporters of the Zn subgroup are ZnT1 and ZnT2 in liver cells of rats. Both share the typical characteristics of the CDF family. ZnT1 is located to the plasma membrane, while ZnT2 is localized in intracellular vesicles (Palmiter & Findley, 1995). In yeast, the two well-characterized members of the CDF family are ZRC1 and COT1. Both proteins are localized to the tonoplast, and while ZRC1 confers tolerance to Zn²⁺ and Cd²⁺, COT1 is able to transport Co²⁺ and Rh²⁺ (Conklin *et al.*, 1992). Proteins of the Mn subgroup share some aspects that set them apart from other CDFs. First, the highly conserved residue (HxxxD; H = histidine, D = aspartate; x = any amino acid) in the 5th TMD is replaced by an aspartate residue (DxxxD). MnCDFs also lack the histidine-rich loop between the 4th and 5th TMD (Delhaize *et al.*, 2003).

The genome of *Arabidopsis thaliana* contains 12 CDF members that are usually called MTP for metal tolerance protein. They are also classified into the three major

I Introduction

subgroups mentioned above. AtMTP1, a Zn^{2+} transporter that is localized to the tonoplast, is described to sequester Zn^{2+} into vacuoles and confers tolerance to Zn^{2+} toxicity (Kobae *et al.*, 2004). Its ortholog PtdMTP1 is thought to have the same function in poplar (Blaudez *et al.*, 2003). Another CDF that mediates Zn^{2+} tolerance by sequestration into vacuoles is AtMTP3 (Arrivault *et al.*, 2006). It was shown to restore the growth and increase the cellular concentrations of Zn and Co of the sensitive yeast mutant *zrc1 Δ cot1 Δ* . High concentrations of Zn or Co as also Fe deficiency induced an increase in the expression of *AtMTP3*. Due to the expression of *AtMTP3* with *AtIRT1* and *AtFRO2*, which are involved in Fe uptake, in root epidermis and cortex, and the induction of its expression by Fe deficiency, it was concluded that AtMTP3 is responsible for the detoxification of Zn that enters the root via AtIRT1 (Arrivault *et al.*, 2006).

In *Stylosanthes hamata*, a highly Mn-tolerant legume, *ShMTP8* encodes for a tonoplast-localized Mn^{2+} transporter which translocate Mn^{2+} into vacuoles (Delhaize *et al.*, 2003). This transporter was the first described transporter of the Mn subgroup and previously called ShMTP1. Sequence analysis of ShMTP8 showed that this protein lacks the complete N-terminal sequence as also the histidine-rich loop that is common for members of the CDF family. ShMTP8 was able to complement the Mn-sensitive yeast strain *pmr1 Δ* and, when expressed in Arabidopsis, ShMTP8 was shown to confer tolerance to Mn toxicity (Delhaize *et al.*, 2003).

Due to their phylogenetic relationship, four members of the CDF family in Arabidopsis, *AtMTP8* to *AtMTP11*, may also encode for Mn transporters (Montanini *et al.*, 2007). To date, the only characterized proteins of this subgroup are *AtMTP8* and *AtMTP11*. Similar to ShMTP8, AtMTP8 is localized to the tonoplast. The promoter of *AtMTP8* was shown to be active in cells of the epidermis and the cortex of Fe-deficient roots. Studies on knockout mutants showed that AtMTP8 mediates the detoxification of Mn that enters the root via the poorly specific Fe transporter AtIRT1 (Eroglu *et al.*, 2016). Another function of AtMTP8 in plants is the allocation of Mn in developing seeds. Its expression in subepidermal cells on the abaxial side of the cotyledons and in the cortical cells of the hypocotyl, confer the storage of Mn specifically in those tissues (Eroglu *et al.*, 2017, Chu *et al.*, 2017). MTP8 loss-of-function mutants showed a distribution of Mn in the cells surrounding the vasculature as it was shown for Fe in wild type seeds before (Kim *et*

I Introduction

al., 2006, Eroglu *et al.*, 2017). MTP8 was also able to complement the Fe-sensitive yeast strain *ccc1Δ* and to take on the role of AtVIT1 in Fe distribution in seeds of *vit1* mutants. Both findings identified AtMTP8 as the first protein of the Mn-CDF subgroup to exhibit a function as a transporter of Fe next to Mn (Eroglu *et al.*, 2017, Chu *et al.*, 2017).

AtMTP11, localized to vesicular compartments, has been proposed to confer tolerance to Mn toxicity by a vesicle trafficking-based mechanism of Mn secretion via exocytosis. Heterologous expression of *AtMTP11* in the Mn-sensitive yeast strain *pmr1Δ* alleviated its sensitivity to Mn toxicity (Peiter *et al.*, 2007, Delhaize *et al.*, 2007).

From other plant species, only a few members of the Mn subgroup within the CDF family have been described yet: ShMTP8 from the legume *Stylosanthes hamata* (Delhaize *et al.*, 2003), as mentioned above, HvMTP8.1 and HvMTP8.2 from barley (*Hordeum vulgare*) (Pedas *et al.*, 2014), OsMTP8.1 from rice (*Oryza sativa*) (Chen *et al.*, 2013), CsMTP8 and CsMTP9 from cucumber (*Cucumis sativus*) (Migocka *et al.*, 2014, Migocka *et al.*, 2015), OsMTP9 from rice (Ueno *et al.*, 2015), BvMTP10 and BvMTP11 from beet (*Beta vulgaris*) (Erbasol *et al.*, 2013), PtMTP11.1 and PtMTP11.2 from poplar (*Populus trichocarpa*) (Peiter *et al.*, 2007), and OsMTP11 from rice (Zhang & Liu, 2017). Whereas PtMTP11.1 and PtMTP11.2 share the same localization as AtMTP11 in vesicles of the Golgi apparatus (Peiter *et al.*, 2007), the localization of HvMTP8s is different compared to its ortholog in Arabidopsis. Both HvMTP8 transporters are localized to the Golgi apparatus and were able to complement the Mn-sensitive yeast strain *pmr1Δ* (Pedas *et al.*, 2014). It was suggested that both genes are important for the delivery of Mn to Golgi vesicles and thus for its transport to Mn-dependent enzymes or for the efflux via the secretory pathway, as previously postulated for AtMTP11 (Peiter *et al.*, 2007, Pedas *et al.*, 2014). In contrast to its barley counterpart, MTP8 from rice was shown to be located to the tonoplast, and it was also able to complement the Mn sensitive yeast strain *pmr1Δ*. Knockout lines of this gene showed decreased Mn uptake rates and a decreased Mn accumulation in the roots (Chen *et al.*, 2013). MTP8 from cucumber was also located in the vacuolar membrane and able to restore the growth of *pmr1Δ* yeast on media containing elevated levels of Mn (Migocka *et al.*, 2014). Another Mn transporter of the CDF family in cucumber, CsMTP9, was shown to be localized in the plasma membrane of root endodermal cells, and studies with yeast cells showed that it was able to transport

I Introduction

Mn and Cd. Arabidopsis plants expressing CsMTP9 showed an increased tolerance to excess Mn and Cd, which was suggested to be the result of an increased translocation of both metals from the roots to the shoots. The function of this MTP was proposed to be the transport of Mn and Cd from endodermis cells into the vascular cylinder (Migocka *et al.*, 2015). As mentioned above, MTP9 in rice (OsMTP9) was also described to be localized in the plasma membrane, but here in cells of the exo- and endodermis. Its ability to transport Mn was demonstrated by complementation assays using the *pmr1*Δ yeast strain. Furthermore, expression of *OsMTP9* in another yeast mutant strain, *Δzrc1cot1* resulted in an improved tolerance to Ni. From the localization at the proximal side of the cells and from decreased Mn concentrations in shoots of *Osmtp9* mutant lines, the authors concluded that OsMTP9 functions in releasing Mn from exodermis cells into the aerenchyma and in exporting Mn from endodermis cells into the stelar apoplast (Ueno *et al.*, 2015).

Except for a short report on MTP10 from beet (Erbasol *et al.*, 2013), showing its ability to complement the *pmr1*Δ yeast mutant, our knowledge about the role of AtMTP10 homologs is very limited. This member of the CDF family will therefore be elucidated in this thesis.

1.4 Submergence and the molecular and metabolic changes under limiting oxygen availability

An environmental factor that may lead to an enhanced availability of Mn and thus cause Mn toxicity, is the waterlogging of soils provoked by submergence. Most terrestrial plants are sensitive to submergence, which becomes apparent in a decreased growth. Under submergence the plant encounters three major problems: (i) decreased gas diffusion rate of O₂, CO₂, and ethylene in water, (ii) decreased light intensity that causes a drop in photosynthetic activity, and (iii) decreased redox potential in the soil that can lead to an increased availability of metals, in particular manganese, up to toxic amounts (Blom & Voeselek, 1996, Vervuren *et al.*, 2003, Bailey-Serres & Voeselek, 2008). For the last reason, Mn transporters were hypothesised to play a critical role during submergence.

I Introduction

Upon the decrease in cellular O₂ concentration during submergence, ATP synthesis is mediated by the less efficient fermentation, which results in lower ATP production, altered growth, and lower survival of the plants (Ricard *et al.*, 1994, Geigenberger, 2003). In the fermentation processes one molecule of hexose-equivalent yields only three molecules of ATP, while under aerobic conditions the mitochondrial respiration results in 39 molecules of ATP from this molecule (Geigenberger, 2003). Additionally, an accumulation of toxic fermentation compounds, like ethanol or lactate, poses another challenge to cope with (Drew, 1992).

The analysis of changes in the transcriptome under hypoxic or anoxic conditions has been the subject of many studies investigating the tolerance of plants to those conditions. Typical genes found to be up-regulated are involved in the change of carbon (C) and nitrogen (N) metabolism, e.g. alcohol dehydrogenase (ADH), pyruvate decarboxylase (PDC), lactate dehydrogenase, sucrose synthase (SUS), and alanine aminotransferase (AlaAT) (Loreti *et al.*, 2005, Branco-Price *et al.*, 2008, Mustroph *et al.*, 2009, Christianson *et al.*, 2009, van Dongen *et al.*, 2009, Licausi *et al.*, 2010, Lee *et al.*, 2011, Yang *et al.*, 2011). Furthermore, the up-regulation of genes involved in ethylene biosynthesis, e.g. ACC synthase (ACS) and ACC oxidase (ACO), presents a link between low oxygen availability and the phytohormone ethylene under submergence (Mustroph *et al.*, 2010). Another link to ethylene lies in the transcription factor RAP2.2, the overexpression of which improved the survival of Arabidopsis plants under oxygen depletion. RAP2.2 belongs to the subgroup VII of ethylene response factors (ERFs), like the previously described SUB1A gene cluster and the SNORKEL genes *SK1* and *SK2* that have an impact on the flooding tolerance of rice (Hattori *et al.*, 2009, Hinz *et al.*, 2010). The expression of genes that are involved in the metabolic adaptation to hypoxia is regulated by transcription factors of this ERF subgroup VII in response to ethylene signalling (Bailey-Serres *et al.*, 2012).

In case of oxygen deficiency caused by temporarily occurring floods, plants have also to overcome post-hypoxic conditions. The rehabilitation of the carbon metabolism and the defence of reactive oxygen species (ROS) that lead to post-hypoxic injury during re-aeration, are the most important adaptations under those conditions (Meguro *et al.*, 2006). One mechanism of ROS detoxification during the re-introduction of O₂ is an

I Introduction

increase in superoxide dismutase (SOD) activity. This was previously shown in submergence-tolerant species like *Iris pseudacorus* (Monk *et al.*, 1987b), *Nelumbo nucifera* (Ushimaru *et al.*, 2001), *Lupinus angustifolius* (Yu *et al.*, 1999), and rice (*Oryza sativa*) (Ushimaru *et al.*, 1992). In contrast to that, roots of the intolerant soybean (*Glycine max*) showed a decreased SOD activity during re-oxygenation (Vantoi & Bolles, 1991). SOD catalyses the breakdown of superoxide anions to hydrogen peroxide which is further detoxified by catalases and peroxidases. From studies on wheat it is known that during re-oxygenation the activity of enzymes in the ascorbate-glutathione cycle also increases to provide antioxidants in the reduced form for the detoxification of hydrogen peroxide (Biemelt *et al.*, 1998).

During re-oxygenation, ethanol accumulated during fermentation is metabolized to acetaldehyde by either the reverse reaction of the alcohol dehydrogenase (ADH) and/or by catalase (CAT) through peroxidation during the conversion of hydrogen peroxide to water (Fig. 2). Acetaldehyde can be converted to acetyl CoA by the mitochondrial acetaldehyde dehydrogenase (ALDH) and thus serve as substrate for the rehabilitated TCA cycle. An increase of ALDH activity was only observed in the submergence-tolerant species rice and not in the intolerant species maize during re-oxygenation, and it has thus been proposed that it alleviates post-anoxic injury in submergence-tolerant species (Meguro *et al.*, 2006).

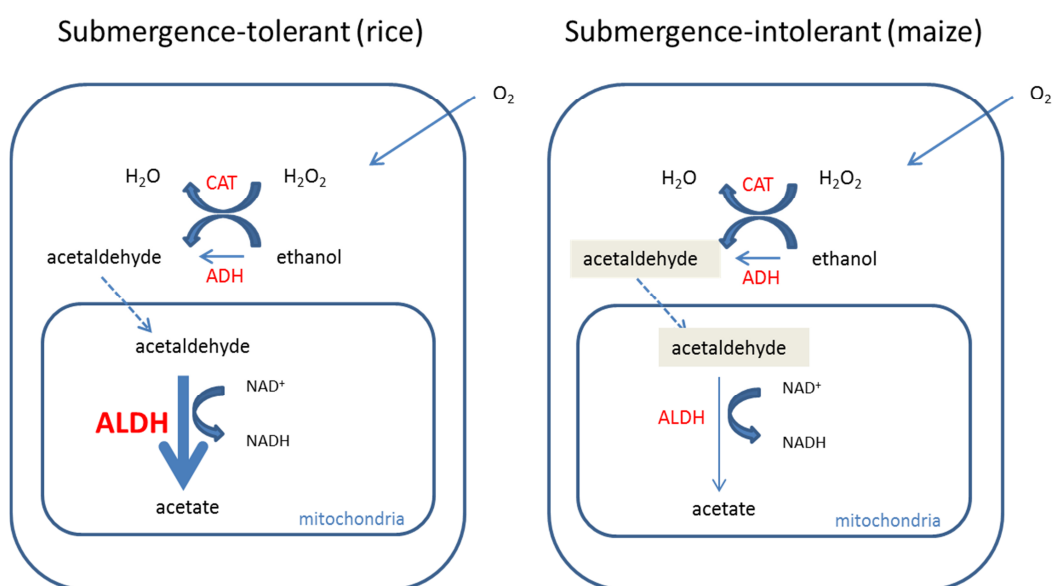


Fig. 2: Schematic representation of metabolic pathways of a submergence-tolerant species (rice) and a submergence-intolerant species (maize) during re-oxygenation (Meguro *et al.*, 2006).

1.5 Objectives of this work

The overall objective of this thesis was the functional characterization of the CDF protein AtMTP10 in *Arabidopsis*. Sequence analysis showed that this transporter belongs to the Mn clade of the CDF family. However, the specificity and the function of this transporter *in planta* had not yet been identified. In this work, the functions of AtMTP10 were thus elucidated in a reverse genetic approach by employing a range of molecular, cell biological, and physiological methods. Since it became apparent during this project that AtMTP10 plays an outstanding role in submergence tolerance of *Arabidopsis*, the mechanistic basis of *mtp10* mutant phenotypes under those conditions was examined.

2 Material and Methods

2.1 Plasmids and Constructs

For cloning of the *AtMTP10* coding region, RNA was isolated from leaves of soil-grown *Arabidopsis thaliana* Col-0 plants using the “Spectrum™ Plant Total RNA Kit” (Sigma Aldrich, St Louis, USA) with an on-column DNase treatment with DNase I (30 U) for 15 min at RT (Omega bio-tek, Norcross, USA). RNA was transcribed to cDNA by SuperScript II reverse transcriptase (Life Technologies, Carlsbad, CA, USA). The coding region of *AtMTP10* was amplified in a thermocycler (iCycler, Biorad, Hercules, USA) by using gene-specific primers containing specific restriction sites (see Appendix) and Phusion DNA polymerase (Invitrogen, Carlsbad, USA).

For DNA extraction, a leaf of soil-grown *Arabidopsis* Col-0 was ground in extraction buffer (200 mM Tris-HCl (pH 7.5); 250 mM NaCl; 25 mM EDTA; 5% SDS (w/v)). After centrifugation (16100 x g, 5 min) the DNA was precipitated with isopropanol. The resulting pellet was washed with 70% ethanol (v/v), air-dried, and resolved in 10 mM Tris-HCl (pH 8.5). For complementation lines and promoter-GUS lines, the genomic DNA was amplified in a thermocycler (iCycler, Biorad) by using gene-specific primers containing specific restriction sites (see Appendix) and Phusion DNA polymerase (Life Technologies, USA).

After amplification of *AtMTP10* DNA or cDNA fragments, a restriction digest was performed as described below for the specific constructs. Digested plasmids were dephosphorylated with Shrimp Alkaline Phosphatase (2 U; NEB, Ipswich, USA) for 15 min at 37°C, and ligation was performed with T₄ ligase (200 U) at 16°C overnight. The amounts of vector and insert were calculated as follows: $((100 \text{ ng vector} \times \text{bp insert}) / \text{bp vector}) \times 3 = \text{insert [ng]}$. All purification steps were performed with the “Wizard® SV Gel and PCR Clean-Up System” (Promega, Madison, USA). Electro-competent *E.coli* cells (TOP10; Thermo Fisher No C4040-xx) were transformed with ligation reactions by electric shock of 2500V in an electroporator (2510, Eppendorf, Hamburg, Germany). After incubation in SOC media (Tab. 1) at 37°C for 1 h and 200 rpm in a shaking incubator (Certomat IS, Sartorius, Göttingen, Germany), transformed bacteria were plated on selective LB media (Tab. 1). Minipreps of single colonies were performed with the “Pure Yield™ Plasmid

I Material and Methods

Miniprep System“ (Promega, Madison, USA). The individual constructs (Tab. 2) will be described in more detail in the respective section.

All enzymes were obtained from New England Biolabs (NEB, Ipswich, USA) and are listed in the Appendix.

Tab. 1: Growth media for *E.coli* cells

media	material	concentration [g L ⁻¹]
SOC	Tryptone	20
	Yeast Extract	5
	NaCl	0.58
	KCl	0.18
	add after autoclaving:	
	MgSO ₄	20 mM
	Glucose	20 mM
LB	Tryptone	10
	Yeast Extract	5
	NaCl	10
	Agar-Agar Kobe I	20

Tab. 2: Constructs used in this study

name	vector	insert	fused to	use
pART7-MTP10-EYFP	pART7 (Gleave, 1992)	cDNA of <i>AtMTP10</i>	EYFP	transient expression in protoplasts for subcellular localization
pART7-EYFP-MTP10	pART7-EYFP_{nostop}	cDNA of <i>AtMTP10</i>	EYFP	transient expression in protoplasts for subcellular localization
pBART-MTP10-EYFP	pBART (Gleave, 1992)	<i>AtMTP10-EYFP</i> expression cassette	---	transient expression in tobacco for subcellular localization
pART7-MTP10	pART7 (Gleave, 1992)	cDNA of <i>AtMTP10</i>	---	construction of pBART-MTP10
pBART-35S-MTP10	pBART (Gleave, 1992)	<i>AtMTP10</i> expression cassette	---	stable transformation in Arabidopsis Col-0 for overexpression of <i>MTP10</i>

name	vector	insert	fused to	use
pGreen-gMTP10	pGreenII (Hellens <i>et al.</i> , 2000) (http://www.pgreen.ac.uk/pGreenII/pGreenII.htm)	gDNA of <i>AtMTP10</i>	---	stable transformation in <i>Arabidopsis mtp10-1</i> plants for complementation
pBI101.3-PrMTP10	pBI101.3 (Jefferson <i>et al.</i> , 1987)	Promoter of <i>AtMTP10</i>	<i>uidA</i>	stable transformation in <i>Arabidopsis Col-0</i> plants for promoter GUS studies
pFL61-MTP10	pFL61 (Minet <i>et al.</i> , 1992)	cDNA of <i>AtMTP10</i>	---	expression in different yeast strains for yeast complementation assays
pJR1138Y-MTP10	pJR1138Y (Yalovsky <i>et al.</i> , 1997)	cDNA of <i>AtMTP10</i>	EYFP	expression in different yeast strains for localization of MTP10 in yeast
ER-mCherry	pFGC19 (Nelson <i>et al.</i> , 2007)	signal peptide of AtWAK2 + ER retention signal HDEL	mCherry	Co-localization with endoplasmatic reticulum (Nelson <i>et al.</i> 2007)
Peroxisome-mCherry	pFGC19 (Nelson <i>et al.</i> , 2007)	<i>PTS1</i>	mCherry	Co-localization with peroxisomes (Nelson <i>et al.</i> 2007)
TGN-mCherry	pBART (Gleave, 1992)	<i>SYP61</i>	mCherry	Co-localization with TGN
Mitochondria-mCherry	pFGC19 (Nelson <i>et al.</i> , 2007)	target sequence of cytochrome C oxidase from yeast	mCherry	Co-localization with mitochondria (Nelson <i>et al.</i> 2007)
Golgi-mCherry	pFGC19 (Nelson <i>et al.</i> , 2007)	alpha-1,2-mannosidase from soybean	mCherry	Co-localization with Golgi apparatus (Nelson <i>et al.</i> 2007)
pSoup	pSOUP (Hellens <i>et al.</i> , 2000) (http://www.pgreen.ac.uk/pGreenII/pGreenII.htm)	---	---	for transformation with pGreen II

2.2 Plant material

T-DNA insertion lines were obtained from the European Arabidopsis stock centre (NASC). Lines with a Columbia-0 (Col-0) background were obtained from the SALK collection [SALK_121470 (*mtp10-1*) and SALK_023321 (*mtp10-2*)] and a line with a Wassilewskija (WS) background from the FLAG collection [FLAG 239D02 (*mtp10-3*)]. Transposon lines with Nossen-0 (No-0) background were obtained from the RIKEN collection [RATM 13-2493-1 (*mtp10-4*) and RATM 13-0042-1 (*mtp10-5*)]. Homozygous plants were identified by using gene-specific primers as listed in the appendix. The insertions were identified with SALK_Lb(A) and SALK_Rb(A) primers for the lines of the SALK collection, FLAG_Lb (4a) and FLAG_Rb (4a) primers for the line of the FLAG collection, and Ds5-2a_G-edge for the lines of the RIKEN collection (see Appendix).

For identification of gene knockout, RNA was extracted with the „Total Purification from Plant“ Kit (Macherey-Nagel, Düren, Germany), and cDNA synthesis was performed by SuperScript II reverse transcriptase (Life Technologies, Carlsbad, CA, USA). For reverse transcriptase PCR, gene-specific primers were used. Amplification of *Actin2* (*ACT2*; At3g18780) was performed to test the quality of the cDNA.

2.2.1 Complementation lines: *mtp10-1::gMTP10*

For complementation of the mutant line *mtp10-1*, genomic DNA of *AtMTP10* including the 5'UTR and promoter region (2037 bp upstream of the ATG) and the 3'UTR (586 bp downstream of the TAG) was amplified from Col-0 genomic DNA and cloned into pGreenII (Hellens *et al.*, 2000) with *Sma*I-containing primers. The vector and the amplified product were digested with *Sma*I, purified, dephosphorylated, and ligated as described above. *Agrobacterium tumefaciens* (GV3101) bacteria were transformed with the resulting construct by electric shock of 2500V in an electroporator (2510, Eppendorf). After incubation in SOC media (s. 2.1) at 28°C for 2 h and 200 rpm in a shaking incubator (Certomat IS, Sartorius), transformed bacteria were plated on selective YEB media (Tab. 3) containing kanamycin (50 µg mL⁻¹) and gentamycin (25 µg mL⁻¹). A single positive colony was plated on a fresh selective YEB plate containing the same antibiotics and incubated for three days at 28°C. Homozygous *mtp10-1* plants were stably transformed with that A.

I Material and Methods

tumefaciens culture by the floral-dip method (Clough & Bent, 1998). Seedlings were selected by kanamycin on sterile agar plates (s. 2.3.1), and expression level of *AtMTP10* was determined in four independent lines by quantitative real time RT-PCR (s. 2.9). Expression was quantified using a cDNA dilution series and normalized against *Actin2* (*ACT2*; At3g18780).

Tab. 3: Growth media for *Agrobacterium tumefaciens* cells

media	material	concentration [g L ⁻¹]
YEB	Yeast Extract	1
	Beaf Extract	1
	Casein Hydrolysate	5
	Sucrose	5
	MgSO ₄ x 7 H ₂ O	0.49
	Agar-Agar Kobe I	20
SOC	Tryptone	20
	Yeast Extract	5
	NaCl	0.58
	KCl	0.18
	add after autoclaving:	
	MgSO ₄	20mM
	Glucose	20mM

2.2.2 Overexpressor lines: *CaMV35S-MTP10*

For overexpressing *AtMTP10*, the coding region of *AtMTP10* was cloned into pART7 downstream of the *CaMV35S* promoter using XmaI-containing primers. The vector and the amplified product were digested with XmaI, purified, dephosphorylated, and ligated as described above. A cassette including the 35S promoter, the coding region of *AtMTP10*, and the 3'ocs terminator was sub-cloned from pART7-*MTP10* into pBART by NotI digestion. *A. tumefaciens* (GV3101) bacteria were transformed with the resulting construct by electric shock of 2500V in an electroporator (2510, Eppendorf). After incubation in SOC media (s. 2.1) at 28°C for 2 h and 200 rpm in a shaking incubator (Certomat IS, Sartorius), transformed bacteria were plated on selective YEB media (s. 2.2.1) containing spectinomycin (25 µg mL⁻¹) and gentamycin (25 µg mL⁻¹). A single positive colony was plated on a fresh selective YEB plate containing the same antibiotics

I Material and Methods

and incubated for three days at 28°C. Arabidopsis Col-0 plants were stably transformed with that *A. tumefaciens* culture by the floral-dip method. The resulting seeds were sown on soil, and the plants were cultivated as described in 2.3.3 and selected by glufosinate-NH₄ (0.2 g L⁻¹; BASTA; Bayer Crop Science, Langenfeld, Germany). The expression level of *AtMTP10* was determined in four independent lines by quantitative real time RT-PCR (s. 2.9). Expression was quantified using a cDNA dilution series and normalized against *Actin2* (*ACT2*; At3g18780).

2.2.3 Promoter GUS lines: *PrMTP10*-GUS

For promoter-GUS studies the *AtMTP10* promoter region 2037 bp upstream of the start codon was amplified from Col-0 genomic DNA using *Sma*I-containing primers and cloned into pBI101 upstream of the *uidA* gene (Jefferson *et al.*, 1987). The amplified promoter and the vector were *Sma*I-digested, purified, dephosphorylated, and ligated as described above. *A. tumefaciens* (GV3101) bacteria were transformed with the resulting construct by electric shock of 2500 V in an electroporator (2510, Eppendorf). After incubation in SOC media (s. 2.1) at 28°C for 2 h and 200 rpm in a shaking incubator (Certomat IS, Sartorius), transformed bacteria were plated on selective YEB media (s. 2.2.1) containing kanamycin (50 µg mL⁻¹) and gentamycin (25 µg mL⁻¹). A single positive colony was plated on a fresh selective YEB plate containing the same antibiotics and incubated for three days at 28°C. Arabidopsis Col-0 plants were stably transformed with that *A. tumefaciens* culture by the floral-dip method, and transformed lines were identified by kanamycin selection (50 mg L⁻¹) on sterile agar plates as described in 2.3.1.

2.3 Plant cultivation

2.3.1 Cultivation on sterile agar plates

Arabidopsis seeds were surface-sterilized in bleach solution [1/3 NaClO (v/v) (Carl Roth, Karlsruhe, Germany) and 0.02% Triton X-100 (v/v)] for 5 min and washed four times with sterile deionized water. Seeds were sown on ½-strength Murashige & Skoog medium (pH 5.8) including Gamborg's B5 vitamins and 0.8% phytoagar (both Duchefa, Haarlem,

I Material and Methods

Netherlands) using BARKY μ tipette™ Capillary Tips (BARKY Instruments International, Folkestone, UK). Seeds were stratified for 2 d at 4°C in the dark, and plants were cultivated either under long-day conditions [16 h light period (22°C; 150 $\mu\text{mol m}^{-2} \text{s}^{-1}$) and 8 h dark period (18°C)] or under short-day conditions [10 h light period (22°C; 150 $\mu\text{mol m}^{-2} \text{s}^{-1}$) and 14 h dark period (18°C)] and a constant relative humidity of 65% in a plant growth cabinet (AR75, Percival Scientific, Perry, USA).

2.3.2 Cultivation in liquid media

For analysis of metals in shoots, roots, and xylem exudates, plants were grown in liquid culture medium according to (Arteca & Arteca, 2000) with minor modifications (0.5 mM $(\text{NH}_4)_2\text{SO}_4$, 2 mM KNO_3 , 2 mM CaCl_2 , 0.5 mM MgSO_4 , 0.3125 mM KH_2PO_4 , 42.5 μM FeNaEDTA, 0.125 μM CuSO_4 , 0.25 μM ZnSO_4 , 17.5 μM H_3BO_3 , 0.05 μM NaMoO_4 , 0.0025 μM CoCl_2 , and 3.5 μM MnSO_4 . Medium pH was adjusted to 5.8. Before stratification for 2 d at 4°C in the dark, seeds were sown on rock wool (Grodan; Grodania A/S, Hedehusene, Denmark) inserted into 1.5 mL microtubes (Eppendorf) with a cut bottom. Plants were pre-cultured in boxes containing 1 L of the medium under short-day conditions in a plant growth cabinet (ATC26, Conviron, Winnipeg, Canada) as described in 2.3.1. After two weeks, plants were transferred to boxes containing 5 L of the media (16 plants per box) and cultivated further under the same conditions as indicated in the specific experiments. Media were changed twice a week and aerated with 0.4 L h^{-1} atmospheric air, controlled by a flow-meter (Cole&Parmer, Vernon Hills, USA).

2.3.3 Cultivation on soil

For propagation and for submergence experiments, plants were cultivated in standardized ED73 soil (Einheitserde Werkverband e.V., Sinntal-Altengronau, Germany) mixed with 1/3 vermiculite (w/w) (Gärtnereibedarf Kammlott GmbH, Erfurt, Germany). BioMükk® (BioFa AG, Münsingen, Germany) was added to the soil: vermiculite mixture in a concentration of 10 g L^{-1} (w/w).

2.4 Examination of Mn toxicity effects on agar plates

For monitoring the growth of *AtMTP10* loss-of-function mutants, and complementation lines under Mn toxicity, seeds were surface-sterilized and sown on ½ MS plates as described in 2.3.1. The medium was supplemented with different Mn concentrations as indicated. After stratification, the plates were placed vertically in a growth cabinet (AR75, Percival Scientific) set to long-day conditions. The root length was determined every second day, and fresh weight was determined at the end of the experiment. The root growth rate was calculated by means of a linear regression of the root lengths.

2.5 Examination of Mn deficiency effects in liquid culture media

Plants were cultivated for six weeks under short-day conditions in liquid culture media containing either 0 or 3.5 µM MnSO₄ as described under 2.3.2. After harvesting, the plants were separated into shoots and roots. To remove the external nutrient solution, roots were washed in ice-cold washing buffer I (5 mM CaSO₄, 1 mM MES-KOH, pH 5.8) for ten minutes and subsequently in washing buffer II (washing buffer I supplemented with 10 mM EDTA) for five minutes, before they were transferred to deionized water. The remaining deionized water was removed by blotting the plant material in towel paper before it was dried for 3 d at 65°C in a drying oven (Linn High Therm, Eschenfelden, Germany).

2.6 Determination of metal concentrations

Dried shoots and roots were weighed into PFA vessels (CEM, Kamp-Lintfort, Germany) and digested in 32.5% HNO₃ (v/v) and 6% H₂O₂ (v/v) (Carl Roth, Karlsruhe, Germany) for 15 min at 180°C in a MARS 5 Xpress (CEM) microwave oven with the temperature ramped to 180°C in 15 min. Elements were analysed by ICP-OES using an Ultima 2 instrument (Horiba Scientific, Tenyamachi, Japan).

2.7 Promoter-GUS studies

The promoter activity of *AtMTP10* was determined by promoter-GUS analysis of homozygous ProMTP10-GUS plants (2.2.3). Plants were cultivated on sterile agar plates or on soil as described in 2.3.1 and 2.3.3, respectively, and transferred to staining solution [100 mM sodium phosphate buffer (pH 7.0), 10 mM EDTA, 3 mM $K_4[Fe(CN)_6]$, 0.5 mM $K_3[Fe(CN)_6]$, 0.1% Triton X-100 (v/v), and 2 mM 5-Bromo-4-chloro-3-indolyl-beta-D-glucuronic acid (X-Gluc; X-Gluc Direct, UK) in DMSO] and stained for GUS activity for 1 h at 37°C. After chlorophyll removal with 80% ethanol (v/v), the tissues were documented with an AxioCam HRc digital camera (Carl Zeiss, Jena, Germany) mounted on a SteREO Discovery V.20 stereomicroscope (Carl Zeiss). For cross sections the respective plant part was embedded in 3% low-melting agarose (w/v) (Biozym Scientific, Hessisch Oldendorf, Germany). 40 µm sections were prepared with a Hyrax V 50 vibrating microtome (Carl Zeiss) and documented with an AxioCam MRc mounted on an Axioskop microscope (Carl Zeiss).

2.7.1 Visualization of the Casparian strip

Cross sections (40 µm) of *Arabidopsis* roots were stained in 0.1% (w/v) berberine hemisulfate for one hour. After 3 wash steps with deionized water, the sections were incubated in 0.5% (w/v) aniline blue for 30 min. The sections were rinsed three times with $FeCl_3$ in 50% (v/v) glycerine (Brundrett *et al.*, 1988), and pictures were taken by fluorescence microscopy, employing an AxioCam MRc mounted on an Axioskop microscope (Carl Zeiss). Samples were excited with a HBO 50 lamp (Carl Zeiss) by using a FS49 filter set (Carl Zeiss) with an 365 nm excitation filter, a 395 nm beam splitter, and a 445/50 nm band pass emission filter.

2.8 Yeast complementation assays

For yeast complementation assays the full-length cDNA of *AtMTP10* was cloned into the yeast expression vector pFL61 (Minet *et al.*, 1992) downstream of the *PGK* promoter by using NotI-containing primers (s. 2.1). The amplified coding region and the vector were NotI-digested, purified, digested, and ligated as described above (2.1). *S. cerevisiae* wild

I Material and Methods

type strain BY4741 (Y00000) and its deletion mutants Y04169 (*ccc1Δ*), Y01613 (*cot1Δ*), Y04533 (*cup2Δ*), Y04534 (*pmr1Δ*), and Y00829 (*zrc1Δ*) [Euroscarf, Frankfurt, Germany (Winzeler *et al.*, 1999)] grown on YPD media (Tab. 4) were transformed with pFL61-*MTP10* or the empty vector by the Li-acetate method according to Elble (1992). For complementation assays yeast strains were grown to log phase under uracil selection in synthetic complete media (SC) (Tab. 4) and spotted in a tenfold dilution series onto plates containing different concentration of the respective metals.

Tab. 4: Growth media for *Saccharomyces cerevisiae*

media	material	concentration [g L ⁻¹]
YPD	Yeast Extract	10
	(Bacto)peptone	20
	Glucose	20
	Agar-Agar Kobe I	20
SC-Uracil	(NH ₄) ₂ SO ₄	5
	Complete Supplement Mixture (CSM)-URA	0,77
	Yeast Nitrogen Base Without Amino Acids & (NH ₄) ₂ SO ₄	1,9
	Glucose	20
	Agar-Agar Kobe I	20

2.8.1 Determination of metal concentration in yeast

Metal concentrations in yeast were also determined by ICP-OES (s. 2.6). SC-URA medium (100 mL) (s. 2.8) was inoculated with a pre-culture of the respective strain and grown to the log phase. Cultures were centrifuged for 5 min (4500 rpm at 4°C) and washed two times in washing buffer (50 mM Tris-HCl and 10 mM EDTA, pH 6.5). Cells were resuspended in 6 mL sterile water and cell density of a 1:400 dilution was determined by counting with a Neubauer-Improved counting chamber. The cell suspension was digested in 25% HNO₃ (v/v) and 4.6% H₂O₂ (v/v) in a total volume of three millilitre (Carl Roth).

2.8.2 Yeast microsomal vesicle transport assays

The microsomal fraction of log phase-grown *pmr1Δ* cells, transformed with the empty vector pFL61 or with pFL61-*MTP10*, was prepared according to Ueoka-Nakanishi *et al.*

I Material and Methods

(2000). Uptake experiments and calculation of uptake rates were performed as previously described by (Peiter *et al.*, 2007) with minor modifications. 500 µg microsomal protein were incubated in 500 µL uptake buffer [5 mM BTP/MES (pH 7.5), 300 mM sorbitol, 25 mM KCl, 5 mM MgCl₂] for 5 min at 25°C. MnCl₂ labelled with ⁵⁴Mn²⁺ with a specific activity of 56.28 mCi mg⁻¹ (≅ 2082.52 MBq mg⁻¹) (Perkin Elmer, Waltham, USA) was added to a final concentration of 100 µM Mn²⁺. MgATP (Sigma Aldrich, St Louis, USA) was added to the respective samples to a final concentration of 1 mM. Aliquots of 100 µg protein were removed and filtered through buffer-premoistened cellulose acetate filters (0.45 µm; Whatmann, Maidstone, UK) at the indicated time points. The filters were washed twice with 1000 µL ice-cold washing buffer [5 mM BTP/MES (pH 7.5), 300 mM sorbitol, 25 mM KCl, 1 mM MnSO₄] and transferred into 4 mL scintillation cocktail (Carl Roth). The β-emission (decays per minute) was determined using a Tri-Carb liquid scintillation counter (Perkin Elmer) with a pre-count delay of 0.2 min and a counting time of 1 min. Prior to the uptake assays, the intactness of the vesicles was tested with Acridine Orange. Vesicle suspension (60 µg protein) was diluted in 1 mL of a buffer containing 5 mM BTP/MES (pH 7.5), 300 mM sorbitol, 25 mM KCl, 5 mM MgCl₂, 1 mM DTT, and 12 µM Acridine Orange. The reaction was started by the addition of 1 mM MgATP added from a 20 mM stock in the same buffer. The proton transport activity was monitored in a Specord 200 photometer (Carl Zeiss Technology, Jena, Germany) by measuring the changes of the absorbance at a wavelength of 492 nm for ~200 s. Afterwards ammonium sulphate [2.5µM] was added to the samples, and the changes in absorbance were measured for another ~100 s.

2.9 Quantitative real time RT-PCR

RNA was extracted with an “RNeasy plant mini kit” (Qiagen, Hilden, Germany) or a “Spectrum™ Plant Total RNA kit” (Sigma Aldrich, St Louis, USA). DNA was removed with an on-column DNase treatment with DNase I (30 U) for 15 min at RT (Omega bio-tek, Norcross, USA). 1 µg of total RNA was transcribed to cDNA with SuperScript® II reverse transcriptase (Life Technologies, Carlsbad, USA) for determination of the expression level upon Mn toxicity and with Protoscript II (NEB, Ipswich, USA) for the other experiments using random hexamer primers. Quantitative real time PCR was performed in a realplex⁴

I Material and Methods

Mastercycler system (Eppendorf, Hamburg, Germany) by using the POWER SYBR Green PCR mastermix (Applied Biosystems, Foster City, USA). Relative expression levels of *AtMTP10* were quantified by employing a cDNA dilution series and normalized against *At5g60390 (EF1 α)*, *At3g18780 (Actin2)*, and *At4g05320 (Ubiquitin10)* as indicated in the different experiments.

2.10 Subcellular localization in mesophyll protoplasts

For subcellular localization of *AtMTP10*, EYFP fusion constructs were prepared. For C-terminal EYFP fusion, the full-length *AtMTP10* cDNA without the stop codon was amplified from pART7-*MTP10* (s. 2.1) by using XmaI-containing primers and cloned into pART7-EYFP (Peiter et al., 2007). For N-terminal EYFP fusion, the *AtMTP10* cDNA including the stop codon was cloned into pART7-EYFP_{nostop} with BamHI-containing primers. To avoid a frameshift, an adenosine was included upstream of the ATG in the forward primer. PCR products and plasmids were digested with the respective enzymes, purified, dephosphorylated, and ligated as described above (s. 2.1). Protoplasts of the Arabidopsis Col-0 wild type and of an ER-GFP or a Golgi-GFP marker line (Hawes & Satiat-Jeunemaitre, 2005) were prepared and transiently transformed with the constructs as described before (Peiter et al., 2007). Briefly, leaves of four-week-old plants grown on soil as described in 2.3.3 were cut in plasmolysis buffer [500 mM mannitol, 10 mM CaCl₂, 10 mM MES-KOH (pH 5.6)]. After two vacuum infiltration steps of five minutes in enzyme solution [1% cellulysin (w/v), 0.3% macerascase (w/v), 400 mM mannitol, 20 mM KCl, 20 mM MES-KOH (pH 5.6), 10 mM CaCl₂, 0.1% BSA (w/v)] the tissue was digested for 3 h at 23°C in the dark. The resulting protoplasts were isolated with the help of a 70 μ m mesh (Becton Dickinson, Franklin Lakes, USA) before CaCl₂ was added to a concentration of 100 mM. Protoplasts were collected by centrifugation (100g, Centrifuge 5804R, Eppendorf, Hamburg, Germany), washed in W5 solution [125 mM CaCl₂, 154 mM NaCl₂, 2 mM MES-KOH (pH 5.6), 5 mM KCl] and incubated on ice for 30 min in the dark. For transformation, W5 solution was substituted by MaMG solution [400 mM mannitol, 15 mM MgCl₂, 5 mM MES-KOH (pH 5.6)]. 2×10^4 cells were mixed with 10 μ g plasmid DNA and PEG-CMS solution [1 g PEG4000 (Fluka 95904) (\cong 154 mM with an average molecular weight of 4000 g mol⁻¹), 308 mM mannitol, 154 mM Ca(NO₃)₂] and incubated for 20 min at 23°C in

I Material and Methods

the dark. Transformed protoplasts were washed in protoplast culture medium [4.4 g L⁻¹ MS salt with vitamins (Duchefa, Amsterdam, Netherlands), 350 mM mannitol, 50 mM glucose, 3 mM CaCl₂, 0.1 mg ml⁻¹ ampicillin, pH 5.8] and resuspended in 50 µL of the same medium. All centrifugation steps were performed in a MiniSpin centrifuge (Eppendorf) for two minutes and 100g. After 20 hours of incubation in the dark, EGFP and EYFP fluorescence was observed by confocal laser scanning microscopy using a LSM 510 META (PMT detector) equipped with a Plan-apochromatic lens (63x/1.4 Oil) (Carl Zeiss). Pictures were taken in Lambda mode (497-668nm) with a resolution of 1024x1024 in plane scan mode for single lines with four repetitions. As excitation light source an argon laser with an excitation wavelength of 488 nm and a main dichroic beam splitter 405/488 nm was used. EYFP and EGFP signals were separated by linear unmixing with previously generated spectra. Spectra were obtained from protoplasts transiently transformed with the pART7 empty vector containing the respective fluorophore. Co-localization of CFP and EYFP was performed with the same microscope in channel mode by using the multitrack function. Excitation light source was the 488 nm argon laser (EYFP) and a 458 nm argon laser (CFP) with a 458 nm HFT and a 545 nm NFT. EYFP and auto fluorescence were detected by using a band pass filter with 505-530 nm and a long pass filter with 615 nm, respectively. The CFP signal was detected by using a band pass filter with 470-500 nm.

2.11 Subcellular localization in tobacco

For subcellular localization in tobacco, electro-competent cells of the *A. tumefaciens* strain GV3101 were transformed with pBART-*MTP10-EYFP* and different marker plasmids (Nelson *et al.*, 2007) (s. 2.1 and Appendix) by electroporation with an electroporator (2510, Eppendorf). After an incubation in SOC media (Tab. 3) for two hours at 28°C in a shaking incubator with 200 rpm (Certomat IS, Sartorius), transformed bacteria were cultivated on selective YEB-media (Tab. 3) containing the respective antibiotics (25 µg ml⁻¹ spectinomycin and 25 µg ml⁻¹ gentamycin for pBART, or 50 µg ml⁻¹ kanamycin and 25 µg ml⁻¹ gentamycin for pFGC19). 1.5 mL of a liquid YEB overnight culture of a single colony was centrifuged and resuspended in 250 µL infiltration media [10 mM MgCl₂, 5 mM MES (pH 5.3), 0.15 mM acetosyringone] . The OD₆₀₀ was adjusted to 0.8, and 1 mL of suspension was infiltrated into leaves of six-week-old soil-grown *Nicotina benthamiana*

I Material and Methods

plants. Microscopic analysis was performed 48 hours post-infiltration. For co-localization with marker plasmids overnight cultures were mixed 1:1 before the infiltration of tobacco leaves. For studies with Tyrphostin (TYR) A23 or Mn^{2+} , protoplasts of infiltrated tobacco leaves were isolated as described above (s. 2.10). Treatments with TYR A23 (100 μ M) or Mn^{2+} (100 μ M) were performed with approximately 0.5×10^7 cells in W5 solution for 15 min at room temperature. All pictures were taken with an AxioCam MRm mounted on an Axio Observer Z1 microscope equipped with a Plan Apochromatic lens (40x/1.3 oil) (all Carl Zeiss). Pictures were taken with a multi-track function and an excitation by a HXP120 UV lamp (Carl Zeiss). For detection of the EYFP signal, the filter set FS46HE (Carl Zeiss) with an excitation band pass filter 500/25 nm and an emission band pass filter 535/30 nm was used. For detection of the mCherry signal, the filter set FS31 (Carl Zeiss) with a bandpass filter 565/30 nm for excitation and a band pass filter 620/60 nm for emission was used.

2.12 Growth experiments under oxygen-deficient conditions

2.12.1 Submergence of soil-grown plants

Arabidopsis Col-0, *mtp8-1* (Eroglu *et al.*, 2016), *mtp9-1* (SALK_102733.45.10), *mtp10-1*, *mtp10-4*, *mtp10-1::gMTP10.2*, and *mtp11-1* (Peiter *et al.*, 2007) were pre-cultured for one week on vertical ½ MS agar plates under long-day conditions in a growth cabinet (AR75, Percival Scientific) (s. 2.3.1). Seedlings were transferred to soil (2.3.3) and grown for another 14 days before they were submerged for 21 days and re-aerated for another 14 days or 21 days under the same conditions. Pictures were taken at the end of the respective recovering phase.

2.12.2 Anoxic conditions on agar plates

Col-0 and *mtp10-1* seeds were sown on ½ MS agar plates as described in 2.3.1 and cultivated for 7 days under long-day conditions in a growth cabinet (AR75, Percival Scientific, Perry, USA). Subsequently, plates were mounted in a dessicator for 24 hours, which was flooded with N_2 to trigger anoxic conditions. Flow rate was controlled by a

I Material and Methods

flow-meter (Cole&Parmer, Vernon Hills, USA) and adjusted to 0.4 L h^{-1} . To mimic the conditions of the growth cabinet, the light intensity was adjusted to $100 -120 \mu\text{mol m}^{-2} \text{ s}^{-1}$. Plants were allowed to recover under different conditions for ten days before fresh and dry weight were determined.

2.13 Analysis of xylem exudates

For collecting xylem exudates, shoots of hydroponically-grown plants (see 2.3.2) were cut off, and the hypocotyl was connected to a silicon tube (diameter 1 mm; VWR, Radnor, USA). Xylem exudates were collected for two hours in a microtube (Eppendorf). Metals were analysed by ICP-MS using a Thermo Element 2 instrument (Thermo Fisher Scientific, Waltham, USA).

3 Results

3.1 Plant material

3.1.1 Genotypical analysis of *AtMTP10* insertional mutants

Five mutant lines defective in *AtMTP10* were analysed for the position of the T-DNA insertion or the transposon by sequencing of the insert borders (Fig. 3). In the main mutant line used in this thesis, SALK_121470 (*mtp10-1*), the T-DNA insertion was identified in the second exon. The left border was located 821 bp and the right border 842 bp downstream of the ATG. For SALK_023321 (*mtp10-2*), the left border was identified 2174 bp and the right border 2197 bp downstream of the ATG, both in the 3'UTR. In the line FLAG 239D02 (*mtp10-3*), the insertion was detected in the promoter of *AtMTP10*. The left border was 597 bp and the right border 525 bp upstream of the ATG. For the transposon lines of the Riken collection, only the GUS-end could be determined. In both lines the transposon was located in the sixth exon. For RATM 13-2493-1 (*mtp10-4*) and for RATM 13-0042-1 (*mtp10-5*), it was detected 1954 bp and 2131 bp downstream of the ATG, respectively.

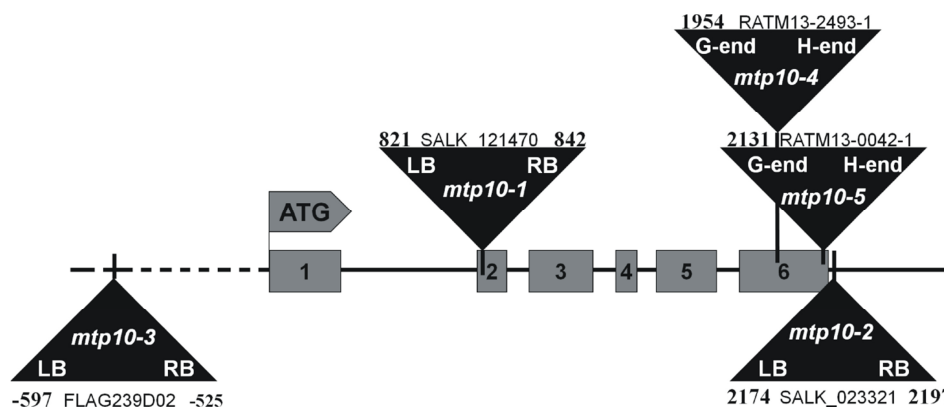


Fig. 3: Structure of *AtMTP10* and locations of mutations. Dotted line represents the promoter region, grey boxes the six exons, and the lines between the introns. Insertion sites in T-DNA or transposon lines are represented by black triangles. (LB= left border; RB= right border; G-end= β -glucuronidase (GUS) end; H-end= bacterial aph4 gene (resistance to hygromycin) end).

The *AtMTP10* expression levels of these lines were determined by reverse transcriptase PCR on leaf material using primers spanning the insertions (Fig. 4). The quality of the cDNA preparations was assessed by the amplification of *Actin2* (At3g18780). The mutant lines *mtp10-1*, *mtp10-4*, and *mtp10-5* showed no transcript of *AtMTP10*. The mutant

I Results

mtp10-3 showed a transcript, even though its abundance was decreased compared to the wild type. So this line was considered as knocked down for *AtMTP10*. This was verified by quantitative real time PCR (qRT-PCR), which showed that the transcript level of *AtMTP10* in *mtp10-3* was reduced to 3.6% of that in the wild type. The line *mtp10-2* showed no difference to the wild type in the expression of *AtMTP10*.

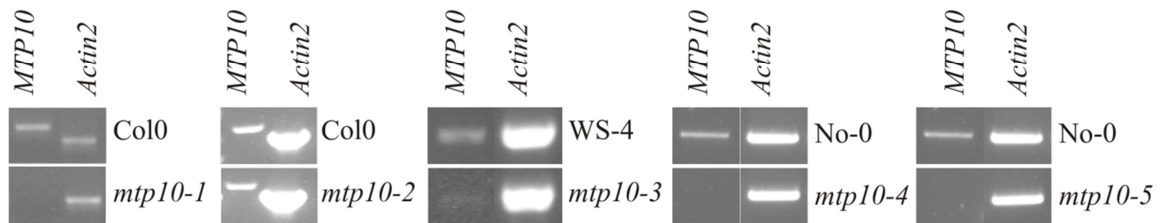


Fig. 4: Presence of *AtMTP10* transcript in the mutant lines *mtp10-1* through *mtp10-5* and the corresponding wild types as analysed by RT-PCR. *Actin2* served as positive control.

3.1.2 Generation of *AtMTP10*-overexpressing lines

For analysis of the functions of *AtMTP10* *in planta*, overexpressors were generated. To this end, Col-0 plants were transformed by floral dipping with a construct expressing the coding region of *AtMTP10* under the control of the CaMV35S promoter. Resulting seeds were sown on soil and selected by BASTA. RNA of four independent lines was translated to cDNA and analysed for *AtMTP10* expression level (Fig. 5 A). Homozygous lines were selected on sterile agar plates containing DL-Phosphinothricin (Fig. 5 B). Further experiments were performed with homozygous seeds of line 3, which showed an increased expression of *AtMTP10* by ~3100fold.

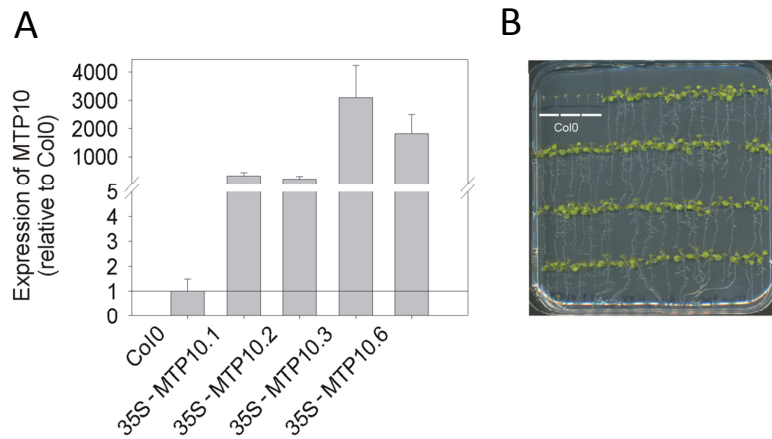


Fig. 5: Expression of *AtMTP10* in four overexpressor lines as determined by quantitative real time PCR. Expression was quantified against a cDNA dilution series and normalized to *Actin2* (A). Col-0 and 35S-MTP10.3 seedlings grown on $\frac{1}{2}$ MS agar plate containing DL-Phosphinothricin (B).

3.1.3 Generation of *AtMTP10* complementation lines

For complementation of the *mtp10-1* mutant, plants were transformed with a construct containing the genomic DNA of *AtMTP10* including its native promoter and terminator. The genomic sequence of *AtMTP10* ranging from 2037 bp upstream of the ATG until 586 bp downstream of the stop codon was amplified from Col-0 genomic DNA and cloned into pGreenII. The construct was transformed in *mtp10-1* plants by floral dipping, and resulting seeds were selected with BASTA. RNA of different lines was translated to cDNA and analysed for transcript level of *AtMTP10*. Expression of *AtMTP10* in *mtp10-1::gMTP10.1* and *mtp10-1::gMTP10.2* was comparable with that in the Col-0 wild type (Fig. 6). *mtp10-1::gMTP10.1* showed a two fold higher expression whereas *mtp10-1::gMTP10.2* showed half of the expression of *AtMTP10* compared to the wild type. The other two lines showed an increased expression (*mtp10-1::gMTP10.3*: 8-fold; *mtp10-1::gMTP10.4*: 4.4 fold) and were considered as slight overexpressors.

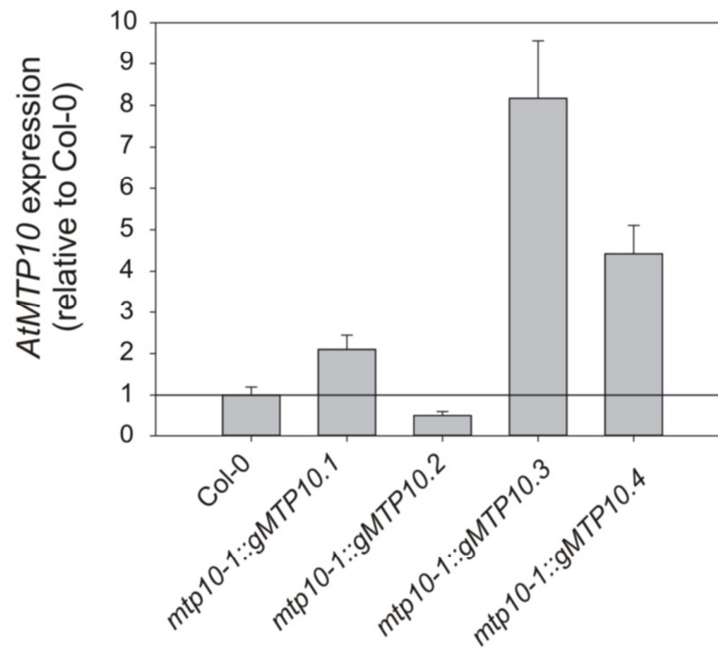


Fig. 6: Expression of *AtMTP10* in four complementation lines determined by quantitative real time PCR. Expression was quantified against a cDNA dilution series and normalized to *Ubiquitin*.

3.2 Functional characterization of *AtMTP10*

3.2.1 Experiments on the model yeast *Saccharomyces cerevisiae*

3.2.1.1 Yeast complementation assays

To determine the metals transported by *AtMTP10*, yeast complementation assays were performed. Metal-hypersensitive yeast mutants were transformed with *AtMTP10* and grown on plates containing the respective metal in a toxic concentration (Fig. 7). *AtMTP10* was able to complement a Mn-sensitive yeast strain (*pmr1Δ*) and an Fe-sensitive one (*ccc1Δ*), but not yeast strains sensitive to other divalent cations like Cu^{2+} (*cup1Δ*), Co^{2+} (*cot1Δ*), or Zn^{2+} (*zrc1Δ*). The growth of *pmr1Δ* was restored on media with up to 24 mM Mn, a concentration that even the parental strain BY4741 was not able to tolerate.

I Results

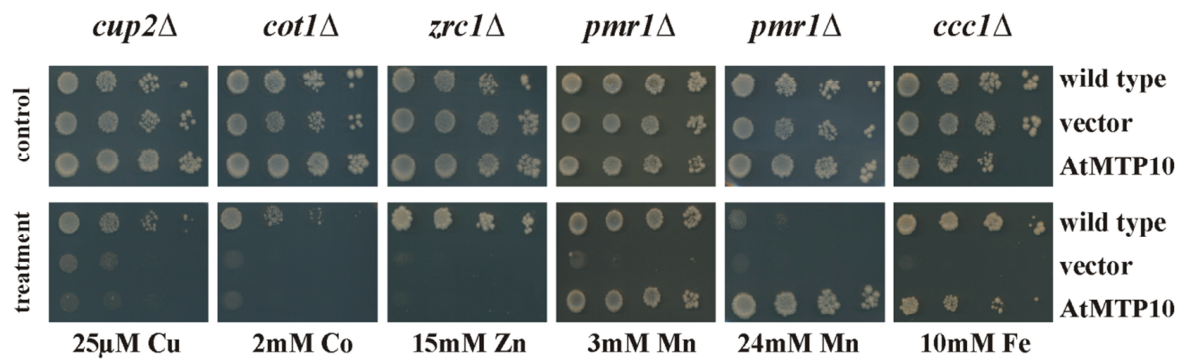


Fig. 7: Ten-fold dilution series of *Saccharomyces cerevisiae* wild type and deletion strains carrying the vector pFL61 with or without *AtMTP10* grown on selective media containing the indicated metal concentrations.

3.2.1.2 Localization of *AtMTP10* in *S. cerevisiae*

Due to the fact that PMR1 mediates Mn tolerance by secretion via the Golgi and *AtMTP10* complements the *pmr1Δ* deletion strain, it was assessed if both proteins share the same localization in yeast. Fluorescence microscopy of *pmr1Δ* yeast cells expressing an *AtMTP10-EYFP* construct showed a punctate pattern and a weak signal in the cytosol, indeed suggesting a subcellular localization to the ER and to vesicles of the Golgi apparatus (Fig. 8).

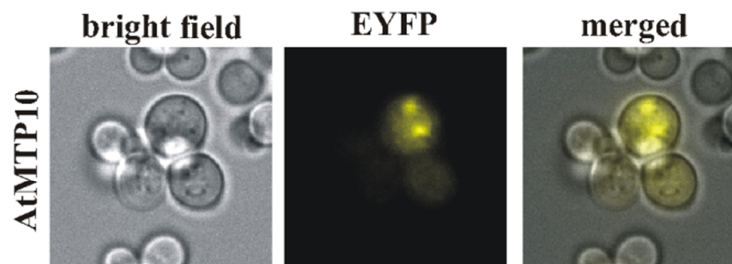


Fig. 8: *pmr1Δ* yeast cells expressing *AtMTP10-EYFP*. Bright field, EYFP, and merged image (from left to right).

3.2.1.3 Mn contents in yeast cells

To examine if the restored tolerance of *pmr1Δ* cells expressing *AtMTP10* is due to an increase in Mn efflux or Mn sequestration, Mn concentrations were determined by ICP-OES analysis (s. 2.8.1). Yeast cells were cultivated until early log phase in liquid SC media supplemented with different Mn concentrations and washed twice to remove the

I Results

extracellular-bound Mn. Irrespective of the Mn concentration in the medium, yeast cells of the Mn-sensitive *pmr1Δ* strain expressing *AtMTP10* showed decreased Mn concentrations compared to those harbouring the empty vector pFL61 (Fig. 9). This indicated that *AtMTP10* mediated an exclusion of Mn.

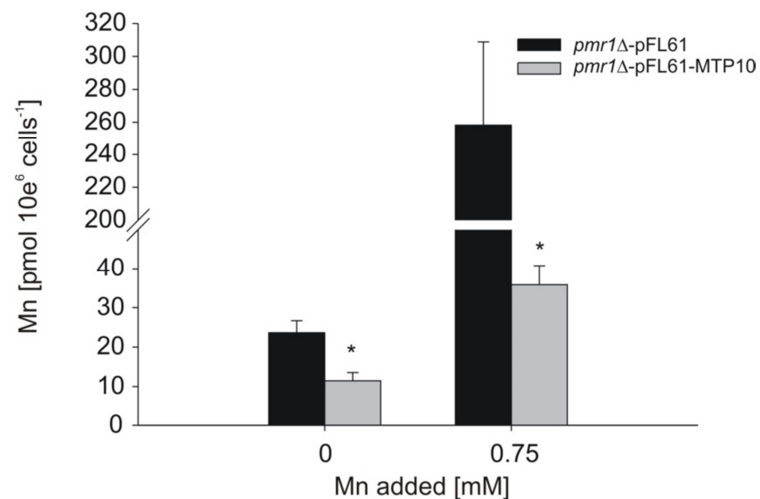


Fig. 9: Mn contents in *pmr1Δ* pFL61 (black bars) and *pmr1Δ* pFL61-MTP10 (grey bars) strains cultivated in liquid SC media with 0.75 mM or no additional Mn. Bars represent the means \pm SE of three biological replicates of three independent cell cultures, and asterisks indicate significant differences according to Student's t-test (* = P<0.05).

3.2.1.4 ATP-dependent ⁵⁴Mn²⁺ uptake by yeast microsomal vesicles

For analysis of the Mn transport ability of *AtMTP10*, microsomal vesicles were prepared from *pmr1Δ* yeast cultures, and ATP-dependent uptake assays with radioactively labelled ⁵⁴Mn²⁺ were performed in collaboration with the Division of Molecular Microbiology of the MLU Halle-Wittenberg (Andreas Kirsten). Vesicles from cells expressing *AtMTP10* showed an elevated rate of ⁵⁴Mn influx compared to vesicles from cells transformed with the empty vector, which supports the assumption that *AtMTP10* is able to transport Mn (Fig. 10). To ensure the intactness of the vesicles and a comparable rate of ATP-dependent proton influx, an Acridin Orange assay was performed on each vesicle preparation. Figure 11 shows an example of vesicles of one preparation. Both strains were capable of proton influx, and the proton gradient collapsed after a treatment with ammonium sulphate.

I Results

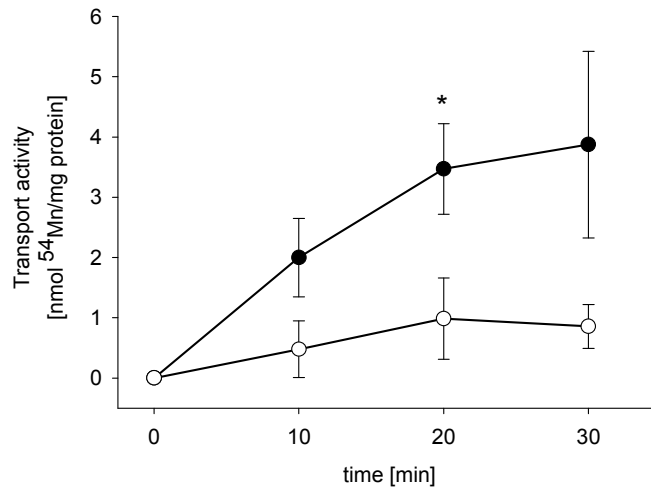


Fig. 10: $^{54}\text{Mn}^{2+}$ transport assay with microsomal membrane vesicles isolated from *pmr1Δ* yeast expressing *AtMTP10* (filled circles) or containing the empty vector pFL61 (open circles). Data represent the means \pm SE of three biological replicates of three independent vesicle preparations, and asterisks indicate significant differences according to Student's t-test (* = $P < 0.05$).

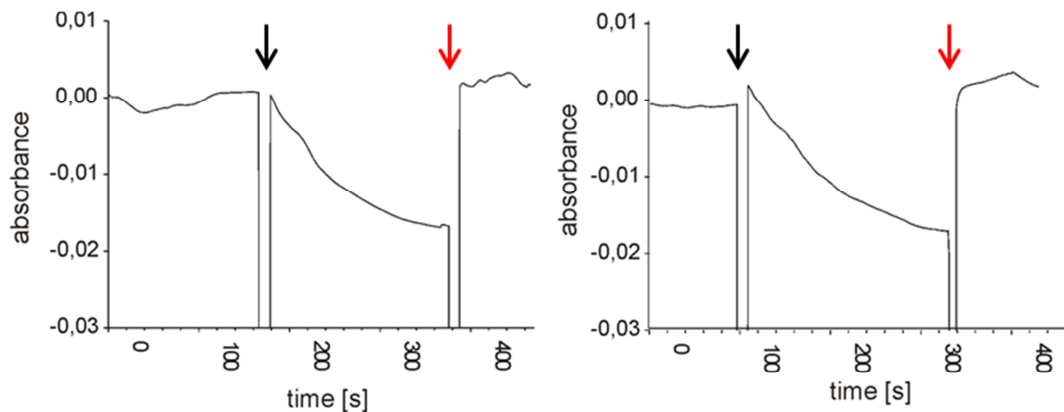


Fig. 11: Acridin Orange test on microsomal membrane vesicles from *pmr1Δ* cells containing the empty vector pFL61 (left) or expressing *AtMTP10* (right). The addition of ATP [1 mM] and $(\text{NH}_4)_2\text{SO}_4$ [2.5 μM] is indicated by a black arrow, and a red arrow, respectively.

3.2.2 Promoter-GUS studies for localization of *AtMTP10* expression *in planta*

For analysis of *AtMTP10* expression *in planta*, its promoter was fused to the *uidA* reporter gene by cloning into pBI101.3. The construct was transformed in Arabidopsis Col-0 plants. To determine the tissues in which the promoter of *AtMTP10* is active, promoter GUS studies were performed. Five independent lines were cultivated on sterile agar plates

I Results

under kanamycin selection. All of the selected lines showed the same staining pattern in cotyledons (Fig. 12), with the promoter activity being specific to the vasculature. Further studies were performed with homozygous plants of line 1.

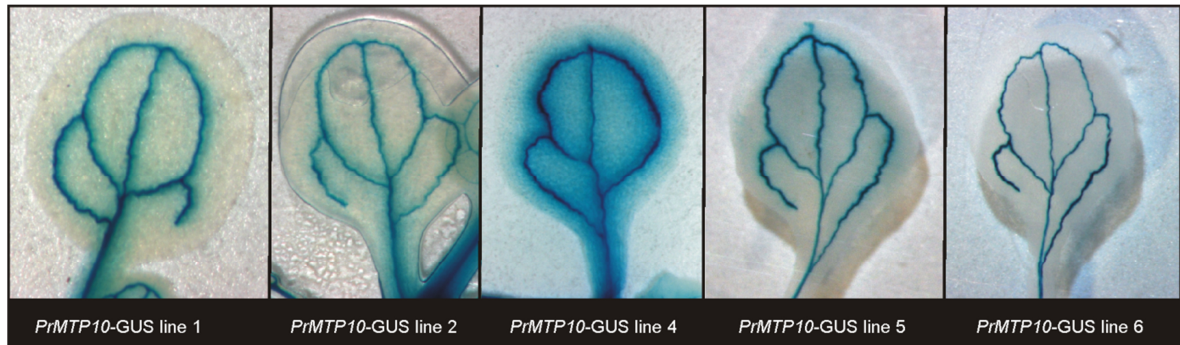


Fig. 12: Cotyledons of five independent *PrMTP10*-GUS lines stained for GUS activity.

The promoter of *AtMTP10* was active in the vasculature of the whole plant (Fig. 13 A). In roots, staining was specific to cells of the pericycle (Fig. 13 C) and absent in the root tip (Fig. 13 B and E). To identify the pericycle, the casparian strip in the endodermis, which is formed distal to the pericycle, was visualized by Berberine-Aniline blue fluorescent staining according to Brundrett *et al.* (1988) (Fig. 13 D). Early lateral roots showed no activity of the promoter of *AtMTP10* (Fig. 13 F). As mentioned before, the cotyledons (Fig. 13 G) and also older leaves (Fig. 13 H) showed a promoter activity of *AtMTP10* in the veins of the leaves. To investigate this staining pattern in detail, cross sections of petioles were made. Microscopic analysis showed GUS activity in cells surrounding the xylem (Fig. 13 I). In addition to roots and leaves, also the flower organs showed GUS activity in the vascular system (Fig. 13 J). In the stamen, the GUS activity was specific to the vasculature of the filament and the connective of the anther (Fig. 13 K). The petal remained unstained (Fig. 13 L) and the pistil showed a GUS activity specific to the abscission zone of the later developing siliques (Fig. 13 M). Furthermore, the ripening siliques showed an activity of the *AtMTP10* promoter in the vasculature and the abscission zone (Fig. 13 N and O), but this activity was not visible in matured siliques anymore (Fig. 13 P).

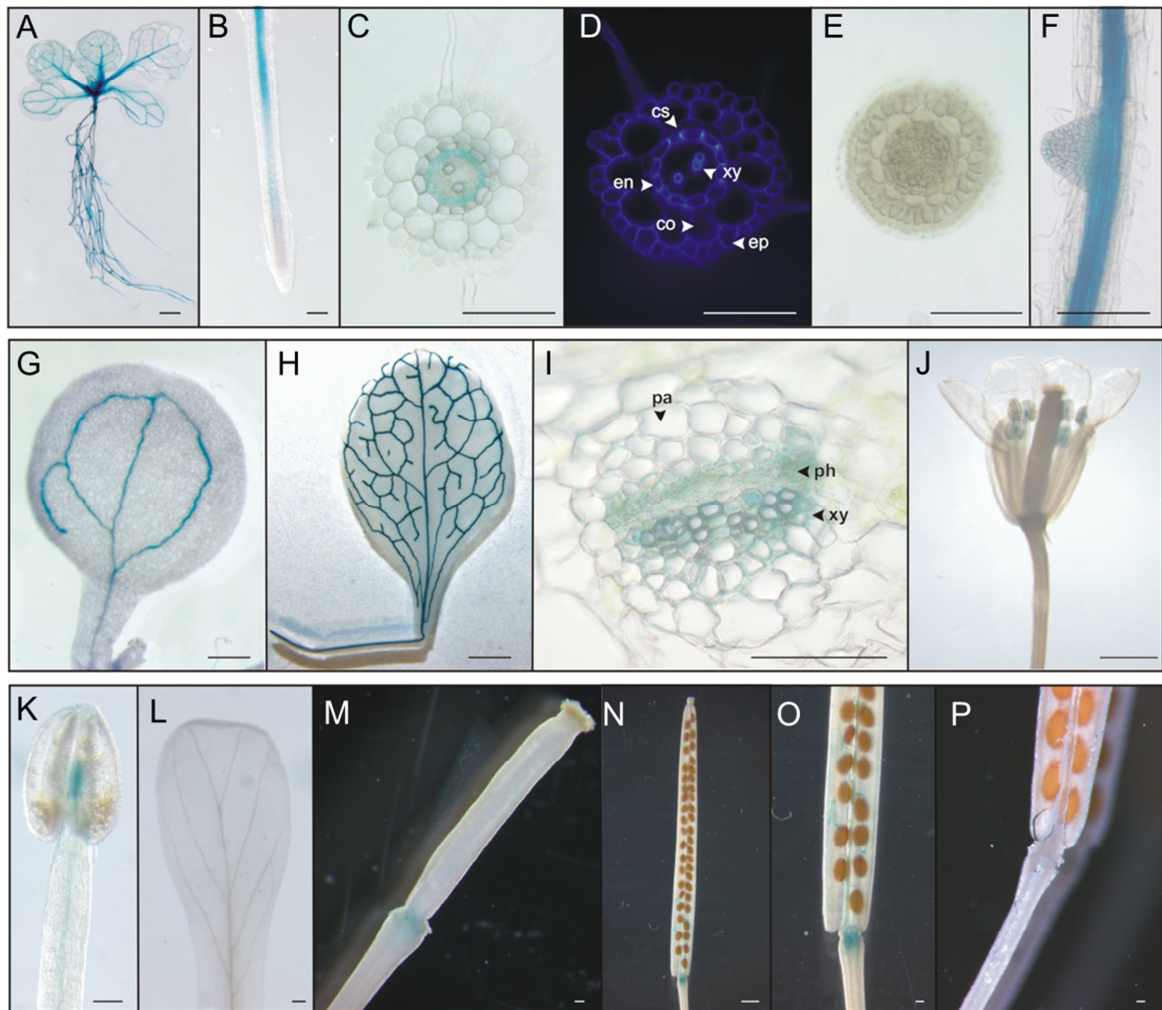


Fig. 13: Promoter activity of *AtMTP10*. (A) GUS activity driven by the *AtMTP10* promoter is present in roots and shoots. (B) In roots, GUS activity increases with root age. (C) Cross section of the root shows that GUS activity is specific to the cells of the pericycle. (D) Berberine-Aniline blue fluorescent staining of a root cross section shows the casparian strip (cs) in the endodermis (en). Xylem (xy), cortex (co), and epidermis (ep) are also indicated. (E) GUS activity is absent in the root tip. (F) Early lateral roots show no activity of the *AtMTP10* promoter. (G, H) *PrMTP10* is also active in the vasculature of cotyledons and in older leaves. (I) Cross sections of the leaves show GUS activity in cells surrounding the xylem vessels (xy). Cells of the phloem (ph) and the parenchyma (pa) are also indicated. (J) Flowers show an *AtMTP10* promoter activity in the vasculature of the stamen and in the abscission zone of the receptacle but not in the petals. Magnification of the stamen (K), the petal (L), and the abscission zone of the receptacle (M). (N-O) Maturing siliques show GUS activity in the abscission zone and also in the vasculature. (P) GUS activity is absent in matured siliques. Bars: 2 mm (H), 1 mm (A, B, G, J, K, N), 100 μ m (C, D, E, F, I, L, M, O, P).

3.2.3 Subcellular localization of AtMTP10 in transiently transformed *Arabidopsis* mesophyll protoplasts

The subcellular localization of a protein determines its functions in the cell. To determine the localization of AtMTP10, protoplasts of the Col-0 wild type were transiently transformed with the fusion construct pART7-*MTP10-EYFP*. Fluorescence of EYFP was detected by confocal laser microscopy. This approach showed that AtMTP10 was distributed throughout the cytoplasm and additionally in small punctate structures (Fig. 14). To test if AtMTP10 may be located in the ER, protoplasts of an ER-GFP marker line (Hawes & Satiat-Jeunemaitre, 2005) were transformed with the *AtMTP10-EYFP* construct. The overlap of GFP and EYFP signals indicated the presence of AtMTP10 in the ER (Fig. 14 A). However, the small EYFP-labelled dots did not overlap with the GFP signal of the ER-marker (Fig. 14 A). To identify these punctate compartments, co-localization studies with markers of the Golgi apparatus (Fig. 14 B) (Hawes & Satiat-Jeunemaitre, 2005), mitochondria (Fig. 14 C) (Nelson *et al.*, 2007), and peroxisomes (Fig. 14 D) (Nelson *et al.*, 2007) were performed. Virtual line scans showed that AtMTP10 was frequently localized adjacent to the Golgi apparatus or co-localized with this compartment. This suggests that AtMTP10 is, next to the ER, localized to a vesicular structure. Further studies showed that AtMTP10 co-localized with AtMTP11 (Fig. 12 E), which has been previously shown to localize to the Golgi apparatus (Peiter *et al.*, 2007).

I Results

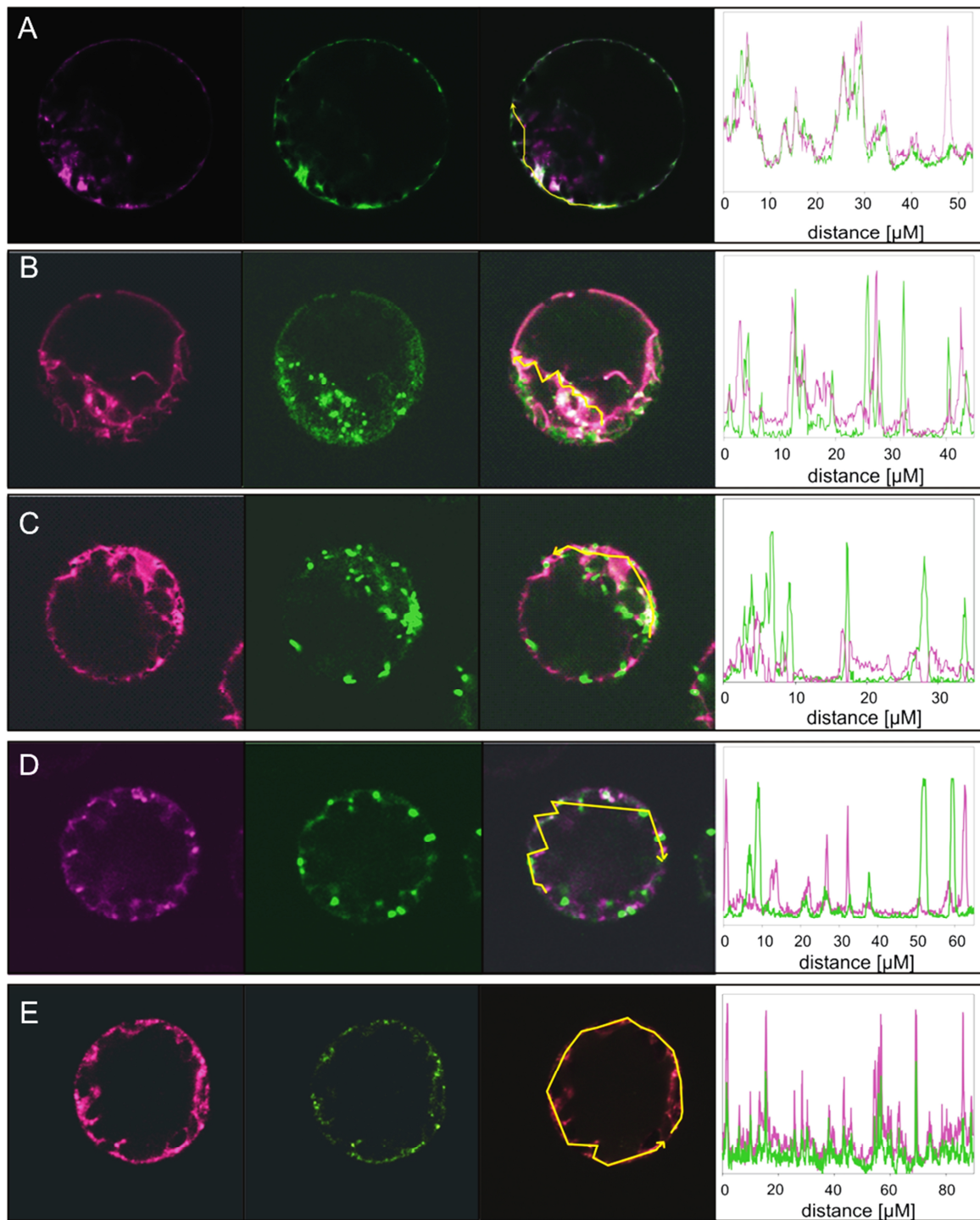


Fig. 14: Arabidopsis mesophyll protoplasts of an ER-GFP (A) or Golgi-GFP (B) marker line transiently expressing *AtMTP10-EYFP*. Arabidopsis Col-0 mesophyll protoplasts co-transformed with *AtMTP10-EYFP* and a GFP/CFP marker for mitochondria (C), a CFP marker for peroxisomes (D), and with *AtMTP11-mGFP* (E). From left to right: EYFP signal of *AtMTP10-EYFP*; GFP/CFP signal of the marker; merged image; virtual line scan diagrams showing the EYFP (pink line) and GFP/CFP (green line) intensity of the arrow in the merged image.

3.2.4 Subcellular localization of AtMTP10 in tobacco cells

For confirmation of the results obtained by protoplast transformation and a more detailed identification of the vesicular compartment in which AtMTP10 is present, further localization studies were performed in tobacco cells. Leaves were infiltrated with *A. tumefaciens* carrying either pBART-MTP10-EYFP (s. 2.1) or a specific organelle marker. For ER localization, the plasmid pFGC19 with the signal peptide of AtWAK2 and the ER retention signal HDEL fused to the fluorescent protein mCherry was used (Nelson *et al.*, 2007). Comparable to the localization that was observed in *Arabidopsis* mesophyll protoplasts (Fig. 14), the EYFP signal co-localized with the ER and additionally to small spots (Fig. 15).

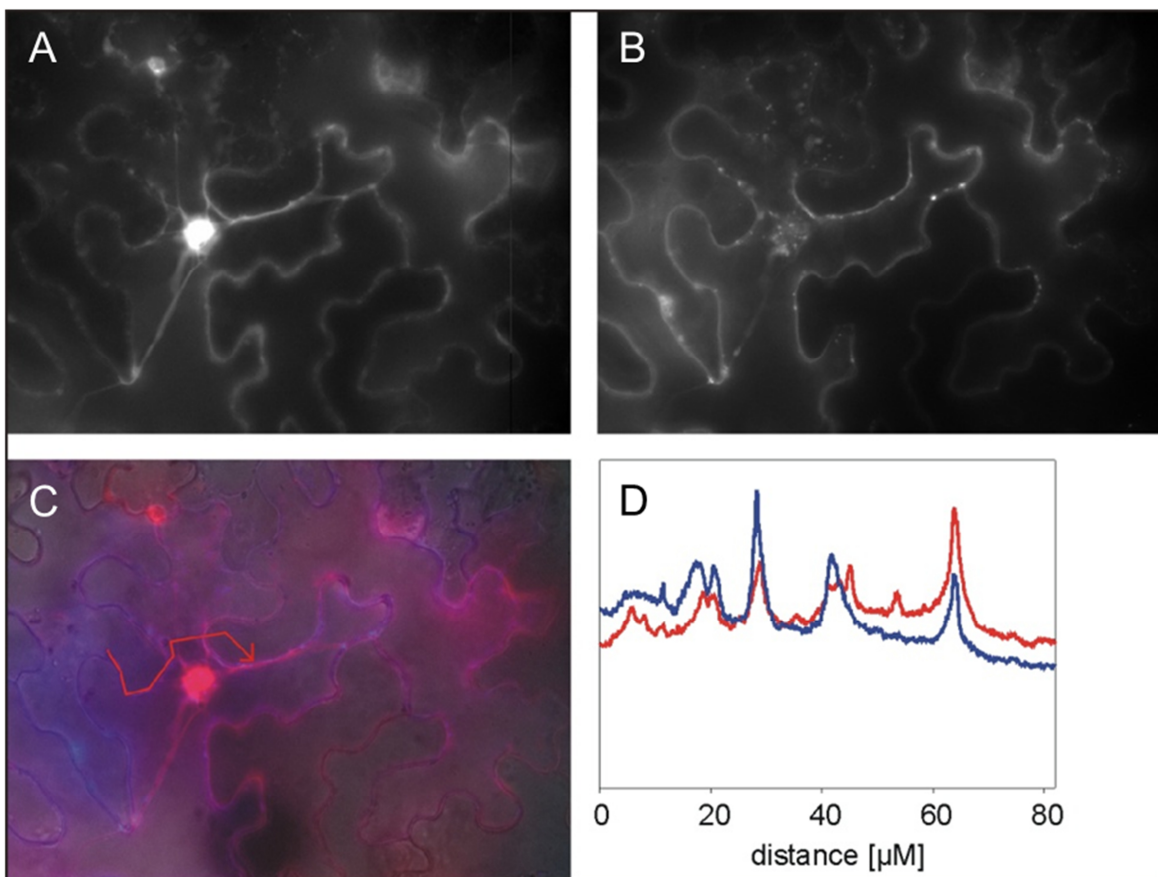


Fig. 15: Co-localization of AtMTP10-EYFP with ER-mCherry. Pictures were taken 48 h post infiltration. (A) mCherry signal, (B) EYFP signal, (C) merged image, (D) virtual line scan diagram showing the mCherry (red line) and EYFP (blue line) intensity of the arrow in the merged image.

I Results

To identify the AtMTP10-labelled spots, tobacco cells co-transformed with pBART-*MTP10-EYFP* and pBART-*SYP61-mCherry* (Groen *et al.*, 2014) were analysed. Both signals overlapped, suggesting a partial localization of AtMTP10 in the *trans*-Golgi network (TGN) (Fig. 16).

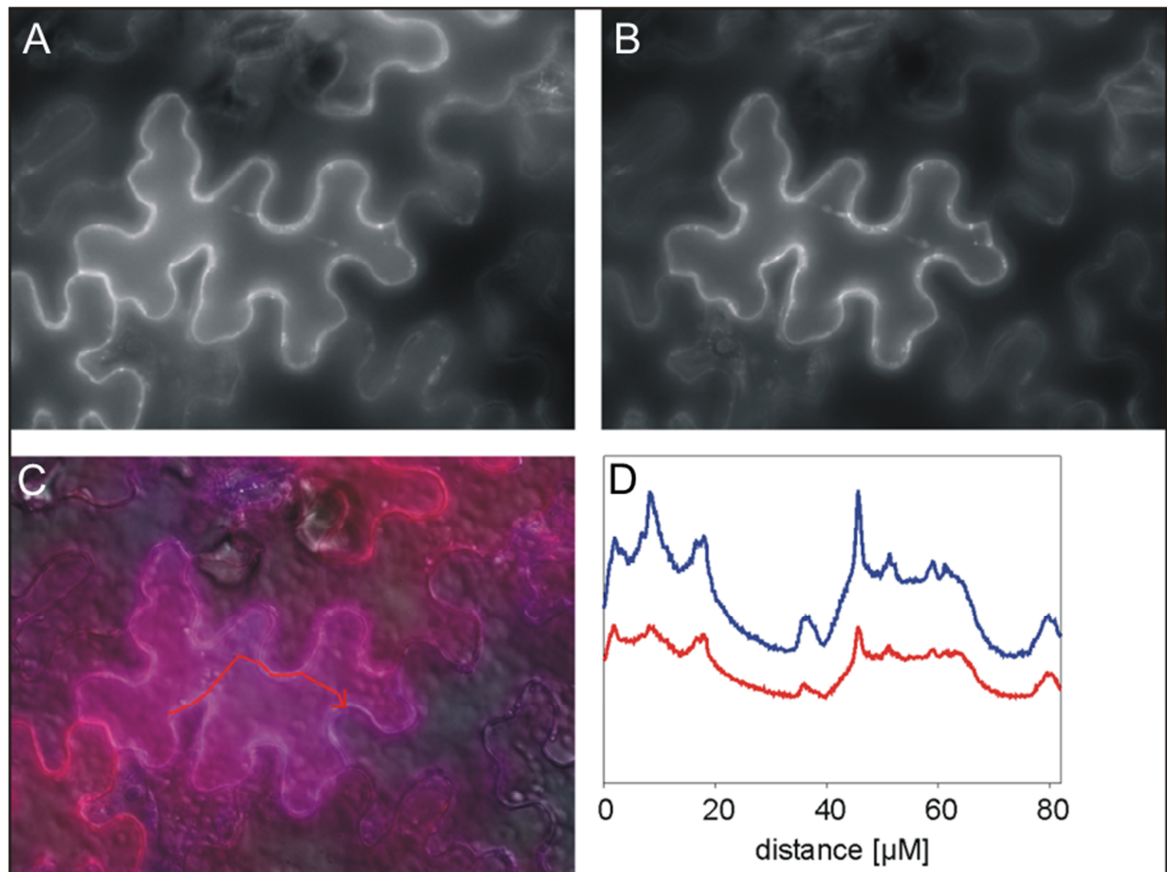


Fig. 16: Co-localization of AtMTP10-EYFP with SYP61-mCherry. Pictures were taken 48 h post infiltration. (A) mCherry signal, (B) EYFP signal, (C) merged image, (D) virtual line scan diagram showing the mCherry (red line) and EYFP (blue line) intensity of the arrow in the merged image.

In some cases, the sorting of transport proteins has been shown to be dynamic and affected by environmental conditions, such as metal load (Barberon *et al.*, 2011). To analyse if the localization of AtMTP10 changes under different conditions, further studies were performed. With the help of the drug Tyrphostin A23 (TYR A23) that prevents the sorting of proteins to clathrin-coated vesicles for internalization (Banbury *et al.*, 2003), possible changes of the localization of AtMTP10 may be uncovered. However, infiltration of intact leaves may cause an inhomogeneous distribution of the treatment agent. To treat cells in a more controlled way, protoplasts of the pBART-*MTP10-EYFP*-transformed

I Results

tissue were isolated and treated with 100 μ M TYR A23 or 100 μ M Mn. After 15 min of incubation, the protoplasts were analysed. These treatments did not lead to a change in the punctate localization of AtMTP10-EYFP (Fig. 17).

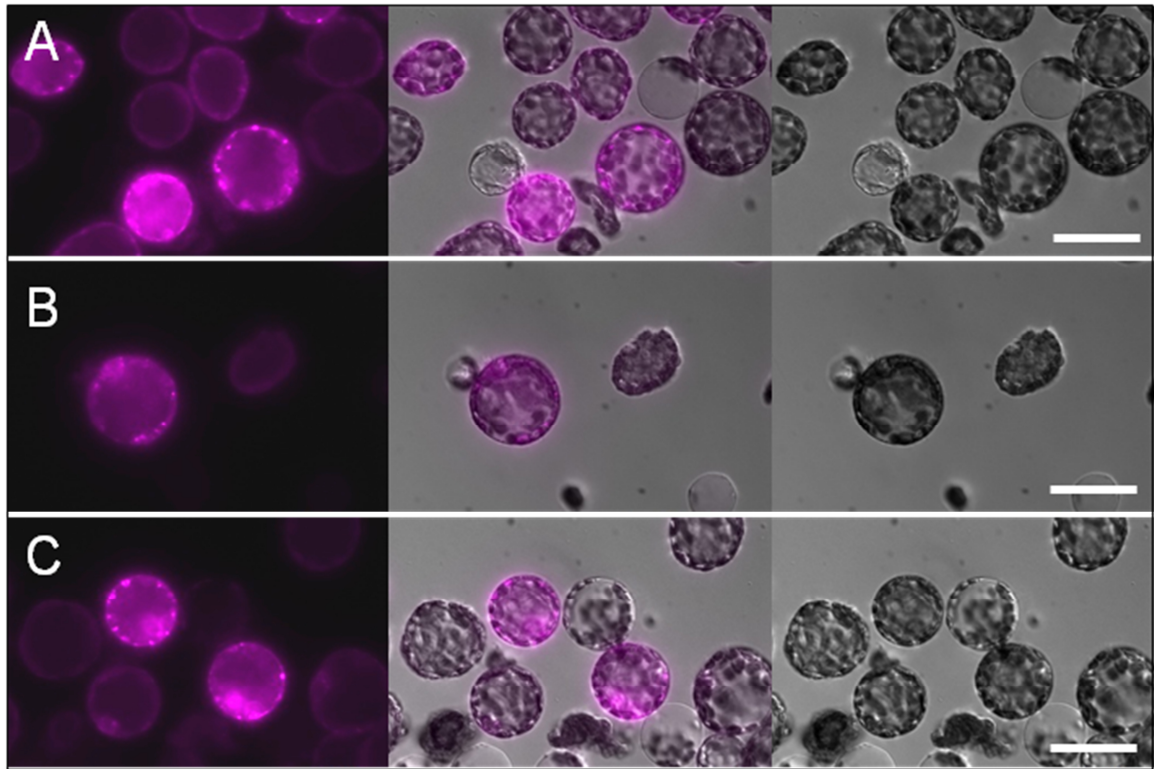


Fig. 17: Localization analysis of *AtMTP10-EYFP*-expressing tobacco protoplasts treated with Tyrphostin A23 or Mn. Microscopic analysis was performed 48 h post infiltration and after 15 min of treatment. Pictures show mock-treated protoplasts (A), protoplasts treated with 100 μ M Tyrphostin A23 (B), and protoplasts treated with 100 μ M Mn (C). From left to right: EYFP signal, merged image, and DIC image.

Collectively, these studies showed that AtMTP10 is localized to the ER and additionally to the Golgi and the TGN. This localization pattern did neither change after treatment with the drug Tyrphostin A23 nor under exposure to a high Mn concentration.

3.3 Phenotypes of *mtp10* mutant plants

3.3.1 Growth of *mtp10-1*, *mtp10-4*, and *mtp10-1::gMTP10* under Mn toxicity

As shown in the yeast complementation assays (s. 3.2.1.1), AtMTP10 was able to complement the Mn-sensitive yeast strain *pmr1Δ*. To identify the role of AtMTP10 *in planta*, the growth of *mtp10-1*, a knockout mutant, was monitored on media with elevated levels of Mn. Seedlings of Col-0 and *mtp10-1* were cultivated on sterile agar plates with different Mn concentrations under long-day conditions, and root length was measured every second day. Interestingly, at elevated Mn concentrations, the roots of *mtp10-1* showed an enhanced growth compared to the wild type, suggesting an increased tolerance to Mn under those conditions (Fig. 18 A and B). The Mn hypertolerance of *mtp10-1* was also reflected in an increased final fresh weight and shoot size of those plants (Fig. 18 C and E). The expression of *AtMTP10* in the wild type, determined by quantitative real time RT-PCR, did not change consistently under elevated Mn concentrations, neither in roots nor in shoots (Fig. 18 D).

I Results

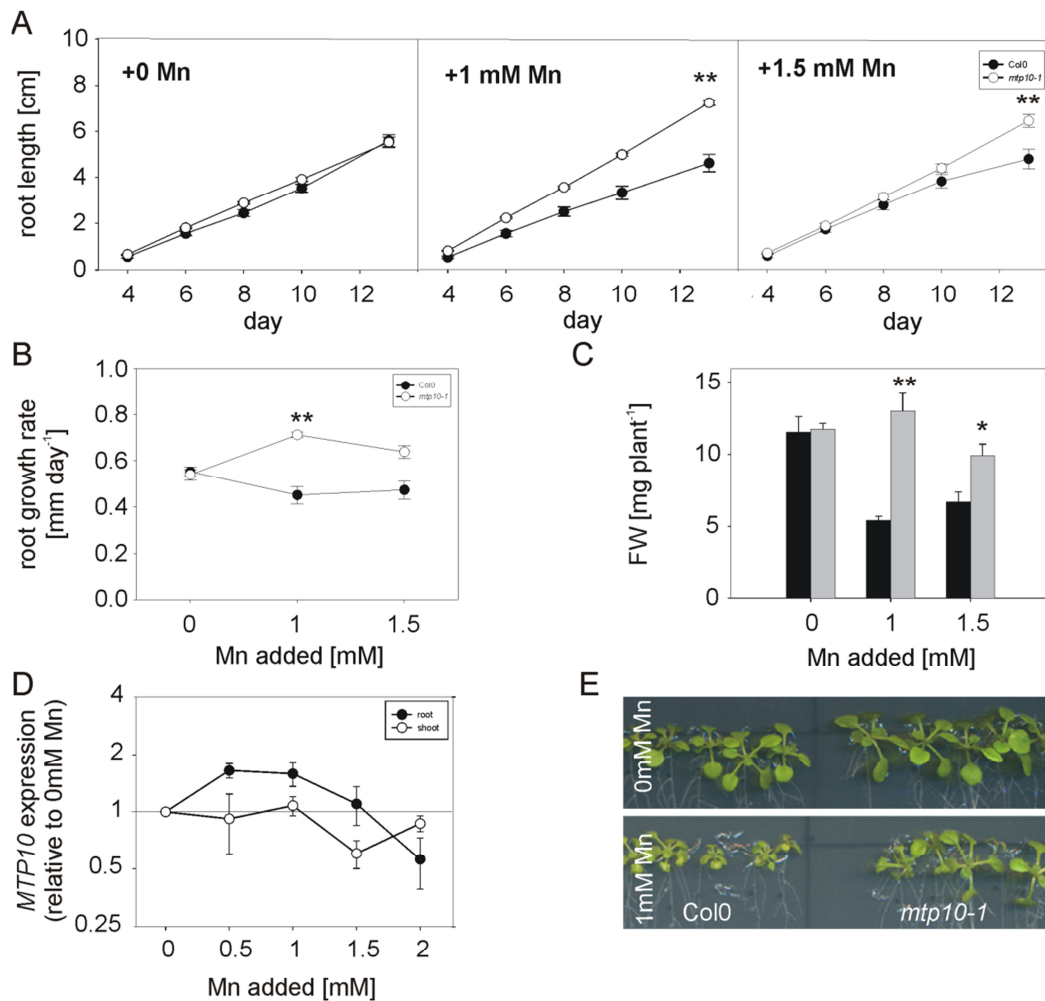


Fig. 18: Root length of Col-0 wild type (●) and *mtp10-1* (○) under different Mn concentrations (A). Root growth rate of those seedlings (B). Each data point represents the mean \pm SE of the linear regression of the root lengths of 10 seedlings determined as shown in (A). Fresh weight of wild type and *mtp10-1* under different Mn concentrations (C). Expression of *AtMTP10* under different Mn concentrations (D). Growth of Col-0 and *mtp10-1* under control conditions or with 1 mM MnSO_4 (E). Asterisks indicate significant differences according to Student's t-test (* = $P < 0.05$; ** = $P < 0.01$). The experiment was repeated three times with comparable results.

For confirmation of the phenotype, this experiment was also performed with a second knockout line, *mtp10-4*. Also *mtp10-4* showed a hypertolerance to Mn toxicity which was reflected in increased root lengths, increased root growth rate and increased fresh weight under Mn toxicity compared to its wild type (Fig. 19 A-C). The addition of 1.5 mM Mn to the half-strength MS media was sufficient to provoke a tolerance phenotype of *mtp10-1* whereas it needed 2.5 mM to provoke the tolerance in *mtp10-4*, which may be explained by the different ecotypes of both mutant lines. The similar phenotype of *mtp10-1*, a T-DNA insertion mutant in a Col-0 background, and *mtp10-4*, a transposon mutant in a No-0

I Results

background, demonstrates that the increased Mn tolerance is not mediated by the sequence of the T-DNA insert or the transposon.

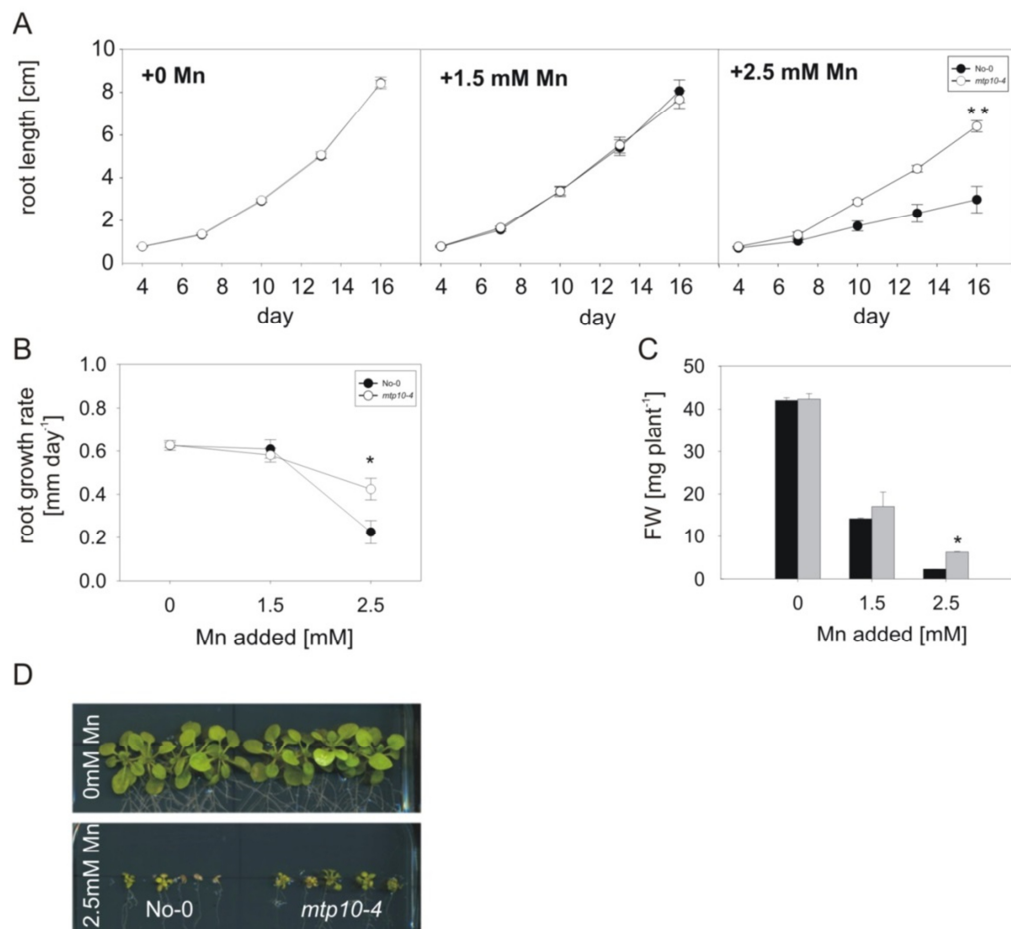


Fig. 19: Root length of No-0 wild type (●) and *mtp10-4* (○) under different Mn concentrations (A). Root growth rate of those seedlings (B). Each data point represents the mean \pm SE of the linear regression of the root lengths of 10 seedlings determined as shown in (A). Fresh weight of wild type and *mtp10-4* under different Mn concentrations (C). Growth of No-0 and *mtp10-4* under control conditions or with 2.5 mM MnSO₄ (D). Asterisks indicate significant differences according to Student's t-test (* = $P < 0.05$; ** = $P < 0.01$). The experiment was repeated twice with comparable results.

The complementation of a mutant line with the genomic DNA of the respective gene is a possibility to verify that a mutant phenotype is not due to mutations in other genes. To this end, the *mtp10-1* mutant was complemented with genomic DNA encompassing the promoter, coding sequence, and terminator of *AtMTP10*. Complementation lines that showed a similar *AtMTP10* expression as the wild type were selected (Fig. 6). The enhanced tolerance of *mtp10-1* (Fig. 18) and *mtp10-4* (Fig. 19) to Mn toxicity was

I Results

abolished in the complementation line *mtp10-1::gMTP10.1* (Fig. 20 A-D). Its root growth rate was comparable to that of the wild type (Fig. 20 A and B), while there was a tendentially but not significantly increased fresh weight of *mtp10-1::gMTP10.1* under elevated Mn concentrations (Fig. 20 C).

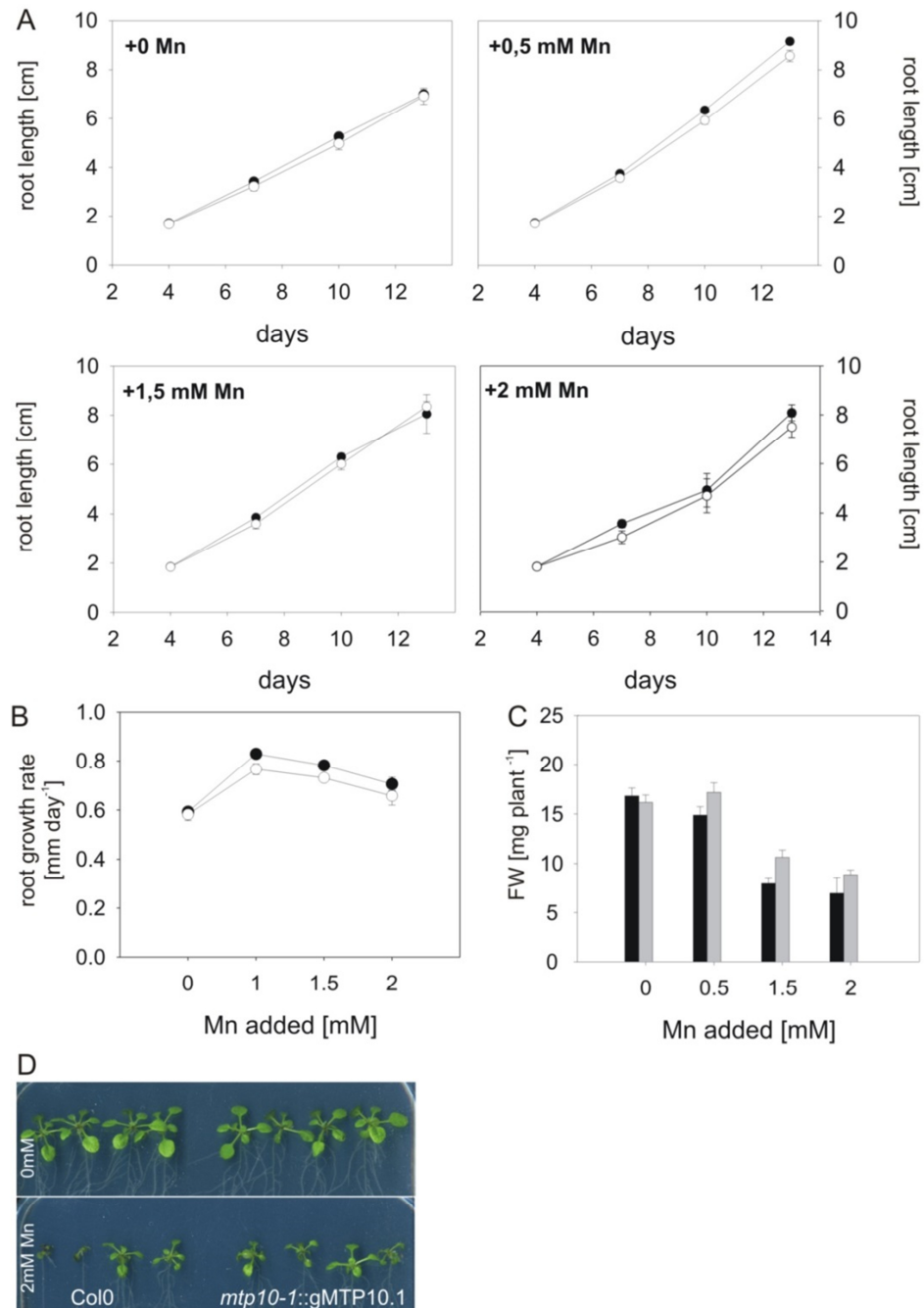


Fig. 20: Root length of wild type (●) and *mtp10-1::gMTP10.1* (○) under different Mn concentrations (A). Root growth rate of those seedlings under different Mn concentrations (B). Each data point represents the mean \pm SE of the linear regression of the root lengths of eight seedlings determined as shown in (A). Fresh weight of wild type and *mtp10-1::gMTP10.1* under different Mn concentrations (C). Growth of Col-0 and *mtp10-1::gMTP10.1* under control conditions or with 2 mM MnSO₄ (D).

3.3.2 Growth of *mtp10-1* under Mn-deficient conditions

Since *mtp10-1* was hypertolerant to Mn toxicity, its growth under Mn deficiency was also examined. Because agar contains traces of Mn, the use of an agar-based system, as used in the previous experiments, is not the best choice for monitoring growth under Mn deficiency. Therefore a system with liquid culture media was employed to grow plants under Mn-limiting conditions. Two-week-old seedlings grown in nutrient solution were transferred from Mn-sufficient (3.5 μ M MnSO₄) to the same or to Mn-deficient (0 MnSO₄) conditions and cultivated for another three weeks. *mtp10-1* showed comparable growth to the wild type under control conditions (3.5 μ M Mn), but a decreased growth under Mn deficiency (Fig. 21 A). This was reflected in the dry weight of those plants (Fig. 21 B). Under Mn-deficient conditions, *mtp10-1* plants showed a shoot dry weight of only 62% of that of the wild type; dry weight of the *mtp10-1* roots reached only 55% of the wild type. Under control conditions the shoot and root dry weights were not significantly different between Col-0 and *mtp10-1*. Metals in shoots and roots of those plants were determined by ICP-OES. Under Mn starvation, there was the tendency that the Mn concentrations in shoots, as also the Fe concentrations, but not the Zn concentrations, were slightly decreased in *mtp10-1* (Fig. 21 C). Interestingly, under control conditions, the shoot Mn concentration was significantly lower in *mtp10-1* as compared to the wild type, while Fe and Zn concentrations were not significantly altered (Fig. 21 D). No differences between both genotypes were observed for root metal concentrations.

I Results

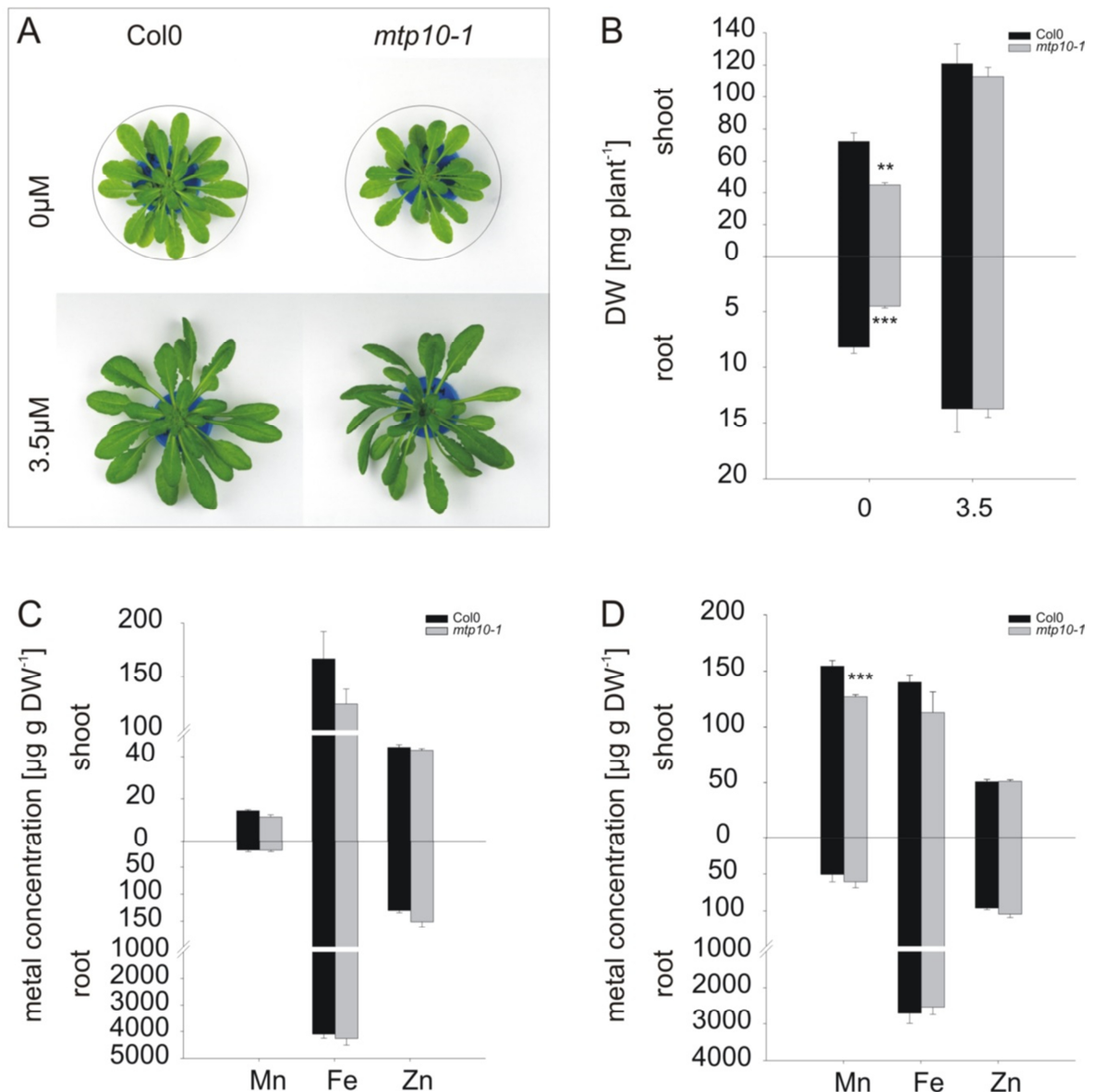


Fig. 21: Growth of plants in liquid culture media with 0 and 3.5 μM Mn (A). Dry weight of shoots and roots (B). Mn, Fe, and Zn concentrations in roots and shoots of plants grown in media with 0 μM Mn (C) or 3.5 μM Mn (D). Values represent the means (\pm SE) of four plants per genotype and treatment. Asterisks indicate significant differences according to Student's t-test (** = $P < 0.01$; *** = $P < 0.001$). This experiment was repeated twice with comparable results.

3.3.3 Metal contents in xylem exudates

Due to the promoter activity of *AtMTP10* in the vasculature (Fig. 13) and the decreased Mn concentrations in the shoots of *mtp10-1* (Fig. 21 D), the xylem exudate was analysed for Mn content by ICP-MS. To this end, xylem exudates of eight-weeks-old, hydroponically, under short-day conditions grown plants, were collected for two hours at 1 pm. Collecting the xylem exudates comprised cutting off the shoots and connecting the

I Results

hypocotyl to a silicon tube. Xylem exudation was related to root dry matter, which was comparable between both genotypes (Fig. 22 A). The comparable growth of both genotypes was also reflected in their shoot dry weights (Fig. 22 A). The exudation rate per hour was also in the same range (Fig. 22 B). Surprisingly, the Mn exudation rates did not differ between wild type and *mtp10-1* (Fig. 22 C). The same was true for Fe and Zn contents in the exudates (Fig. 22 C).

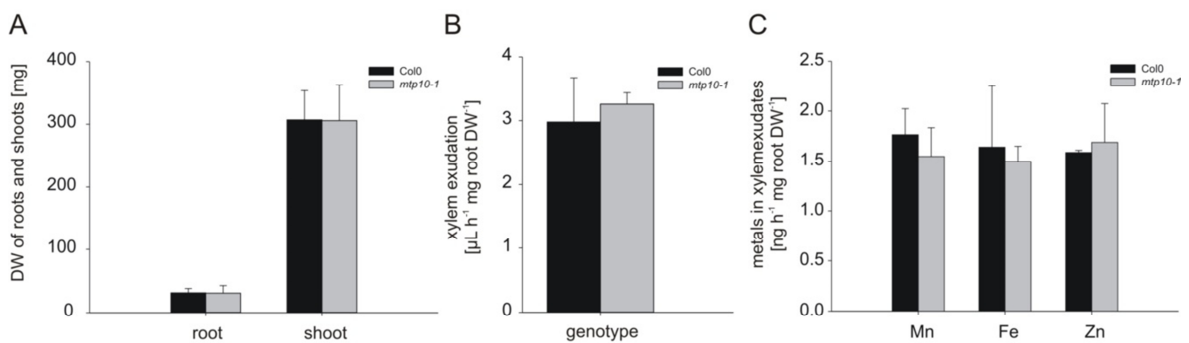


Fig. 22: Dry weight of eight-week-old wild type (black bars) and *mtp10-1* (grey bars) plants grown in liquid media containing 3.5 µM Mn (A). Xylem exudation rates (B) and the exudation rates of Mn, Fe, and Zn of those plants (C). Values represent the means (±SE) of three plants per genotype. This experiment was repeated in a modified way, and data of these experiments are shown in the following parts.

3.3.4 Diurnal rhythm of xylem exudation

A possible explanation for the decreased Mn concentrations in shoots of *mtp10-1* compared to the wild type with a simultaneously comparable Mn translocation rate in the xylem may lie in temporal differences of Mn translocation. The results shown in Figure 22 were obtained in the mid of the day (1 pm). To examine a possible temporal effect, exudation rates and metal composition of the exudates of short-day-grown plants were determined at different times of the day. Three time points were chosen, and the results are displayed in Figure 23. The dry weights of the roots analysed for xylem exudation were comparable at the time points 1 pm and 8 pm, but were lower in *mtp10-1* at the time point 6 am (Fig. 23 A). The exudation rate per root dry weight was slightly, but not significant decreased in *mtp10-1* plants at this time point and comparable at the other time points (Fig. 23 B). Metal analysis showed that translocation of Mn in *mtp10-1* plants

I Results

was significantly lower than that of the wild type when sampled at 6 am in the morning, but not at 1 pm or 8 pm (Fig. 23 C). The translocation of Fe (Fig. 23 D) and Zn (Fig. 23 E) in the exudates showed no significant difference between the genotypes.

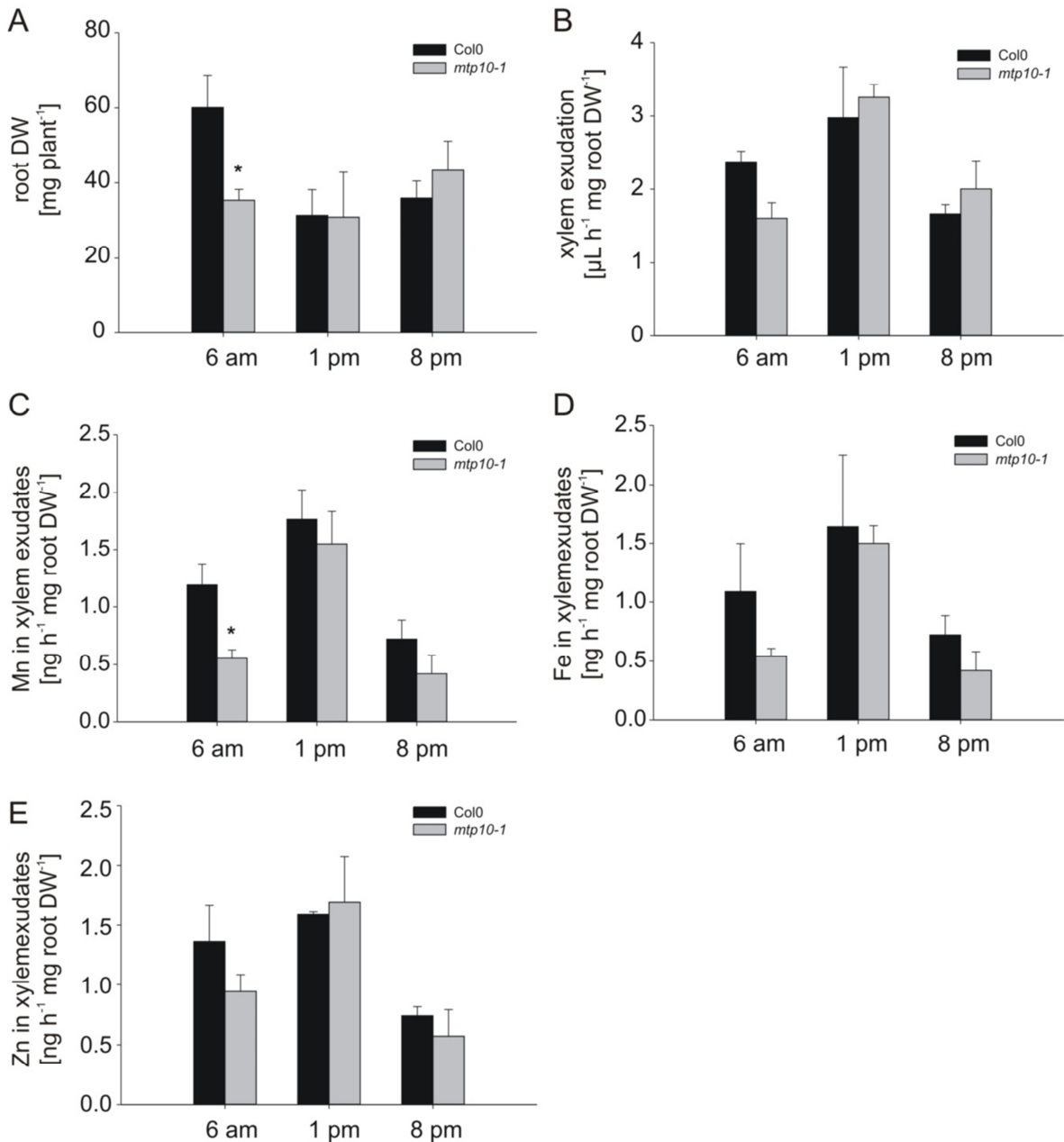


Fig. 23: Xylem exudation of wild type (black bars) and *mtp10-1* (grey bars) plants grown in liquid media containing 3.5 μM Mn in the course of the day. Dry weights of the roots of plants analysed for the metal composition of exudates (A). Xylem exudation rate (B), Mn exudation rate (C), Fe exudation rate (D), and Zn exudation rate (E). Values represent the means (±SE) of three plants per genotype and time point. Asterisks indicate significant differences according to Student's t-test (* = P<0.05).

I Results

Because of the significant differences in plant growth at the 6 am time point that was caused by the small sample number due to limited cabinet space, the experiment was repeated. The results of this experiment, in which two additional time points were analysed, are displayed in Figure 24. A trend of increased exudation rates at the beginning of the day that decreased again at noon was observed. Both genotypes had comparable root dry weights and exudate volumes at all time-points that were sampled (Fig. 24 A and B). Interestingly, Mn exudation rates differed very strongly between the genotypes in the dark, but they were comparable during the light period (Fig. 24 C), which confirms the results of the previous experiment shown in figure 23 C. At 6 am, Col-0 plants translocated $1.28 \text{ ng Mn h}^{-1} (\text{mg root dry weight})^{-1}$ compared to $0.54 \text{ ng h}^{-1} (\text{mg root dry weight})^{-1}$ in *mtp10-1*, while at 1 pm the Mn translocation of $1.45 \text{ ng h}^{-1} (\text{mg root dry weight})^{-1}$ in Col-0 and $1.43 \text{ ng h}^{-1} (\text{mg root dry weight})^{-1}$ in *mtp10-1* was comparable (Fig. 24 C). Fe and Zn translocation showed no consistent variation in the course of the day and was comparable between Col-0 and *mtp10-1* (Fig. 24 D and E), with one exception: At 8 pm the Fe translocation rate in the xylem exudate of *mtp10-1* was significantly decreased, similar to the Mn translocation rate (Fig. 24 D).

I Results

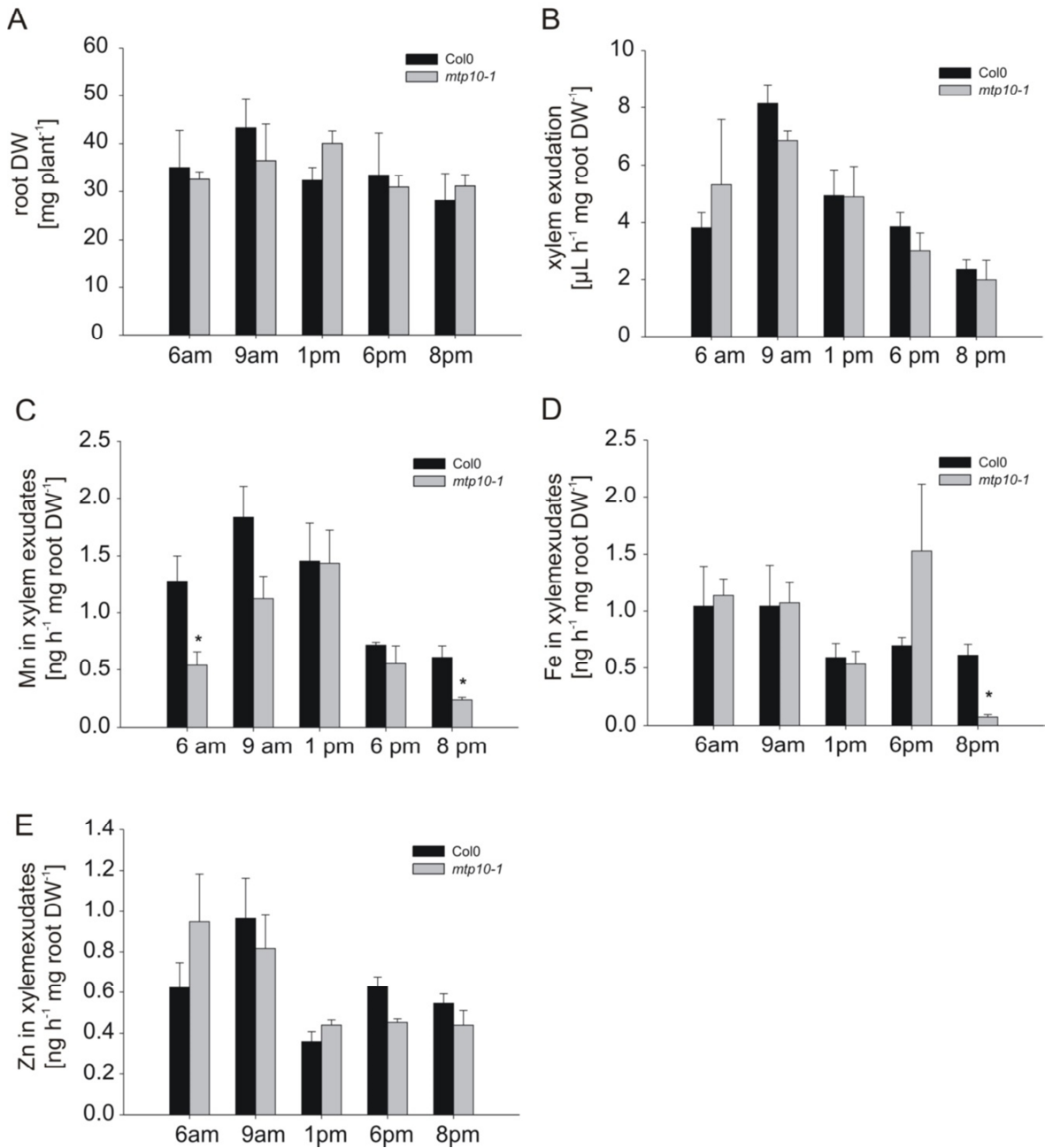


Fig. 24: Xylem exudation of wild type (black bars) and *mtp10-1* (grey bars) plants grown in liquid media containing 3.5 μM Mn in the course of the day. Dry weights of the roots of plants analysed for the metal composition of exudates (A). Xylem exudation rate (B), Mn exudation rate (C), Fe exudation rate (D), and Zn exudation rate (E). Values represent the means ($\pm\text{SE}$) of three plants per genotype and time point. Asterisks indicate significant differences according to Student's t-test (* = $P < 0.05$).

I Results

The metal composition of the shoots of the plants sampled in Figure 24 was analysed. Shoot dry weights did not differ between both genotypes (Fig. 25 A). The shoot Mn concentrations of *mtp10-1* were significantly decreased compared to the wild type (Fig. 25 B), which is in agreement with previous experiments (Fig. 21). Fe and Zn concentrations showed no differences between Col-0 and *mtp10-1* (Fig. 25 B).

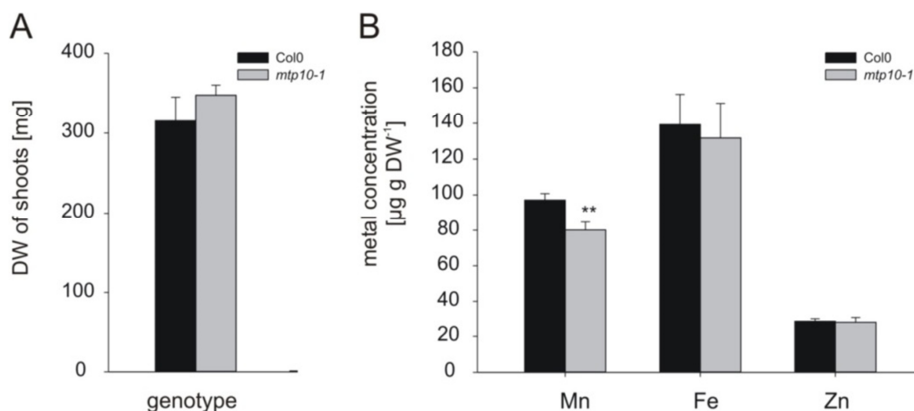


Fig. 25: Dry weight of Col-0 (black bars) and *mtp10-1* (grey bars) shoots of plants sampled for xylem exudate analysis (Fig. 24) (A). Metal concentration of these shoots (B). Values represent the means (\pm SE) of 15 plants per genotype. Asterisks indicates the significant differences according to Student's t-test (** = $P < 0.01$).

3.3.5 Diurnal rhythm of *AtMTP10* expression

A possible explanation for the differences in the xylem exudation of Mn throughout the day may lie in the expression of *AtMTP10*. To test this hypothesis, RNA was isolated from roots at different time points, and *AtMTP10* expression was analysed by quantitative real time RT-PCR. Relative to 6 am, when the plants were not yet exposed to light, the expression of *AtMTP10* showed a more than four-fold decrease until 2 pm. The expression increased again until 10 pm to a similar level as in the early morning and showed a further rise at 11 pm (Fig. 26).

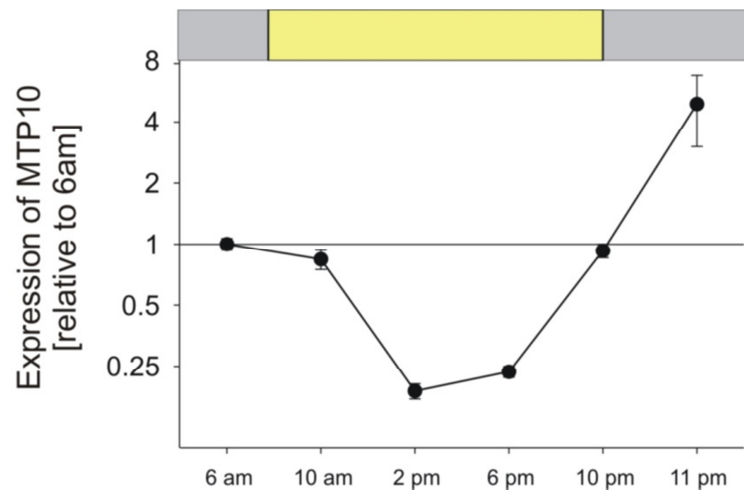


Fig. 26: Expression of *AtMTP10* in the course of the day (grey bars: darkness; yellow bar: light). RNA was isolated from roots of Col-0 plants harvested at indicated time points. Quantitative real time RT-PCR values are normalized to *Actin2*, relative to 6 am, and represent the means of three biological replicates.

3.3.6 The involvement of *AtMTP10* in submergence tolerance of *Arabidopsis*

3.3.6.1 Regulation of *AtMTP10* under oxygen deprivation

To elucidate physiological roles of *AtMTP10*, an analysis of published transcriptomics data, obtained by the Affymetrics ATH1 gene chip and collected in the publically available database GENEVESTIGATOR (Zimmermann *et al.*, 2004), was performed. This database indicated the transcriptional regulation of *AtMTP10* in a number of studies related to anoxia or hypoxia, carried out under different environmental conditions. In one study underlying those data, seven-day-old seedlings grown on sterile plates were exposed to oxygen deprivation triggered by argon flushing for two hours (Mustroph *et al.*, 2009). The experiment started at the end of the light period and was performed under low light ($6.5 \mu\text{M m}^{-2} \text{s}^{-1}$). Figure 27 A shows that the expression of *AtMTP10* was increased in roots, and by trend also in shoots, that were exposed to oxygen deprivation. In another study, five-week-old *Arabidopsis* Col-0 rosettes of plants grown on soil under short-day conditions were exposed to hypoxia (1% oxygen) or control conditions (21% oxygen) for 90 minutes (Licausi *et al.*, 2011). Also under this experimental setup the expression of *AtMTP10* was slightly but significantly increased in shoots of plants exposed to hypoxia (Fig. 27 B). In a third study, *Arabidopsis* seedlings were exposed to hypoxia stress for either two or nine hours (Branco-Price *et al.*, 2008). *AtMTP10* expression was increased compared to control conditions, and this increase was higher when seedlings were

I Results

exposed for only two hours to the stress. Seedlings exposed to nine hours of hypoxia followed by one hour of re-oxygenation did not show an increased *AtMTP10* expression (Fig. 27 C). In another study, that addressed the regulation of genes during hypoxia, Col-0 seedlings were grown for ten days on agar plates containing ½ MS media with 1% sucrose under long day conditions (Chang *et al.*, 2012). Hypoxia stress was triggered by argon flushing of a lucite chamber for two hours, similar to the study of Mustroph *et al.* (2009). Abundance of *AtMTP10* RNA was increased after the hypoxia treatment compared to the control conditions, whereby the abundance was higher in roots compared to shoots (Fig. 27 D). Collectively, all published studies indicate that the expression of *AtMTP10* is robustly upregulated by oxygen deprivation, which points to a role of the gene under those conditions.

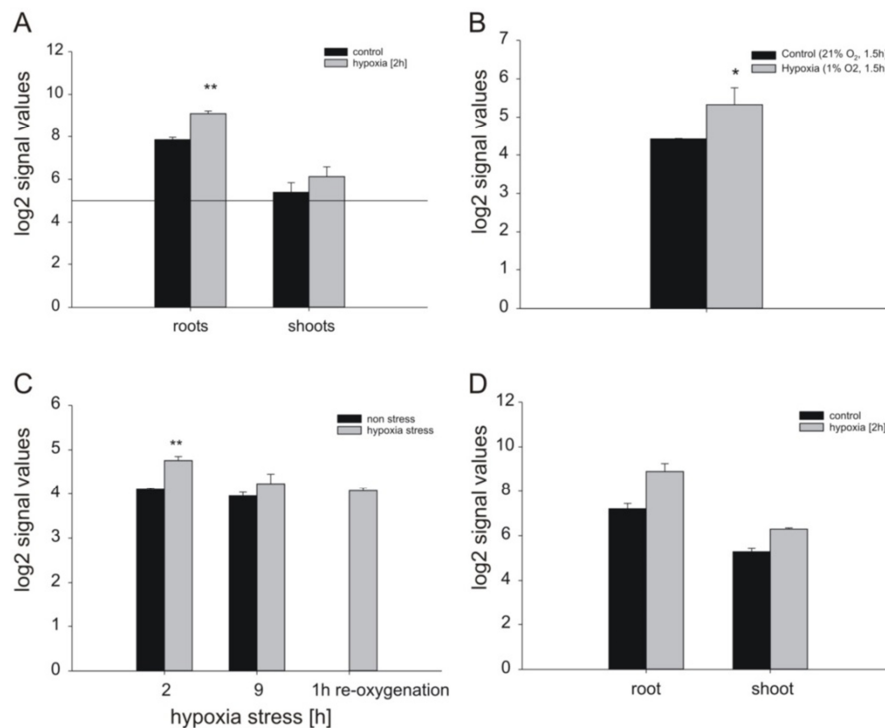


Fig. 27: Published transcriptome and translato-me studies analysing the regulation of *AtMTP10* during or after transient hypoxia stress. *AtMTP10* mRNA abundance in roots and shoots after 2 h of hypoxia stress (A). Horizontal line represent the threshold of abundance (*log₂* signal = 5). *AtMTP10* mRNA abundance in Col-0 shoots after hypoxia stress for 1.5 hours (B). *AtMTP10* mRNA abundance in seedlings exposed to two or nine hours of hypoxia stress and after one hour of re-oxygenation following nine hours of hypoxia stress (C). *AtMTP10* mRNA abundance in roots and shoots of seedlings after two hours of hypoxia stress (D). Samples of the control conditions (black bars) and samples of the hypoxia stress (grey bars). Data were obtained from GEO repository (<https://www.ncbi.nlm.nih.gov/geo/>) of the individual studies (A) Mustroph *et al.* (2009), (B) Licausi *et al.* (2011), (C) Branco-Price *et al.* (2008), (D) Chang *et al.* (2012). Bars represent the means \pm SE of three replicates [except for D (two replicates)]. Asterisks indicate significant differences according to Student's t-test (* = P<0.05; ** = P<0.01).

3.3.6.2 Submergence of *mtp* mutant lines

The analysis of published transcriptomic data pointed to an involvement of *AtMTP10* during hypoxia stress. Furthermore, as shown above, the knockout of *AtMTP10* led to an increased tolerance to Mn toxicity (Figs. 18 and 19), which is opposite to *AtMTP8* and *AtMTP11*, the knockout of which has a negative effect on the tolerance of Arabidopsis to Mn toxicity (Peiter *et al.*, 2007, Eroglu *et al.*, 2016). Under field conditions, in water-saturated paddy soils high amounts of Mn are plant-available. This phenomenon also occurs when fields are flooded, e.g. in spring during the snowmelt. Additionally, submerged plants are exposed to hypoxia stress. To assess an involvement in submergence tolerance, Arabidopsis T-DNA insertional knockout lines of all four members of the Mn subgroup of the CDF family were examined. The plants were pre-cultured on soil and flooded for 21 days. Pictures taken after a recovering period of another 14 days show that, interestingly, only the mutation in *AtMTP10* led to an altered tolerance to submergence (Fig. 28 A). This line performed worse than the wild type, which was against the expectation because before it was less sensitive to high Mn levels (Fig. 18). The link of this phenotype to *AtMTP10* was confirmed with the help of a complementation line expressing the genomic DNA of *AtMTP10* (*mtp10-1::gMTP10.2*), as well as by a second mutant (*mtp10-4*) in No-0 background (Fig. 28 B). During re-oxygenation, the *mtp10* mutants showed an accelerated decay, although they appeared indistinguishable from the wild type directly after submergence (Fig. 28 C). The role of *AtMTP10* during re-oxygenation may be related to the regulation of the gene. To test this, its transcript level was determined during submergence and in the first six hours of the reintroduction of oxygen. During submergence, plants showed a weak increase in transcript-level of *AtMTP10* compared to control conditions (Fig. 28 D), which confirms the results of the transcriptomics studies described above (3.3.6.1). Interestingly, during re-oxygenation *AtMTP10* was up-regulated very strongly, by up to 16 times, with a peak in transcript level at one hour after the resupply of oxygen (Fig. 28 E).

I Results

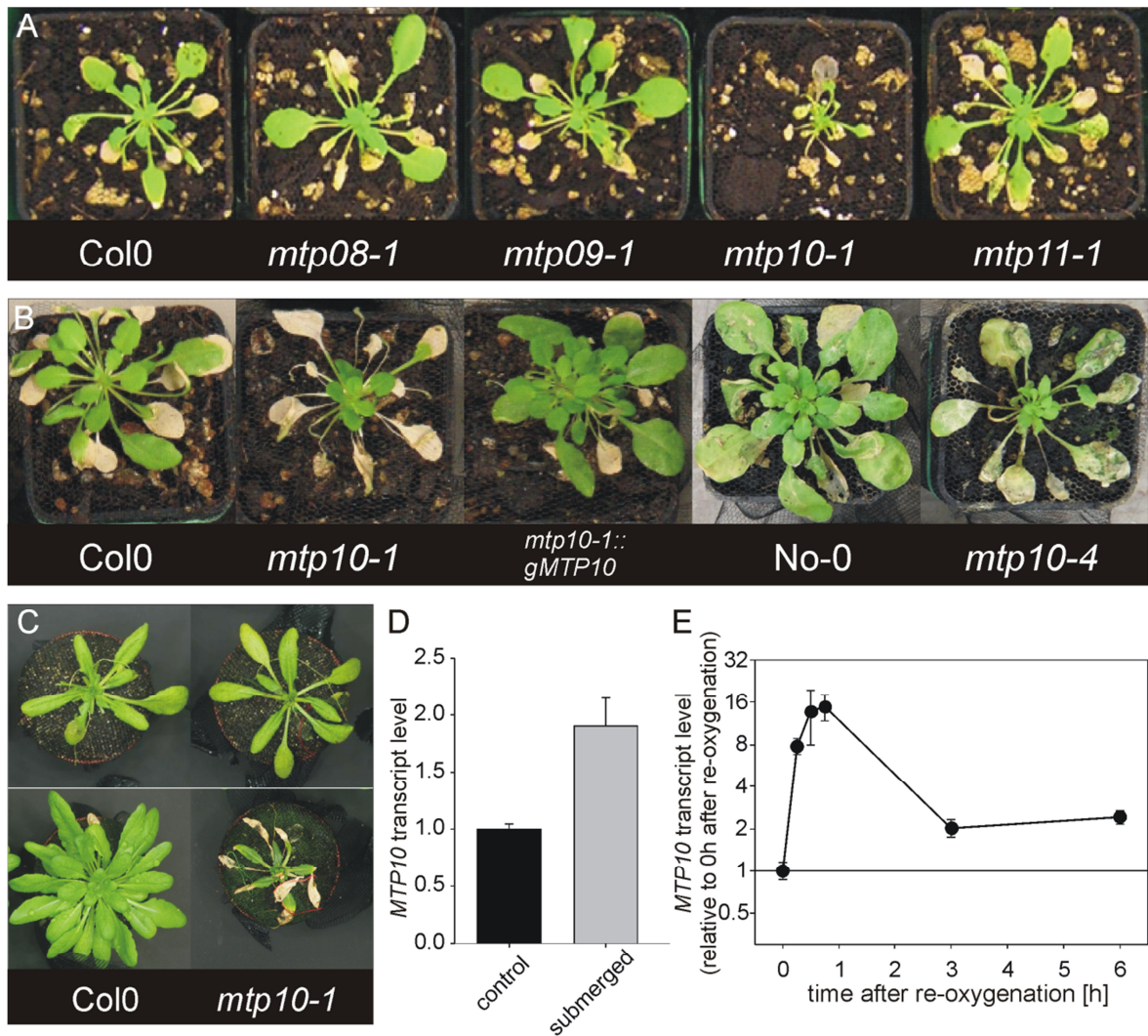


Fig. 28: T-DNA insertion lines of *AtMTP* genes after 21 d of submergence and 14 d of recovering (A). Replication of the experiment shown in (A) including a complementation line (*mtp10-1::gMTP10.2*) and another mutant of *AtMTP10* (*mtp10-4*) in another background (No-0) (B). Phenotype of Col-0 and *mtp10-1* at the beginning of the re-oxygenation period (upper row) and at the end (lower row) (C). Expression of *AtMTP10* in leaves after 11 d of submergence (D) and during re-oxygenation (E). Quantitative real time RT-PCR values are relative to control conditions (D) or to submergence (E) and represent the means of three technical replicates. Expression is normalized to *Actin2*.

During early re-oxygenation the transcript level of *AtMTP10* increased strongly. To study if the localization of *AtMTP10* expression *in planta* remained unchanged, promoter-GUS studies were performed. At all time-points the promoter was only active in the vasculature of the shoots (Fig. 29), similar to unstressed plants (Fig. 13). An increased promoter activity, which would have been reflected in an increase of the blue staining, was not visible, which may be due to the highly transient nature of *AtMTP10* upregulation and the largely qualitative nature of the blue staining. After 24 hours of re-oxygenation the GUS staining intensity was less strong, indicating a decreased promoter activity of

I Results

AtMTP10 (Fig. 29). A staining of roots was not possible because of the soil system that was used to introduce submergence.

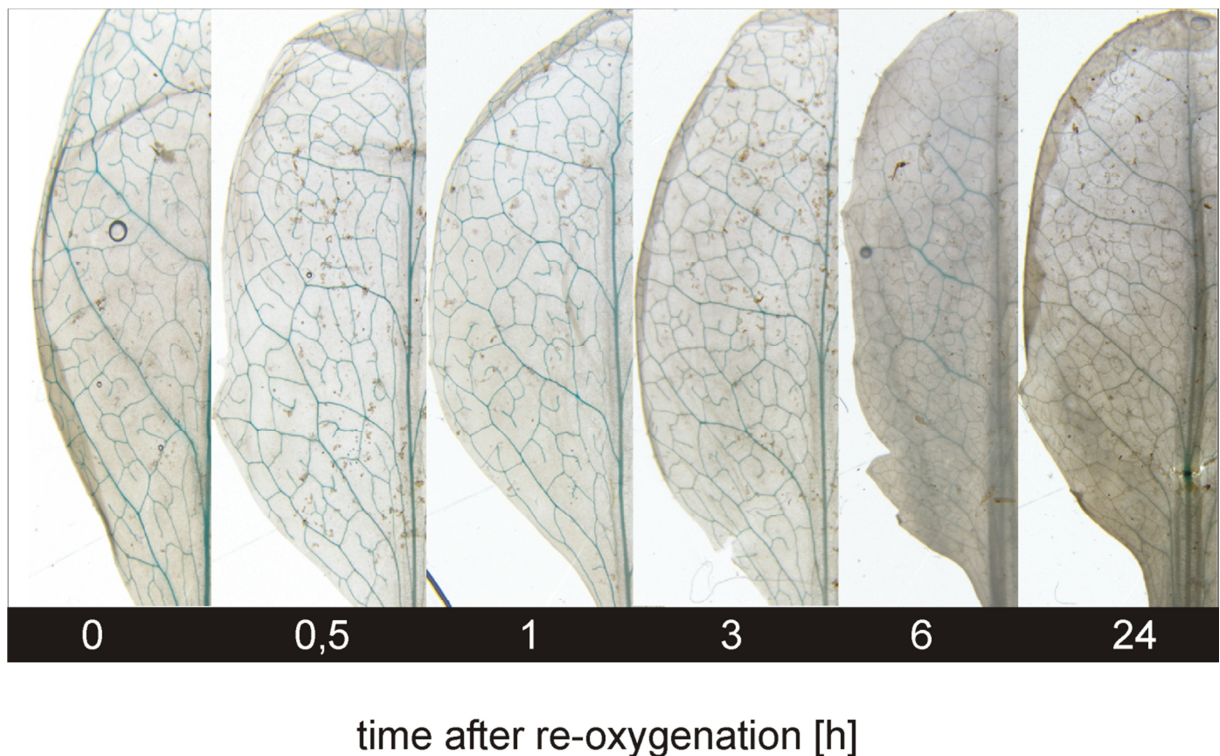


Fig. 29: *AtMTP10* promoter activity in leaves after re-oxygenation. *PrMTP10-GUS* plants were cultivated under submergence for 21 d, and GUS staining was performed after re-oxygenation at the indicated time points.

3.3.7 Growth of seedlings on ½ MS agar plates under anoxic conditions triggered by N₂ aeration

The soil-based submergence experiments were initially conducted to assess effects of increased availability of Mn. However, the mutant with an increased Mn tolerance, *mtp10-1*, was submergence-sensitive, while Mn-sensitive mutants, *mtp8-1* and *mtp11-1*, did not show a submergence phenotype. Furthermore, the *mtp10* phenotype became only apparent after re-oxygenation. This indicated that the submergence phenotype of *mtp10* mutants may not be linked with Mn availability, but rather with oxygen availability. To test this, an agar-based culture system was used to induce oxygen deficiency. Plants were pre-cultured under long-day conditions for seven days on ½ MS medium and aerated with N₂ for 24 h before plants were allowed to recover for another ten days. N₂ aeration led to a decreased growth of *mtp10-1*, which was reflected in the dry weight of

I Results

roots and shoots, while the wild type was not significantly affected by the treatment (Fig. 30 A and B). To examine if the oxygen deficiency imposed under this experimental setup leads to an up-regulation of *AtMTP10*, which was found in the soil-based submergence experiment (Fig. 28), a quantitative real time RT-PCR analysis was performed, employing *Actin2* as housekeeping gene. During re-oxygenation plants were harvested for RNA extraction at different time points. One set of plants was kept under control conditions, i.e. exposed to atmospheric air at all times. The expression of *AtMTP10* under re-oxygenation was normalized to that under control conditions. Compared to aerated plants, the expression of *AtMTP10* was increased by the stress (Fig. 30 C), similar to what was found in the soil-based submergence experiment (Fig. 28 D). *AtMTP10* was slightly up-regulated already during the anoxia conditions, but expression in roots increased strongly upon re-oxygenation, with a maximum at 15 min after re-introduction of oxygen (Fig. 30 C). Unlike in soil-grown submerged plants (Fig. 28 E), the transiently increased expression was not visible in shoots.

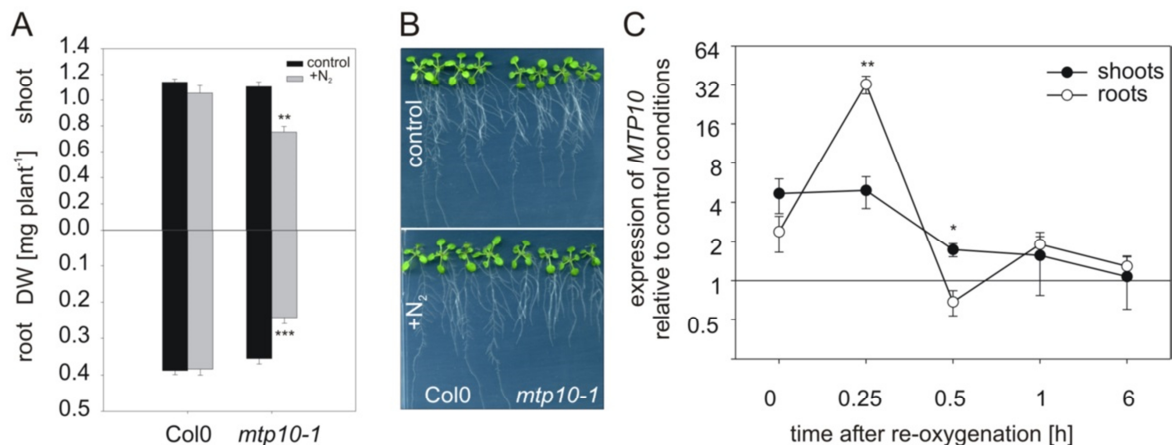


Fig. 30: Dry weight of Col-0 and *mtp10-1* seedlings grown on ½ MS plates at the end of the recovering period of 10 d under control conditions (black bars) or after anoxia conditions triggered by N₂ aeration for 24 h (grey bars) (A). Values represent the means (±SE) of three plates per treatment with four seedlings per genotype. Asterisks indicate significant differences according to Student's t-test (** = P<0.01; *** = P<0.001). Growth of those seedlings under control conditions (upper picture) and after N₂ aeration (lower picture) at the end of the recovering period (B). Expression of *AtMTP10* in *Arabidopsis* seedlings during re-oxygenation after 24 h of oxygen deprivation triggered by N₂ aeration relative to control conditions. Values represent the means ± SE of seedlings from three plates determined in three technical replicates and are normalized to *Actin2*. Asterisks indicate significant differences according to Student's t-test (* = P<0.05; ** = P<0.01) (C). This experiment was repeated twice with comparable results.

3.3.8 Growth of plants in liquid culture media under anoxic conditions of the root zone triggered by N₂ aeration

The uptake of Mn from the soil as also the xylem loading takes place in the roots. As shown above, growth of *mtp10* plants was decreased after exposure to oxygen deficiency caused by either submergence (hypoxia) (Fig. 28) or N₂ aeration (anoxia) (Fig. 30). Additionally, it was shown that shoot Mn concentrations were decreased in *mtp10-1* (Fig. 21), and that the promoter of *AtMTP10* was active in cells of the pericycle (Fig. 13). Furthermore, Mn translocation rates in the xylem were decreased in *mtp10-1* under dark conditions (Figs. 23 and 24). Collectively, these results provoked the hypothesis that the diminished growth of *mtp10* mutants after the recovery from oxygen deprivation is based on an altered xylem loading with Mn. Because of the requirement of larger plants to collect xylem exudates, the experimental setup had to be changed to test this hypothesis. To first address the question whether oxygen deficiency in the root zone alone is sufficient to provoke the *mtp10* phenotype, the roots of six-week-old hydroponically-grown plants were exposed to oxygen-deficient conditions by aeration of the culture media with N₂. The plants were exposed to oxygen deficiency for 24 h prior to a period of regeneration for another ten days. Also this experimental setup led to a decreased tolerance of *mtp10-1* to oxygen deficiency, which was reflected in the dry weight of the shoots as also of the roots (Fig. 31 A and B). The differences in Mn concentration in shoots of *mtp10-1* and Col-0 were similar after oxygen deprivation and control conditions (Fig. 31 C). Fe and Zn concentrations of *mtp10-1* were comparable to those of the wild type. This also holds true for the metal composition of the roots; there were no significant differences in Mn, Fe, and Zn concentrations of the roots (Fig. 31 C). Relative to control conditions, the expression of *AtMTP10* in roots was slightly increased during the anoxic stress (Fig. 31 D). Similar to the previous experiment (Fig. 30 C), relative *AtMTP10* expression increased further after the initiation of the re-oxygenation period. However, this increase was delayed by one hour (Fig. 31 D).

I Results

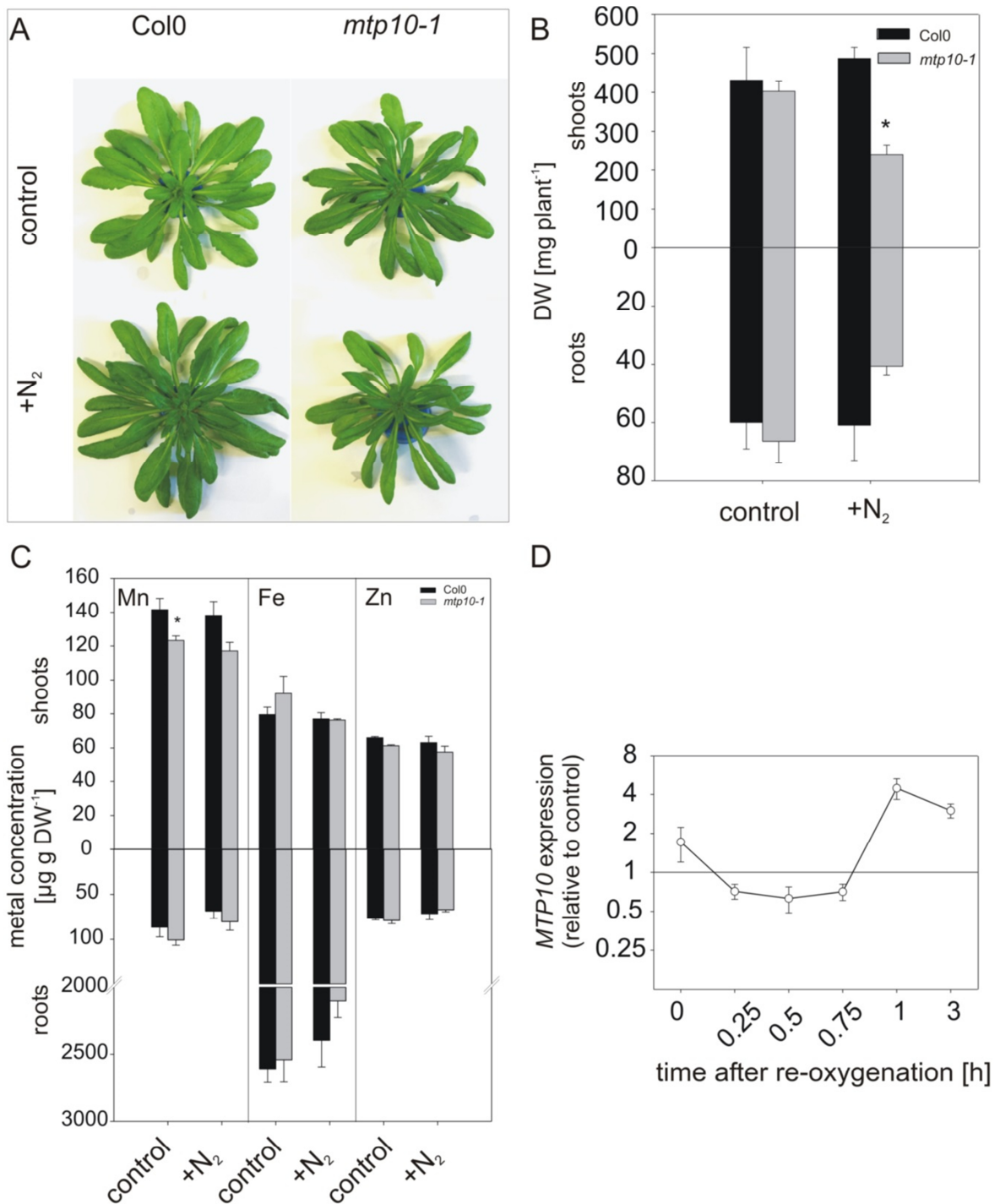


Fig. 31: Phenotype of six-week-old plants grown hydroponically under control conditions (upper part) and after N₂ aeration for 24 h with a following regeneration period of 10 d (lower part) (A). Dry weight of those plants (B) and metal concentrations of the shoots and roots (C). Values represent the means (±SE) of four plants per treatment and genotype. Asterisk indicates significant difference according to Student's t-test (* = P<0.05). Expression of *AtMTP10* in six-week-old plants grown on liquid culture media during re-oxygenation after 24 h of oxygen deprivation triggered by N₂ aeration of the media. Values represent the means ± SE of four plants, each determined in three technical replicates and are normalized to *Actin2* (D). This experiment was repeated twice with comparable results.

3.3.9 Xylem exudation of plants after anoxia conditions in the root zone

After the finding that an exposure to oxygen deficiency only in the root zone is sufficient to affect the growth of *mtp10-1*, the metal composition of xylem exudates was analysed (s. 2.13). To identify a possible role of AtMTP10 in xylem loading of Mn during the re-oxygenation period, exudates were collected for 2 h at the beginning of this period, which followed a N₂ aeration of the liquid culture media for 24 h. This experiment, which was performed twice with similar results, is shown in Figures 32 and 33. The shoot and the root dry weight of Col-0 and *mtp10-1* plants was comparable in both experiments (Fig. 32 A and B, Fig. 33 A and B). After 24 h of anoxia conditions in the root zone the exudate volume was increased tendentially (Fig. 32 C) or significantly (Fig. 33 C) in both genotypes compared to control conditions. Interestingly, also the Mn translocation rate from roots to the shoots, normalized to root mass, increased in Col-0 plants during re-oxygenation significantly (Fig. 32 D) or tendentially (Fig. 33 D). However, this increased Mn translocation was not apparent in *mtp10-1* plants. The xylem exudation rate of Fe was increased in *mtp10-1* under control conditions in the first experiment (Fig. 32 E), but this was not reproducible in the repetition (Fig. 33 E). Zn xylem exudation rates were comparable between the genotypes as also between the treatments (Fig. 32 F, Fig. 33 F). The shoots of the plants sampled for xylem exudates were also analysed for their metal composition. Mn concentrations in shoots of *mtp10-1* plants were significantly decreased (Fig. 32 G, Fig. 33 G), while there were no differences in concentrations of Fe (Fig. 32 H, Fig. 33 H) or zinc (Fig. 32 I, Fig. 33 I) in the shoots.

The different Mn translocation rates in wild type and *mtp10-1* led to the assumption that AtMTP10 plays a role particularly in roots during re-oxygenation because shoots were removed directly at the beginning of re-oxygenation period.

I Results

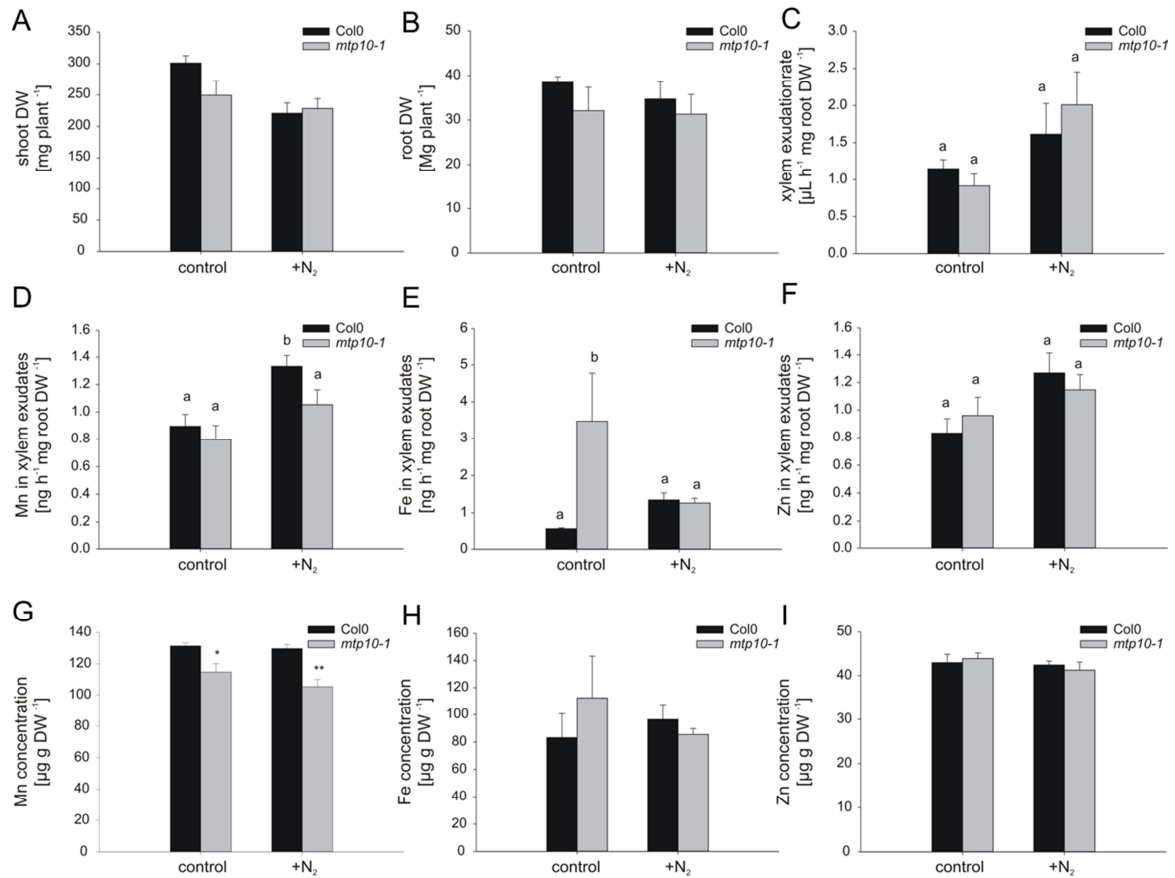


Fig. 32: Dry weight of Col-0 (black bars) and *mtp10-1* (grey bars) shoots (A) and roots (B) grown on liquid culture media and exposed to oxygen deficiency for 24 h. Exudation rates (C) and Mn (D), Fe (E), and Zn (F) translocation in xylem exudates. Mn (G), Fe (H), and Zn (I) concentration in shoots harvested directly at the beginning of the re-oxygenation period. Values represent the means (\pm SE) of three plants per treatment and genotype. Asterisks indicate significant differences according to Student's t-test (* = P < 0.05; ** = P < 0.01). Letters represent significant differences according to a one-factorial analysis of variance (One way ANOVA) followed by a Tukey-test.

I Results

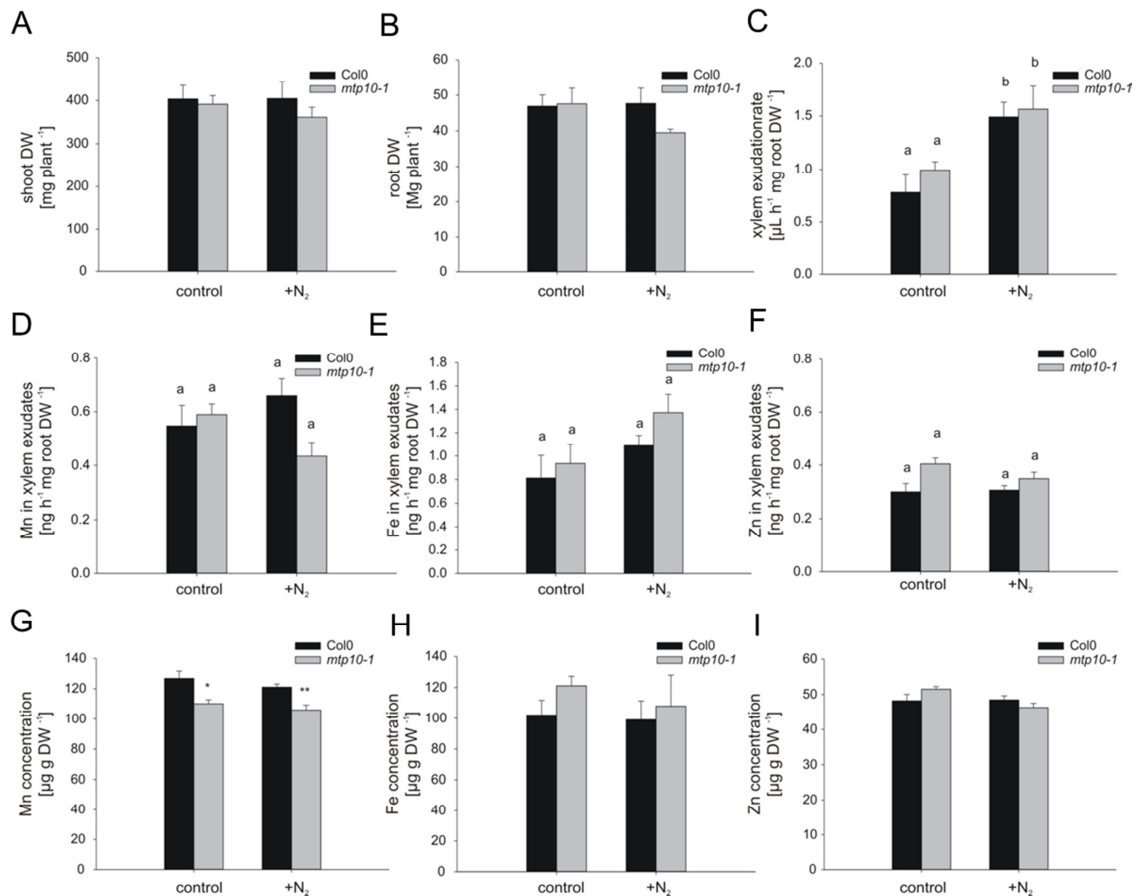


Fig. 33: Dry weight of Col-0 (black bars) and *mtp10-1* (grey bars) shoots (A) and roots (B) grown on liquid culture media and exposed to oxygen deficiency for 24 h. Exudation rates (C) and Mn (D), Fe (E), and Zn (F) translocation in xylem exudates. Mn (G), Fe (H), and Zn (I) concentration in shoots harvested directly at the beginning of the re-oxygenation period. Values represent the means (\pm SE) of three plants per treatment and genotype. Asterisks indicate significant differences according to Student's t-test (* = $P < 0.05$; ** = $P < 0.01$). Letters represent significant differences according to an one-factorial analysis of variance (One way ANOVA) followed by a Tukey-test.

3.3.10 Xylem exudates of *mtp10-1::gMTP10.2* after anoxia conditions in the root zone

To further confirm the oxygen deprivation-associated exudation phenotype of *mtp10*, the complementation line *mtp10-1::gMTP10.2* was also analysed for the metal composition in xylem exudates during re-oxygenation. The dry weights of shoots and roots were comparable to those of the wild type (Fig. 34 A and B) and also an increase in the exudation rate of the wild type and *mtp10-1::gMTP10.2* was found (Fig. 34 C). There were no significant differences in metal translocation in the exudates between the wild type and the complementation line, neither in Mn nor in Fe or Zn (Fig. 34 D-F). The shoot

I Results

concentrations of Mn, Fe, and Zn were also comparable between the genotypes and conditions (Fig. 34 G-I).

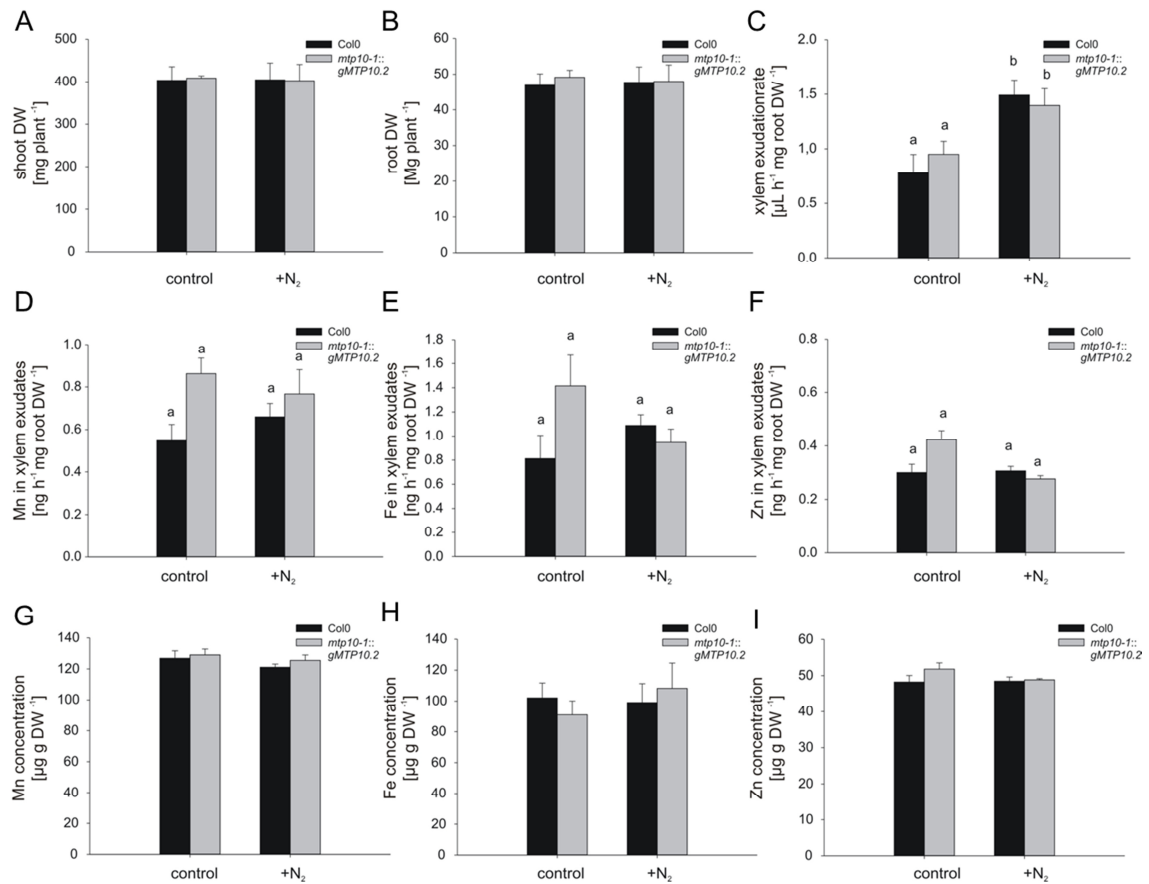


Fig. 34: Dry weight of Col-0 (black bars) and *mtp10-1::gMTP10.2* (grey bars) shoots (A) and roots (B) grown on liquid culture media and exposed to oxygen deficiency for 24 h. Exudation rates (C) and Mn (D), Fe (E), and Zn (F) translocation in xylem exudates. Mn (G), Fe (H), and Zn (I) concentration in shoots harvested directly at the beginning of the re-oxygenation period. Values represent the means (\pm SE) of three plants per treatment and genotype. Letters represent significant differences according to a one-factorial analysis of variance (One way ANOVA) followed by a Tukey-test.

3.4 The possible involvement of alanine in the AtMTP10-dependent submergence tolerance

A principal question that arises from the obtained results is the role of Mn in the recovery from oxygen deprivation. As described in the introduction, Mn is important for the activation of numerous enzymes and as a co-factor of enzymes, a number of which has been shown to play a role in the switch from oxygen-deficient to oxygen-sufficient conditions. In particular, the conversion of alanine and 2-oxoglutarate to pyruvate and glutamate by an alanine aminotransferase (AlaAT) has an influence on the regeneration of

I Results

the plants (Miyashita *et al.*, 2007, Tsai *et al.*, 2014, Diab & Limami, 2016). The pyruvate can be directly used to feed the deprived TCA cycle in mitochondrial respiration. It is known that during oxygen deprivation alanine biosynthesis increases to store carbon that would be otherwise lost during fermentation. During the period of re-oxygenation the expression of AlaAT-encoding genes increases, and *AlaAT1* and *AlaAT2* show a vascular system-specific promoter activity similar to that of *AtMTP10* (Miyashita *et al.*, 2007). Due to the importance of alanine during re-oxygenation, an involvement of *AtMTP10* in alanine metabolism was tested. To get an insight if the *mtp10-1* mutant has defects in alanine breakdown, growth on plates containing half-strength MS media with different nitrogen sources was monitored. Interestingly, the growth of *mtp10-1* was decreased when alanine was the main nitrogen source in the media (Fig. 35). This growth defect was alleviated in the complementation line *mtp10-1::gMTP10.2*, indeed supporting a role of *AtMTP10* in alanine metabolization.

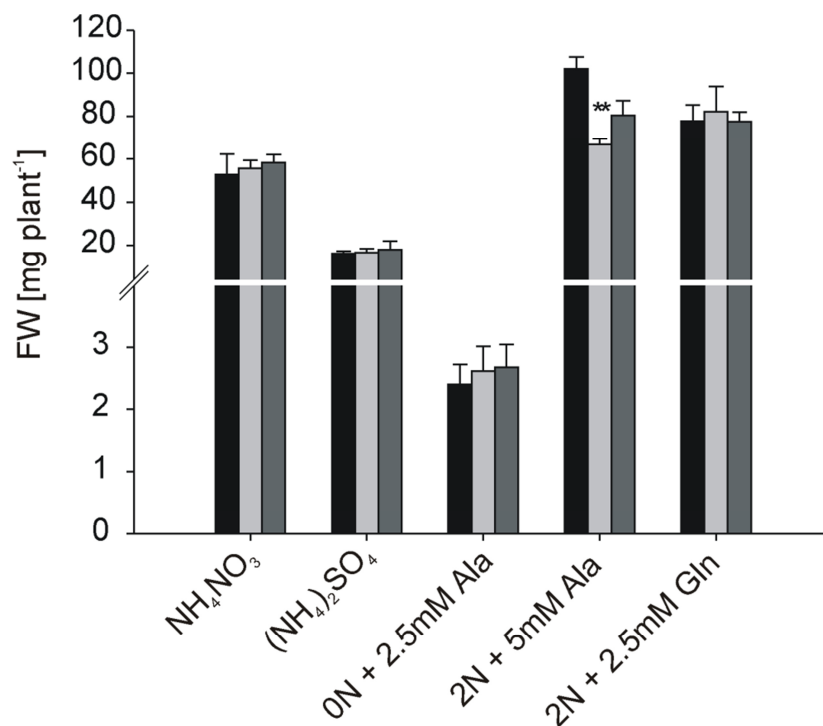


Fig. 35: Fresh weight of Col-0 (black bars), *mtp10-1* (light grey bars), and *mtp10-1::gMTP10.2* (dark grey bars) seedlings grown for 10 d on ½ MS media with different N sources (0.5 mM NH₄NO₃ or 0.5 mM (NH₄)₂SO₄). 2 N = 2 mM nitrogen composed of 0.5 mM NH₄NO₃ and 0.5 mM (NH₄)₂SO₄. Values represent the means (±SE) of three plates per treatment, each containing 5 seedlings. Asterisks indicate significant difference according to Student's t-test (** = P < 0.01).

4 Discussion

4.1 AtMTP10 is a Mn and Fe transporter expressed in the vascular system and localized in intracellular compartments

This thesis aimed to elucidate the function of the Cation Diffusion Facilitator (CDF) member AtMTP10 and the role it plays in *Arabidopsis thaliana*. Consistent with the phylogenetic classification (Montanini *et al.*, 2007) the results strongly indicate that AtMTP10 has a high selectivity for Mn and that this transporter contributes to Mn translocation under specific circumstances.

The CDF family has been classified into three subgroups relating to the main transported metal. Zinc is the major metal transported by members of the first subgroup, while transporters of the second subgroup are able to transport iron and zinc. The third subgroup contains Mn transporters. Besides *AtMTP10*, the *Arabidopsis* genome encodes for three additional confirmed or putative Mn transporters, which all show a close phylogenetic relationship to the Mn transporter ShMTP8 from *Stylosanthes hamata* (Montanini *et al.*, 2007, Delhaize *et al.*, 2003), the founding member of this subgroup. Among these four genes in *Arabidopsis*, *AtMTP8* and *AtMTP11* are so far the only described ones (Delhaize *et al.*, 2007, Peiter *et al.*, 2007, Eroglu *et al.*, 2016, Eroglu *et al.*, 2017, Chu *et al.*, 2017). Like *AtMTP8* and *AtMTP11*, *AtMTP10* was able to complement the Mn-sensitive yeast strain *pmr1Δ* (Fig. 7). PMR1, a Golgi-located Mn and Ca pump, mediates tolerance to Mn toxicity by secretion of Mn via the secretory pathway, and a mutation of *PMR1* leads to an increased Mn sensitivity (Lapinskas *et al.*, 1995, Durr *et al.*, 1998). ICP-OES analysis of *pmr1Δ* cells expressing *AtMTP10* showed a decreased Mn content compared to cells harbouring the empty vector (Fig. 9), and EYFP fusion revealed a localization of AtMTP10 in intracellular vesicles of the transformed yeast (Fig. 8). Collectively, the restored Mn tolerance of *pmr1Δ* by *AtMTP10*, the vesicular localization of AtMTP10, and the decreased Mn concentrations in *AtMTP10*-expressing cells lead to the assumption that AtMTP10 adopts the role of PMR1 in excluding Mn by secretion. The capability of AtMTP10 to transport Mn was furthermore confirmed by ⁵⁴Mn uptake assays with microsomal membrane vesicles isolated from *AtMTP10*-expressing yeast. Vesicles of

I Discussion

this strain showed elevated $^{54}\text{Mn}^{2+}$ influx as compared to the empty vector control (Fig. 10).

AtMTP10 was not able to complement yeast strains sensitive to other divalent cations, like Co (*cot1Δ*), Cu (*cup1Δ*), or Zn (*zrc1Δ*), which is in agreement with the phylogenetic classification to the group of manganese transporters (Montanini *et al.*, 2007). However, a yeast strain defective in the vacuolar iron transporter CCC1 (*ccc1Δ*) (Li *et al.*, 2001) was complemented by *AtMTP10* (Fig. 7). In yeast, tolerance to Fe toxicity is mediated by Fe sequestration into the vacuole by CCC1. In case of the restored growth of *ccc1Δ* yeast expressing *AtMTP10* on high-Fe media, it can be assumed that *AtMTP10* works as in Mn detoxification, meaning that Fe is loaded into secretory vesicles by *AtMTP10* and subsequently excluded via exocytosis. The complementation of *ccc1Δ* is an indication for the ability of *AtMTP10* to transport Fe besides Mn, albeit Fe-specific roles of the transporter *in planta* have not been found in the present study. Thus, this function identified by heterologous expression of *AtMTP10* in yeast might not reflect its function in the plant. However, for another member of the Mn subgroup of CDFs, *AtMTP8*, a role in Fe homeostasis has indeed been recently reported. This vacuolar transporter was initially described to be Mn-specific and to mediate Mn detoxification (Eroglu *et al.*, 2016), but further studies showed that it also complemented the Fe sensitivity of the *ccc1Δ* mutant, like *AtMTP10* in the present study (Eroglu *et al.*, 2017). This ability of *AtMTP10* to complement a Fe-sensitive yeast strain is in contrast to a study of another group (Chu *et al.*, 2017), in which *MTP8* of *Arabidopsis* and orthologues of other plant species shared a putative Fe-binding motif (E/DxxE/D) that is not conserved in the other three MTPs in *Arabidopsis*. In that study, *AtMTP10* was also not able to complement the Fe-sensitive yeast strain *ccc1Δ* (Chu *et al.*, 2017). This inconsistency with the present data may lay in differences between the experimental setups. Instead of SC medium supplemented with iron chloride, Chu *et al.* (2017) used SD medium supplemented with iron sulphate. The presence or absence of traces of other metals like Mn or Zn may also have had an influence on the complementation assays. In addition to complementing the *ccc1Δ* mutant, *in planta* *AtMTP8* was responsible for Fe localization in mature seeds in the absence of the vacuolar iron transporter VIT1 and for Fe storage in subepidermal cells of the cotyledons during germination (Eroglu *et al.*, 2017). The roles of the Mn subgroup

of CDFs therefore extend to Fe homeostasis, although this remains to be shown *in planta* for AtMTP10.

Similar to the Mn-CDFs, transporters of the NRAMP family have been shown to have a dual functionality for Mn and Fe. NRAMP1, for example, is able to transport Fe next to Mn and was found to interact functionally with IRT1 in Fe uptake by complementing the mutant of the Fe transporter *irt1* (Curie *et al.*, 2000, Cailliatte *et al.*, 2009, Cailliatte *et al.*, 2010). Castaings and co-workers found that a double mutant of both transporters, *nramp1-1 irt1-1*, showed severe symptoms of Fe deficiency albeit the concentration of Fe in the growth medium was sufficient (Castaings *et al.*, 2016). Elemental analysis showed that the double mutant contained less Mn and Fe compared to the *nramp1* and *irt1* single mutants under sufficient supply of both elements. The authors concluded that NRAMP1 and IRT1 worked in a redundant manner (Castaings *et al.*, 2016).

By locating the expression pattern of *AtMTP10*, assumptions about its role may be inferred. For this approach, promoter-GUS studies were performed. In agreement with published transcriptomics data (Winter *et al.*, 2007), *AtMTP10* is expressed specifically in the vasculature of the entire plant (Fig. 13). In roots, the promoter activity was specific to the pericycle whereas in leaves activity could be detected in cells surrounding the xylem vessels. Interestingly the promoter activity in the developing siliques decreased with increasing age of the siliques and was high in the abscission zone. The mechanisms of shedding leaves or fruits during senescence have been studied intensively. Major processes are a decreased flux of IAA and an increase in ethylene that induces many cell wall-degrading enzymes, like cellulases (Sakamoto *et al.*, 2008). After abscission, the resulting gap must be plugged to avoid water loss and pathogen attack. During abscission, an increased expression of genes encoding pectin and hemicellulose-modifying proteins or proteins that are responsible for the wax production was identified (Gonzalez-Carranza *et al.*, 2012). A specific involvement of Mn in the production of wax has not been uncovered until now. Nevertheless, it was shown that the thickness of the cuticular layer of plants is decreased under Mn deficiency (Hebberner *et al.*, 2009, Alejandro *et al.*, 2017). Although the expression pattern of *AtMTP10* suggests a role during abscission, aberrances were not observed in *mtp10* mutants. A putative involvement of AtMTP10

I Discussion

may lay in the allocation of Mn in that zone, but this remains to be elucidated in more detail.

Especially the profoundly defined localization of *AtMTP10* expression in cells of the pericycle (Fig. 13) makes this transporter a candidate for Mn translocation. The transport of Mn from root to shoot occurs in the xylem via the transpiration stream. After entering peripheral root cells, e.g. by IRT1 (Korshunova *et al.*, 1999), NRAMP1 (Curie *et al.*, 2000, Cailliatte *et al.*, 2010), and possibly also by Ca²⁺ channels (White *et al.*, 2002), Mn moves symplastically through the cortex and endodermis until it reaches the cells of the pericycle. Alternatively, Mn may take the apoplastic way of solutes through the cell wall, which is blocked by the Casparian strip of the endodermis. In this layer, lignin depositions serve as a diffusion barrier; solutes have to be taken up actively and follow the symplastic route to the cells of the pericycle. Once nutrients have reached the cells of the pericycle, they are released into the stele by transporters or channels. In the case of the macronutrient phosphorus, this step is mediated by the pericycle-localized transporter Pho1 (Hamburger *et al.*, 2002). By GFP fusion and expression in mesophyll cells of tobacco or in onion epidermal cells, this transporter was shown to be localized to the Golgi and the *trans*-Golgi network, but not in the plasma membrane. The export activity of PHO1 could be explained by (i) a minor amount of PHO1 in the plasma membrane that is below detection limit, (ii) differences in the localization between different cell types (mesophyll cells and cells of the vasculature), or (iii) internalization of PHO1 under excess phosphate like previously described for IRT1 (Arpat *et al.*, 2012, Barberon *et al.*, 2011). Arpat and co-workers proposed a fourth possibility, namely export of phosphorus into the xylem mediated by the secretory pathway, like previously hypothesized for MTP11. In this model, PHO1 is responsible to load P_i into vesicles that are destined for exocytosis (Arpat *et al.*, 2012, Peiter *et al.*, 2007). Another pericycle-specific exporter is BOR1, which is responsible for the release of boron into the stele. Contrary to PHO1, this transporter is localized to the plasma membrane of cells of the pericycle (Takano *et al.*, 2002). Furthermore, to avoid toxicity, BOR1 was also shown to be degraded under excess boron by boron-induced ubiquitination (Kasai *et al.*, 2011).

The translocation of all elements from roots to shoots is mediated by the xylem stream, which is driven by transpiration or root pressure. If not loaded apoplastically,

I Discussion

those elements are released into the xylem apoplasm by pericycle cells. The pericycle-specific expression of *AtMTP10* in roots therefore pointed to a role in xylem loading, and hence root-to-shoot translocation of Mn, the molecular basis of which has been unresolved so far.

To elucidate the function of *AtMTP10*, its subcellular localization was determined. To this end, the coding region of *AtMTP10* was fused N-terminally to Enhanced Yellow Fluorescent Protein (EYFP). Transient expression of this construct in mesophyll protoplasts of *Arabidopsis* plants showed an EYFP signal distributed throughout the cytoplasm, suggesting a predominant localization to the ER, and additionally in small spots. The ER localization was confirmed with the help of an ER-GFP marker line (Hawes & Satiat-Jeunemaitre, 2005), in which both signals overlapped (Fig. 14). The small spots did not co-localize with the ER-GFP nor with a GFP marker for mitochondria (Logan & Leaver, 2000) or a CFP marker for peroxisomes (Nelson *et al.*, 2007). A co-transformation of Col-0 protoplasts with *AtMTP10*-EYFP and *AtMTP11*-GFP showed an overlap (Fig. 14 E). This indicates that the function of *AtMTP10* on cellular level is similar to that of *AtMTP11*, i.e. the loading of Golgi-associated vesicles destined for secretion (Peiter *et al.*, 2007).

To identify the vesicular compartment in which *AtMTP10* is localized, further co-localization studies were performed in tobacco cells (*Nicotiana benthamiana*). The localization was comparable to that in *Arabidopsis* mesophyll protoplasts, and co-localization with an ER-mCherry marker (Nelson *et al.*, 2007) showed a predominant overlap (Fig. 15). The small spots, in which *AtMTP10* was also found, co-localized with SYP61-mCherry (Fig. 16), a marker for the *trans*-Golgi network (TGN) (Groen *et al.*, 2014).

The function of Golgi- or TGN-localized proteins is often difficult to identify. Those vesicular compartments contain proteins that are in transit from the ER via the Golgi and TGN to the place of their activity, e.g. the plasma membrane, as well as proteins that are supposed to function in the vesicular compartments themselves (Groen *et al.*, 2014) and thus, microscopic analysis can lead to misinterpretation. This difficulty to assign the function from the localization of a protein was previously demonstrated for the Fe uptake transporter IRT1. It was shown that IRT1 was predominantly localized in the *trans*-Golgi network (TGN)/ early endosomes (EE), next to a very minor presence in the plasma membrane, where it mediates Fe uptake. Endocytosis via the TGN/EE for the

I Discussion

internalization of IRT1 in the vacuole appears as a protective mechanism to avoid an accumulation of the other substrates of IRT1, like Mn, Zn, or Co (Barberon *et al.*, 2011). This internalization was demonstrated by the drug Tyrphostin A23 (TYR A23) that inhibits the cargo sorting of proteins to clathrin-coated vesicles for internalization (Banbury *et al.*, 2003): Fluorescent signals of IRT1-GFP were observed in the plasma membrane upon TYR A23 treatment (Barberon *et al.*, 2011).

To test the possibility that the observed localization of AtMTP10 represents the protein in transit from the plasma membrane, a localization experiment with TYR A23 was performed. Unlike the effect on IRT1, an incubation of protoplasts expressing *AtMTP10-EYFP* with TYR A23 did not change the localization of AtMTP10 (Fig. 17). The fluorescent signal was still observed in the ER and in small spots that were identified as vesicles of the TGN before. This experiment indicated that the observed intracellular localization of AtMTP10 is not due to TYR A23-sensitive internalization of a plasma membrane-resident fraction of the transporter. However, the localization experiments on AtMTP10 were not performed on cells where it is naturally active, e.g. the pericycle, but in mesophyll and epidermal cells. Therefore, the observed localization of AtMTP10 in ER and Golgi/TGN may reflect an impeded trafficking of the protein to or from another membrane, such as the plasma membrane. Stable lines expressing *AtMTP10-EYFP* under its native promoter are required for localization studies in intact tissues.

Since AtMTP10 is involved in Mn transport and translocation, its localization may be regulated by the availability of Mn, as shown before for OsMTP9 of rice (Tsunemitsu *et al.*, 2018). To test this hypothesis, protoplasts of tobacco leaves, expressing *AtMTP10-EYFP* were incubated in solutions containing 100 μ M Mn, similar to the TYR A23 treatments described above. Mn did also not cause an altered localization of AtMTP10. Collectively, from the localization studies it can be concluded that AtMTP10 is likely to be constitutively localized to the ER and to vesicles of the TGN and that it may fulfil its function in these compartments. Despite this, it is possible that the localization of AtMTP10 depends on other specific conditions or on the cell type. Further studies, e.g. employing an AtMTP10-specific antibody, may provide further insights into the localization of AtMTP10 in tissues where it is naturally expressed or under conditions other than Mn toxicity.

4.2 AtMTP10 is a negative factor of Mn tolerance, improves growth at low Mn availability, and contributes to xylem loading of Mn

Although Mn is an essential micronutrient for plant growth, an excessive uptake can lead to symptoms of toxicity and diminished plant growth. Mn uptake is not strictly regulated, and, consequently, its sequestration and translocation have to be well-controlled. One mechanism of plants to avoid Mn toxicity is represented by the previously described Mn transporter AtMTP8. This transporter is localized to the tonoplast in the root cortex and transports excess Mn into the vacuoles (Eroglu *et al.*, 2016, Montanini *et al.*, 2007). Conversely, another member of the CDF family, AtMTP11, mediates Mn tolerance by secretion out of the cell (Peiter *et al.*, 2007). On whole-plant level, enhanced tolerance to Mn can be conferred by a decreased Mn translocation from roots to the shoots, such as shown for Douglas fir (*Pseudotsuga menziesii*) (Ducic *et al.*, 2006). To examine if AtMTP10 plays a role in the tolerance to Mn toxicity, the growth of the *mtp10-1* knockout line was monitored on agar plates supplemented with excess Mn. Surprisingly, in contrast to *AtMTP8* and *AtMTP11*, the missing expression of *AtMTP10* led to an increased tolerance to Mn toxicity, which was reflected in an enhanced root growth rate and increased fresh weight of *mtp10-1* plants (Fig. 18). This was confirmed with a second mutant in a different background, *mtp10-4* (Fig. 19), and by the fact that the growth of a complementation line (*mtp10-1::gMTP10.1*) under Mn toxicity was comparable to that of wild type plants (Fig. 20). Hence, the sensitivity to Mn toxicity was unequivocally linked to the *AtMTP10* gene. Considering the localization of *AtMTP10* expression in cells of the pericycle, a possible explanation for the increased tolerance of the *mtp10* knockout plants may lie in a decreased translocation of Mn in those plants. Despite its involvement in Mn tolerance, the expression level of *AtMTP10* was unaffected under increased Mn concentrations (Fig. 18). Such an unresponsiveness of transcript levels to Mn availability was also observed for *AtMTP11* that also belongs to the Mn subgroup of the CDF family (Peiter *et al.*, 2007). The unaffected expression level of *AtMTP10* may indicate that its downregulation under Mn toxicity is, for unknown reasons, not physiologically advantageous.

To assess the role of AtMTP10 during Mn-limiting conditions, the growth of *mtp10-1* was tested on Mn-depleted media. Plants were pre-cultured on media with sufficient amounts of Mn (3.5 μ M) for two weeks and transferred to Mn deficiency (no

Mn) for another three weeks. The size of Mn-limited *mtp10-1* mutants was clearly diminished, which was also reflected in the dry weights of those plants (Fig. 21). An elemental analysis of those plants showed a decreased Mn concentration in the shoot, but not in the root, under both conditions, even if only trend wise under Mn deficiency, (Fig. 21), which provides further evidence for an involvement of AtMTP10 in root-to-shoot translocation that was inferred from its expression in the pericycle. Wild type plants may thus handle the available Mn in a better way. Interestingly, there are some parallels of AtMTP10 in this respect to the BOR1 and PHO1 proteins, which are transporters that are also expressed in the pericycle and that mediate the xylem loading of the micronutrient boron and the macronutrient phosphorus, respectively. Mutation of *BOR1* led to a diminished growth and decreased concentrations of boron in the shoots (Takano *et al.*, 2002). Shoots of *pho1* mutant plants thus showed decreased phosphorus concentrations under sufficient P supply, while P uptake into the root was comparable to that of the wild type (Poirier *et al.*, 1991, Hamburger *et al.*, 2002). This was also the case with Mn in *mtp10-1*: Mn concentrations in roots were comparable under both, limiting and sufficient supply, but shoot concentrations were decreased in *mtp10-1* under Mn-sufficient conditions. However, the phenotypical differences in *bor1* and *pho1* compared to the wild type are stronger compared to the phenotype of *mtp10-1*, suggesting that there are additional mechanisms for Mn translocation in Arabidopsis and that AtMTP10 plays only a minor role under standard conditions. As mentioned before, an essential transporter for the uptake and possibly also the translocation of Mn is NRAMP1. A mutation in *NRAMP1* led to decreased growth and also to a decreased Mn concentration in shoots, whereas root Mn concentrations were comparable to the wild type under Mn deficiency (Cailliatte *et al.*, 2010). Under sufficient Mn supply, Mn concentrations in shoots were also comparable to the wild type, which let the authors conclude that NRAMP1 is a high-affinity transporter that is important during conditions of Mn starvation. However, since NRAMP1 is an importer, its possible role in root-to-shoot translocation is unresolved.

As discussed above, a lower Mn concentration in the shoot of *mtp10-1*, with unchanged Mn concentration in the roots, may be the consequence of a decreased root-to-shoot translocation. This should be reflected in decreased Mn translocation rates in the xylem. This notion was tested by collecting xylem exudate from hypocotyls after

severing of the shoot. Since the shoots of the plants were cut off before exudate collection, the root pressure was the driving force for exudation. Surprisingly, the elemental translocation in xylem exudates was comparable between *mtp10-1* and the wild type (Fig. 22), which at first contradicted a role of AtMTP10 in Mn translocation and indicated that AtMTP10 plays, if at all, only a minor role in Mn xylem loading. However, the transpiration stream and its composition vary between day and night because of differences in stomatal aperture and the regulation of aquaporins, i.e. proteins of the major intrinsic protein (MIP) family, and other transporters (Dodd *et al.*, 2005, Takase *et al.*, 2011). The Arabidopsis genome encodes for about 30 MIPs that are classified into four subgroups. Especially PIP2 proteins, that belong to the subfamily of PIPs (plasma membrane intrinsic proteins), are involved in the water transport across the plasma membrane in Arabidopsis (Lopez *et al.*, 2003). In *Lotus japonicus*, mRNAs hybridising to a probe of the Arabidopsis PIP2 showed an increased abundance at the beginning of the light period (Clarkson *et al.*, 2000). In addition, photosynthesis is a reaction that proceeds only during the day and that also underlies a circadian regulation (Noordally *et al.*, 2013). In the light period, photosynthates accumulate usually as starch in leaves. They are converted back in the night to support metabolism and growth (Blasing *et al.*, 2005, Haydon *et al.*, 2015). The photosynthetic apparatus has a high requirement of Fe, Cu, Mg, and also for Mn as a part of the tetra-Mn cluster in PSII (Merchant & Sawaya, 2005, Pantazis *et al.*, 2012). This may lead to a higher demand of those nutrients during the day, and a diurnal variation of Mn translocation in the xylem was thus supposed. To test this notion, xylem exudates of wild type and *mtp10-1* plants were collected in the course of the day (Fig. 23 and 24). The exudate volumes increased at the beginning of the light period, which was also shown previously in maize (Lopez *et al.*, 2003). This increase in translocation is likely to be at least partially due to an increased abundance of aquaporins, allowing for an increased transcellular flux of water. Besides differences in exudate volume, fluctuations in Mn translocation were apparent. The Mn exudation rate increased at the beginning of the day and decreased again in the mid of the day (Fig. 23 and 24). This pattern of Mn exudation was observed in both the wild type as well the *mtp10-1* mutant. The reason for the increasing amounts of translocated Mn at the beginning of the day may lie in the involvement of Mn in photosynthesis and thus in an increased requirement of Mn, as discussed above. Interestingly, the Mn exudation rates

differed markedly between both genotypes at the end as well as at the beginning of the dark period, which implicates a specific role of AtMTP10 in Mn translocation at night (Fig. 23 and 24). The dependence of Mn exudation on AtMTP10 only under dark conditions was hypothesised to be related to the transcriptional regulation of the gene. Indeed, transcriptomics analyses show that the expression of *AtMTP10* increases at the end of the day (Blasing *et al.*, 2005, Haydon *et al.*, 2011). This trend was confirmed in the present work by quantitative real-time RT-PCR: Arabidopsis roots analysed at different times of the day showed that the expression of *AtMTP10* was decreased in the mid of day and increased again in the night (Fig. 26).

Transport and assimilation of other nutrients is also known to be diurnally regulated. The transcripts of genes encoding for nitrate, ammonium, and sulphate transporters, and also the homeostasis of copper and iron are influenced by the day-and-night rhythm (Haydon *et al.*, 2011). It was also shown that the ammonium uptake by Arabidopsis plants underlie diurnal fluctuations, and that the transcript level of the main ammonium uptake transporter of the *AMT1* family, *AMT1.3*, varied in the same way as the uptake of ammonium (Gazzarrini *et al.*, 1999). The expression level of *AMT1.3* and ammonium influx peaked at the end of the light period when also the levels of carbohydrates in roots are high, suggesting as possible control by the carbon contents in roots that are needed for ammonium assimilation (Gazzarrini *et al.*, 1999). The remobilization of nitrate from source to sink via the phloem is mediated by NRT1.7 (Fan *et al.*, 2009). The transcript level of this transporter peaked in the early beginning of the dark period when the transcript level of the nitrate reductase NIR2 was low, suggesting that NRT1.7 is needed for the translocation of nitrate when the reductase activity is low (Fan *et al.*, 2009). Analyses of published investigations concerning diurnal or circadian regulation of Fe uptake and translocation are impeded by the fact that the genes involved in the Fe acquisition apparatus are not highly expressed under Fe sufficiency (Haydon *et al.*, 2015). Vert and co-workers found in a study with a heterozygous mutant of *IRT1* that this mutant started flowering earlier than the wild type under short-day conditions, leading to the question if Fe uptake depends on light (Vert *et al.*, 2003). They found an increase in expression of *IRT1* and *FRO2* during the light period, but only under Fe sufficiency, not under Fe deficiency. This indicated that in strategy I plants, Fe availability

has a higher impact than light on the regulation of Fe acquisition genes (Vert *et al.*, 2003). In monocots, that use strategy II of Fe acquisition, light plays a more prominent role because the release of phytosiderophores follows a diurnal rhythm with a peak at the early beginning of the light period (Takagi *et al.*, 1984).

The observed trends in diurnal variation of Mn exudation rates, as well as the effect of *AtMTP10* mutation, were specific for Mn. Fe and Zn exudation did not vary throughout the day, and there were no significant differences in Fe and Zn exudation rates between *mtp10-1* and the wild type, except for the second sampling under dark conditions at 8 pm, where Fe exudation was decreased in exudates of *mtp10-1* (Fig. 24). However, this effect did only occur in one of the experiments and thus is considered as an outlier. This indicates that the root-to-shoot translocation of Mn is regulated differently from that of Fe and Zn. The xylem exudation data also show that further, yet unknown, xylem loading mechanisms for Mn operate during the day and support *AtMTP10* at night. The physiological advantage of specific xylem loading mechanisms at different times of the day is unclear. Also, the experiments presented in this thesis do not yet allow a conclusion if the *AtMTP10*-mediated xylem loading of Mn is under diurnal or circadian regulation. The discrimination of both potentially regulatory factors needs to be elaborated in future studies.

4.3 **AtMTP10 is important to overcome post-anoxia conditions**

The response of *AtMTP10* expression to environmental factors was screened *in silico* using the GENEVESTIGATOR database (Zimmermann *et al.*, 2004). This pointed to studies on hypoxia treatments where *AtMTP10* showed a higher transcript level compared to control conditions (Branco-Price *et al.*, 2008, Mustroph *et al.*, 2009, Licausi *et al.*, 2011, Chang *et al.*, 2012) (Fig. 27). Mustroph and co-workers compared the expression of genes after a treatment of 2 h of hypoxia under low light conditions by flushing seven-day-old seedlings with argon. A comparable experimental setting was used by Chang and co-workers with the exception that they used ten-day-old seedlings. Branco-Price *et al.* (2008) treated plants in a similar way, but for two and nine hours, whereas Licausi *et al.* (2011) treated *Arabidopsis* plants for one and a half hours with 1% oxygen in the dark and

analysed the rosettes of those plants. All these studies showed a slight increase of *AtMTP10* transcript levels under hypoxic or anoxic compared to control conditions. This triggered the question if this increase in *AtMTP10* expression under oxygen limitation is physiologically relevant and if *mtp10* mutants show a phenotype in these conditions. In addition, besides oxygen deficiency, Mn toxicity is a major growth-limiting factor on submerged soils. Thus, an involvement of other members of the Mn subgroup of CDF proteins in submergence tolerance appeared possible, too. To test this, six-week-old soil-grown mutants of those genes were flooded for three weeks. After 14 days of regeneration, the phenotype of the plants was assessed. Interestingly, only the *mtp10-1* mutant plants showed a strongly diminished recovery from this stress (Fig. 28). This phenotype was confirmed with a second knockout line (*mtp10-4*) in No-0 background, and it was abolished in a complementation line (*mtp10-1::gMTP10.1*) (Fig. 28).

Flooding events are problematic for most sessile plants. Major problems are a decreased gas diffusion rate of O₂, CO₂, and ethylene; a decreased redox potential in the soil that can lead to an increased availability of metals to toxic amounts; and a decreased light intensity that causes a drop in photosynthetic activity (Blom & Voeselek, 1996, Drew, 1997, Gibbs & Greenway, 2003, Vervuren *et al.*, 2003, Bailey-Serres & Voeselek, 2008). As shown in this thesis, a mutation of *AtMTP10* leads to an increased tolerance to Mn toxicity (Fig. 18 and 19), so that Mn toxicity can be excluded as an explanation for the decreased tolerance of *mtp10* mutants to submergence. A more time-resolved observation showed that the phenotype of *mtp10-1* was comparable to the wild type after de-submergence and that mutant plants did not begin to decay until the beginning of the recovery phase (Fig. 28). This indicates a specific involvement of *AtMTP10* in the recovery from submergence rather than during this abiotic stress.

Several genes that have an impact on the recovery from transient oxygen deficiency are known to be already up-regulated during the stress (Branco-Price *et al.*, 2008). The abundance of many mRNAs increases during hypoxic stress, but their translation only rises after the relief of the stress. This includes mRNAs encoding enzymes with catalytic, transferase, kinase, as well as protein-binding activity (Branco-Price *et al.*, 2008). Interestingly, analysis of the transcript levels of *AtMTP10* uncovered that this gene also showed those characteristics of a slight increase already during submergence (Fig. 27

and 28 D), which might be attributed to the preparation of plant cells to re-oxygenation. However, most notable was a rapid increase in transcript abundance during the first hour after re-introduction of oxygen (Fig. 28 E), suggesting a major role of *AtMTP10* during re-oxygenation.

Due to undefined fluctuations in nutrient availability and interactions with soil microorganisms, soil systems are difficult to define, and the causality of phenotypes is difficult to determine. Thus, the experimental setup was changed back to an agar-based system. The most obvious change in the plant's environment during submergence is the oxygen deprivation due to the altered gas diffusion rate. Oxygen, as a resulting product of photosynthesis, is essential for plant growth on the one hand, but on the other hand, it can lead to injuries caused by oxidative stress (Monk *et al.*, 1989, Steffens *et al.*, 2013). Oxygen is involved in approximately 200 reactions of a plant cell. This reaches from the most important demand for mitochondrial respiration to ensure the energetic needs (95% of the cellular oxygen) to its integration in a double bond in fatty acyl chains to modulate the fluidity of membranes (0.007% of the cellular oxygen) (Rawlyer *et al.*, 2002). To check if the diminished growth of *mtp10* mutants during re-oxygenation was triggered by oxygen deficiency, ten-day-old seedlings grown on half-strength MS agar plates were exposed to oxygen deficiency for 24 h in a desiccator. Oxygen-deficient conditions were created by flushing the desiccator with N₂. After the following recovery period, *mtp10-1* plants showed a diminished growth, as seen before in the soil-based submergence experiments (Fig. 30). Also the previously observed up-regulation of *AtMTP10* in the early phase of re-oxygenation was apparent, but only in roots. Interestingly, the response of seedlings to anoxia conditions was much faster compared to that of adult plants to submergence (Fig. 30). A possible explanation may lie in the differences between anoxia and hypoxia conditions. Under submergence the oxygen contents are not completely zero, and the photosynthetic activity of submerged plants is decreased, but not totally interrupted. Due to the decreased diffusion rate of gases in water, the produced oxygen remains at the leaf surface and hence plant-available. Such conditions are therefore rather hypoxic than anoxic (Müstroph *et al.*, 2014). In contrast, oxygen produced by seedlings that are permanently flushed with N₂, diffuses away and is not plant-available (Ellis *et al.*, 1999). The physiological changes in the re-aeration period after anoxia are

therefore much worse than after hypoxia (Biemelt *et al.*, 1998). Due to the faster increase of *AtMTP10* expression level after anoxic conditions compared to the hypoxic conditions during submergence, it may be concluded that *AtMTP10* plays a greater role after the transient anoxic stress. Another factor that may have an impact on the kinetics of *AtMTP10* expression is the age of the plants. For experiments with transient anoxia stress, seedlings grown on agar plates were much younger compared to the plants growing on soil for the submergence experiments.

The expression of *AtMTP10* in roots increased during re-aeration (Fig. 30 C). For the plant, oxygen deficiency of roots is much more difficult to overcome. While oxygen contents in the soil decline faster because of consumption by the root and by soil microorganisms, shoots have access to oxygen from the water and from the residual, although reduced, photosynthetic activity (Sauter, 2013, Mustroph *et al.*, 2014). Uptake of nutrients is also critical, if energy supply, membrane integrity, and ion transport are hampered under oxygen deprivation. Also, a flooding-induced decrease in root water conductivity mediated by changes in aquaporin activity leads to stomatal closure in leaves and wilting, and thus to a reduced translocation of nutrients (Colmer & Greenway, 2011, Sauter, 2013). Furthermore, root survival depends on carbohydrate transport from the shoot, which is decreased due to the reduced photosynthesis rate under submergence (Mustroph *et al.*, 2014). To test the presumed specific importance of *AtMTP10* in roots, the experimental setup was changed to a hydroponic system that allowed root-specific exposure to anoxic conditions. Six-week-old plants grown in nutrient solution were exposed to oxygen deficiency in the root zone by N₂ aeration of the media. Also under this setup, a diminished growth of *mtp10-1* plants was registered after a regeneration period of ten days (Fig. 31). The expression level of *AtMTP10* in roots was slightly increased during anoxia, and decreased somewhat in the early phase of re-oxygenation relative to control conditions. This was followed by an increase of expression by around four fold compared to control conditions at 1 h after re-introduction of oxygen (Fig. 31 D). The increase of *AtMTP10* transcript level in roots during the anoxic period might again be attributed to the preparation of plant cell to re-oxygenation, as discussed above.

These results indicated that an exposure to oxygen deprivation only in the root zone was sufficient to cause a decreased capacity of *mtp10* mutants to recover from the stress. This provokes the question to the possible function of *AtMTP10* during this period.

4.4 Function of *AtMTP10* during post-anoxic conditions

So far, it has been concluded that *AtMTP10* plays a role in plant recovery during post-anoxic stress. Directly after submergence or anoxia, *mtp10* mutants looked comparable to the wild type but deteriorated thereafter. Furthermore, the expression of *AtMTP10* increased in the early phase of re-oxygenation in shoots after submergence, as well as after anoxia triggered by N₂ aeration in roots. The weakened growth of *mtp10-1* also occurred when only the root zone was exposed to anoxia conditions. In all of those experimental setups the plants were allowed to recover for 10 d. It was hypothesised that the need for *AtMTP10*, which is largely specific for Mn²⁺ (Fig. 7 and 10) and expressed in the vasculature of the whole plant (Fig. 13), lies in an involvement of this transporter in Mn²⁺ translocation into the xylem. As previously discussed, the involvement of *AtMTP10* in Fe homeostasis was only shown in yeast (Fig. 7), and there was no evidence from elemental analyses that *AtMTP10* plays a role in Fe transport *in planta*. The idea of a participation of *AtMTP10* in xylem loading of Mn during re-oxygenation was underlined by the decreased Mn translocation in xylem exudates of *mtp10-1* in the dark period (Fig. 23 and 24). To test this hypothesis, the elemental composition of xylem exudates in the early phase of re-oxygenation after root anoxia was analysed. The collection of shoot tissue and xylem exudates of plants cultivated under submergence was not feasible because of contaminations from suspended soil and water surrounding the shoots. In contrast, hydroponic cultivation of plants avoids those contaminations. As discussed above, exposure of the root zone of hydroponically-grown plants to oxygen deficiency by N₂ aeration was sufficient to provoke the decreased capacity of *mtp10-1* to recover (Fig. 31). Xylem exudates were collected in the first two hours after re-introduction of oxygen following an oxygen deprivation of the root zone for 24 h. The exudate volume, normalized to root dry weight, increased in the early phase of re-oxygenation compared to control conditions, in which the root zone was continuously supplied with atmospheric air, whereby the mutant did not differ from wild type plants (Fig. 32 and 33).

I Discussion

Interestingly, Mn translocation increased tendentially or significantly in re-oxygenated plants. This increase failed to appear in *mtp10-1* (Fig. 32 and 33). These results demonstrate a likely involvement of AtMTP10 in xylem loading of Mn during re-oxygenation.

To deduce a possible function of AtMTP10 and the increased Mn translocation, the processes that proceed during re-oxygenation following hypoxia or anoxia and their dependence on Mn have to be considered. Upon re-oxygenation plants have to not only to increase photosynthesis again, the prevention of injury mediated by reactive oxygen species (ROS) is also a major task. Oxygen deprivation leads to an up-regulation of many ROS detoxification systems, such as peroxidase, ascorbate peroxidase, monodehydroascorbate reductase, glutathione reductase, and superoxide dismutase (SOD). It has been concluded that genes encoding those enzymes play an essential role to counteract post-anoxia injury (Monk *et al.*, 1989, Klok *et al.*, 2002), and it has been known for a long time that plants with an increased SOD activity showed a higher tolerance to re-oxygenation as also throughout the oxygen deprivation stress (reviewed in (Blokhina *et al.*, 2003)). In *Iris pseudacorus*, SOD activity increased in rhizomes during 28 days of anoxia and stayed high during 48 hours of re-oxygenation, when the SOD activity was 13 times higher compared to the beginning of the anoxia stress. This also holds true for anoxia-tolerant Lotus seedlings (*Nelumbo nucifera*) that showed an increase in SOD activity during re-oxygenation after they germinated under submergence (Ushimaru *et al.*, 2001). In contrast to that, the less tolerant species *Iris germanica* showed only a slight increase in SOD activity during anoxia, and during re-oxygenation even a decrease (Monk *et al.*, 1987b). Contrarily, in roots of submergence-intolerant soybean (*Glycine max*), activity of SOD decreased rapidly during a re-oxygenation period by about 70% (Monk *et al.*, 1987b, Vantoai & Bolles, 1991).

SODs contain Cu/Zn, Fe, or Mn in their active site. Next to their co-factors, also the localization of the SODs differs. The three Fe-containing SODs in Arabidopsis are localized to plastids, the Cu/Zn-containing SOD to plastids or the cytosol, and the MnSOD predominantly to the mitochondria (Bowler *et al.*, 1992). There are also studies in higher plants that showed that the Mn- as also the Cu/Zn-containing SODs were localized to peroxisomes (Luis *et al.*, 1983, Schrader & Fahimi, 2006, Bueno *et al.*, 1995). By inhibiting

the Cu/Zn-SOD and the use of plant material without chloroplasts, e.g. rhizomes, it was concluded that 25% of the increase in SOD activity during oxygen deficiency was contributed by the MnSOD (Monk *et al.*, 1987b). Unfortunately, most investigations were performed only under hypoxia or anoxia, and there are only a few studies that investigated the period of re-oxygenation. In *Arabidopsis*, expression of the Mn-containing SOD was not up-regulated during re-oxygenation, which also holds true for the Fe- and Cu/Zn-SODs (Branco-Price *et al.*, 2008, Tsai *et al.*, 2014).

Other mechanisms to combat the burst in oxidative stress during re-oxygenation are low-mass ROS scavengers, like ascorbate and glutathione together with the enzymes co-operating in the ascorbate-glutathione cycle, like the ascorbate peroxidase, glutathione reductase, monodehydroascorbate reductase and dehydroascorbate reductase (Skutnik & Rychter, 2009). It was shown that the activities of enzymes working in the ascorbate-glutathione cycle, namely ascorbate peroxidase and glutathione reductase, decreased in wheat seedlings during root anoxia and increased again upon re-aeration (Biemelt *et al.*, 1998). This effect was also shown in rice seedlings (Ushimaru *et al.*, 1992). In *Arabidopsis*, it was shown that two different accessions performed differently upon re-oxygenation (Yeung *et al.*, 2018), and it was concluded that the ability of the tolerant genotype to regenerate better from transient anoxia stress was connected to a higher ascorbate and glutathione production with simultaneously occurring lower ROS contents (Yeung *et al.*, 2018). Furthermore, it was shown that the regulation of *VTC* and *GSH* gene, encoding enzymes involved in ascorbate and glutathione synthesis, are under control of the transcription factor MYC2 which in turn is activated by a rapid accumulation of jasmonates during re-oxygenation (Yuan *et al.*, 2017). All of these findings showed that the antioxidants ascorbate and glutathione are very important to overcome the period following hypoxia or anoxia stress.

Interestingly, it is known that the glutathione reductase from yeast depends on activation by Mn (Miki *et al.*, 1996), but this has not been examined in the plant enzyme yet. A comparison of the dynamics of those low-mass ROS scavengers between wild type and *mtp10* mutants would be an interesting aspect to uncover the role of the additionally translocated Mn and thus of AtMTP10.

I Discussion

Next to re-initiation of photosynthesis and detoxification of ROS, the third challenge that plants have to handle after oxygen-deficient conditions is the return of carbon metabolism from ethanolic fermentation back to mitochondrial oxidative phosphorylation. Figure 36 shows a schematic pathway of metabolisms during hypoxia and the following period of re-oxygenation.

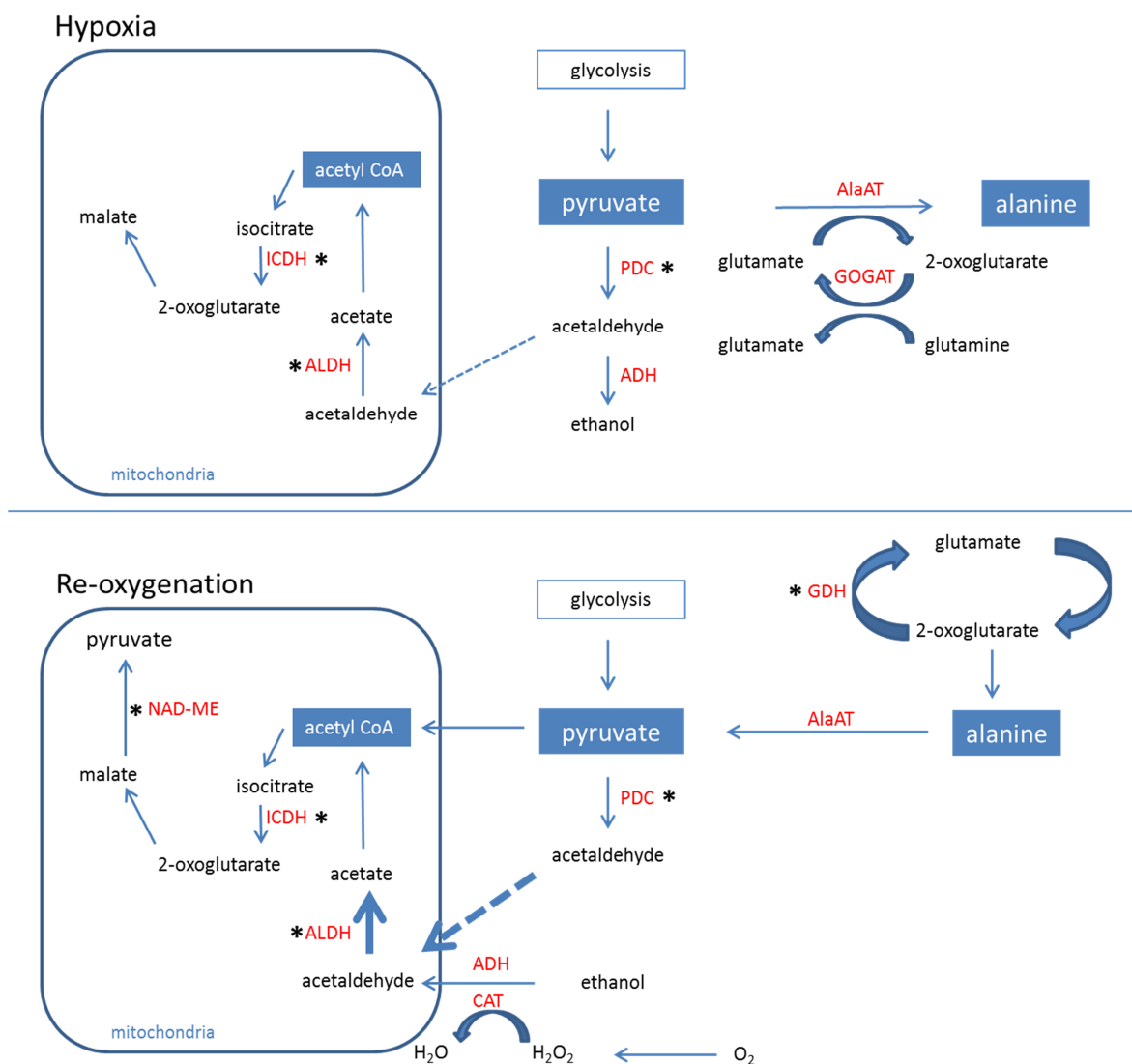


Fig. 36: Proposed pathways of metabolisms under hypoxia and during re-oxygenation. According to (Monk *et al.*, 1987a, Kreuzwieser *et al.*, 2001, Tsuji *et al.*, 2003, Shingaki-Wells *et al.*, 2014, Diab & Limami, 2016). ADH=alcohol dehydrogenase; AlaAT=alanine aminotransferase; ALDH=acetaldehyde dehydrogenase; CAT=catalase; GDH=glutamate dehydrogenase; GOGAT=glutamine oxoglutarate aminotransferase; ICDH=isocitrate dehydrogenase; NAD-ME=NAD-dependent malic enzyme; PDC=pyruvate decarboxylase. An involvement of Mn was shown for the enzymes marked with an asterisk.

The oxidation of ethanol during re-oxygenation by reverse activity of alcohol dehydrogenases (ADH) and/or by the activity of catalases (CAT) or the decarboxylation of pyruvate by pyruvate decarboxylases (PDC) results in the toxic organic compound acetaldehyde (Fig. 36) (Monk *et al.*, 1987a, Kreuzwieser *et al.*, 2001, Shingaki-Wells *et al.*, 2014, Tsuji *et al.*, 2003). Aldehyde dehydrogenase (ALDH) oxidizes aldehydes to acetate that may support the regeneration of the aerobic TCA cycle by providing acetyl-CoA. In rice, a species with a high tolerance to submergence, the activity of an aldehyde dehydrogenase (OsALDH2a) was induced during re-oxygenation, while its mRNA increased already during submergence (Tsuji *et al.*, 2003). In submergence-intolerant species like maize (*Zea mays L.*) the ALDH activity decreased during submergence and reached the initial level during re-aeration much more slowly compared to the submergence-tolerant species rice (Meguro *et al.*, 2006) (Fig. 2). The Arabidopsis genome harbours 14 *ALDH* genes. Two of them were previously characterized to be involved in tolerance to osmotic and oxidative stress, ALDH3II (chloroplastic) and ALDH7B4 (cytoplasmic) (Kirch *et al.*, 2005, Kotchoni *et al.*, 2006). Microarray data indicate an up-regulation of ALDH7B4 during re-oxygenation after 9 h of hypoxia stress (Branco-Price *et al.*, 2008). In *Acinetobacter sp.*, ALDH activity is enhanced by Mn (Zhao *et al.*, 2009). Due to the similarity of ALDH from bacteria to the human mitochondrial ALDH that contains a Mn binding site, it was concluded that all bacterial NAD⁺-dependent ALDHs need Mn for their activation (Ni *et al.*, 1999). For plant ALDHs, a dependence on Mn has not yet been studied.

In contrast to that, a multitude of enzymes that are involved in metabolic processes for the allocation of pyruvate to the TCA cycle and thus for mitochondrial respiration, were previously shown to be Mn-dependent. For example, NAD malic enzymes (NAD-ME) (Fig. 36) were described to depend on Mn in Arabidopsis. They catalyse the conversion of malate and NAD⁺ to pyruvate, CO₂ and NADH/H⁺. The Arabidopsis genome encodes for two NAD malic enzyme isoforms, NAD-ME1 (At2g13560) and NAD-ME2 (At4g00570). Promoter-GUS studies showed that both are expressed in the whole plant while the staining was little increased around the vascular system (Tronconi *et al.*, 2008, Tronconi *et al.*, 2010, Tronconi *et al.*, 2012). Furthermore, both NAD-MEs, as also apparent in this thesis for AtMTP10, have an impact on the nocturnal metabolism

(Tronconi *et al.*, 2008, Lee *et al.*, 2010). A *NAD-ME1 NAD-ME2* double mutant showed no differences in growth, but it was speculated that NAD-MEs may allocate pyruvate for the TCA cycle under conditions of high energy demand (Tronconi *et al.*, 2008, Sweetlove *et al.*, 2010). During re-oxygenation and the ensuing switch to mitochondrial respiration, the pyruvate generated by NAD-ME may be beneficial for regeneration. Another indication for the involvement of NAD-ME in recovering from hypoxia conditions is an increase of its transcript level during re-oxygenation (Branco-Price *et al.*, 2008). Nevertheless, there are no studies that compared the growth of *nad-me* mutant plants during re-oxygenation, but comparing the enzymatic activity of NAD-MEs between *mtp10* mutants and the wild type would be an interesting aspect for future work.

Under low oxygen supply, pyruvate represents the end product of glycolysis and thus the initial carbon source which is either metabolized to the fermentation end products ethanol and lactate, or converted with glutamate to alanine and 2-oxoglutarate (Ismond *et al.*, 2003). Whereas carbon atoms are lost in fermentation products during ethanolic glycolysis, the production of alanine is an effective mechanism to conserve nitrogen and carbon that can be converted to pyruvate again upon re-oxygenation (Liepman & Olsen, 2003). This reaction is mediated by alanine aminotransferases (AlaAT) (Fig. 36). The Arabidopsis genome encodes four alanine aminotransferase isoforms: GGAT1 and GGAT2, that show next to AlaAT activity a glutamate glyoxylate aminotransferase activity, and AlaAT1 and AlaAT2 that exhibit only an AlaAT activity (Miyashita *et al.*, 2007). The activity of AlaAT1 increases during recovery from hypoxia to provides pyruvate from alanine breakdown for the TCA cycle and thus for ATP production via respiration (Klok *et al.*, 2002, Liepman & Olsen, 2003, Loreti *et al.*, 2005, Miyashita *et al.*, 2007). Promoter-GUS studies showed that *AlaAT1* has a vasculature-specific expression pattern which is absent in the root tip, as shown for *AtMTP10* in this thesis (Fig. 13) (Miyashita *et al.*, 2007). Furthermore, an *AlaAT1* null mutant (*alaat1-1*) with a decreased AlaAT activity showed a decreased growth when alanine was the main nitrogen source for plant growth (Miyashita *et al.*, 2007). To test the hypothesis that the decreased recovery of *mtp10* mutants from hypoxia and anoxia is caused by a lower AlaAT activity, mutant plants were thus cultivated on agar plates containing different N sources. Similar to *alaat1-1*, the *mtp10-1* mutant showed a decreased growth compared

to the wild type if alanine was the main nitrogen source. This phenotype was abolished in a complemented mutant line (*mtp10-1-gMTP10.2*), confirming that this sensitivity was due to the mutation of *AtMTP10* (Fig. 35). Interestingly, the *alaat1-1* mutant showed no impaired survival of the primary root tip after hypoxic or anoxic conditions (Miyashita *et al.*, 2007). This may lead to the conclusion that the breakdown of alanine is not essential to overcome the period of re-oxygenation. However, the root survival was only monitored for two days after re-introduction of oxygen after up to 24 h of anoxia. Furthermore, only the survival of the root tip was monitored, albeit from promoter GUS studies it is known that *AlaAT1* and *AlaAT2* are not expressed in root tips (Miyashita *et al.*, 2007). The expression of *AlaAT1* and *AlaAT2* as also the AlaAT enzyme activity were already induced under hypoxic conditions, but upon re-oxygenation the expression of *AlaAT1* decreases whereas *AlaAT2* transcripts showed an increase (Tsai *et al.*, 2014). AlaAT activity was more important for the breakdown of alanine to pyruvate under the ensuing post-hypoxia conditions (Miyashita *et al.*, 2007). This is in agreement with the expression level of *AtMTP10*: compared to control conditions, *AtMTP10* was already up-regulated during hypoxia and anoxia stress, but its expression increased further during re-oxygenation (Fig. 28 D and E; Fig. 30 C; Fig. 31D). Despite the commonalities of *AlaAT2* and *AtMTP10* expression patterns and the alanine phenotype of *mtp10* mutants, an involvement of Mn in AlaAT activity or regulation has not been described so far. It is thus unknown if the additional Mn translocation during re-oxygenation may indeed be necessary for an enhancement of AlaAT activity. The determination of alanine contents in plants during re-oxygenation and a comparison between wild type and *mtp10* mutant plants would be an interesting aspect for future experiments.

The breakdown of alanine, and thus the synthesis of pyruvate and glutamate, by AlaAT require α -ketoglutarate. The breakdown of isocitrate via NADP-dependent isocitrate dehydrogenase (NADP-ICDH) is a central pathway of α -ketoglutarate synthesis (Fig. 36). NADP-ICDHs catalyse the oxidative decarboxylation of isocitrate to α -ketoglutarate and CO₂ while reducing NADP⁺ to NADPH + H⁺. The Arabidopsis genome contains three genes that encode for an ICDH (At1g65930; At5g14590; At1g54340) (Hodges *et al.*, 2003, Leterrier *et al.*, 2012). The activity of NADP-ICDH is mainly important during ammonia assimilation via the GS/GOGAT pathway and therefore for the synthesis

I Discussion

of amino acids like glutamine and glutamate. The enzymatic activity depends on the co-factor NADP⁺ and a divalent cation like Mg²⁺ or Mn²⁺ (Ni *et al.*, 1986). Promoters of *NADP-ICDH* were shown to be active, similar to *AtMTP10*, in the vasculature of the whole plant, but in roots the activity was not shown to be specific for the cells of the pericycle (Lemaitre & Hodges, 2006). Enhanced Mn transport during re-oxygenation may increase NADP-ICDH activity in shoots with two beneficial effects: (i) NADPH+H⁺ could be used directly for ATP synthesis, (ii) or in regeneration of glutathione used in ROS scavenging or (iii) α -ketoglutarate could be used as substrate for alanine breakdown by AlaAT by simultaneously providing pyruvate for the TCA cycle. It would therefore be interesting to compare the enzymatic activities of NADP-ICDH between Col-0 and *mtp10-1* plants during re-oxygenation.

Another pathway to provide α -ketoglutarate for the TCA cycle is based on NADH glutamate dehydrogenases (NADH-GDHs) (Fig. 36) (Fontaine *et al.*, 2012, Diab & Limami, 2016). The NADH-GDH encoding genes *GDH1* and *GDH2* were found to be up-regulated during anoxia, but during re-oxygenation the induction was even higher. Induction of *GDH3* was observed only during re-oxygenation. This up-regulation is another evidence for an increased amino acid catabolism to replenish the carbon pool (Tsai *et al.*, 2014). In *Medicago truncatula* an increased expression of *GDH1*, as also of the mitochondrial alanine amino transferase (*AlaAT*), was determined as a characteristic of hypoxic seedlings (Limami *et al.*, 2008). These adaptations were proposed to be important for the regeneration of α -ketoglutarate. Interestingly, the activity of GDH was increased first after the stress. It was further shown that alanine was the major amino acid accumulated in plants submitted to hypoxia instead of asparagine and proline that are known to accumulate under other abiotic stresses like drought, salt, mineral deficiencies, toxic metals, or pathogen attack. The authors concluded that this accumulation was more meaningful in preparation to normoxia and serves as a nitrogen store during the stress (Miyashita *et al.*, 2007, Limami *et al.*, 2008).

The formation of alanine during hypoxia for storage and the remobilization of alanine to provide pyruvate during re-oxygenation are shown in Figure 36. Both pathways are mediated by AlaAT, whereas GDH and GOGAT are important enzymes to provide the substrates for the reactions. Until now, the activation of GDH by Mn was only shown in

pea (*Pisum sativum*) (Garland & Dennis, 1977). Taken together, both enzymes that were shown to be necessary for the α -ketoglutarate pathway, namely the NADP-dependent isocitrate dehydrogenase (NADP-ICDH) and glutamate dehydrogenase (GDH), were shown to be activated Mn (Garland & Dennis, 1977, Ni *et al.*, 1986). An enhanced Mn translocation during re-oxygenation, which was observed in wild type plants, may be useful for those enzymatic pathways. Thus, a comparison of the α -ketoglutarate contents in wild type and *mtp10* mutants would be an interesting aspect for future experiments.

It can be inferred that the up-regulation of *AtMTP10* during re-oxygenation and the probably ensuing enhanced translocation of Mn may be a plant response in preparation to post-anoxia conditions. This step may be important for the restoration of metabolite composition and mitochondrial respiration to provide ATP for the high energy demand during those conditions. To uncover the function of *AtMTP10* during re-oxygenation, a comparison of the metabolite profile of Col-0 and *mtp10* mutant plants and the analysis of their enzymatic activities would thus be a promising approach. Changes in the metabolism of plants during re-oxygenation are aimed to provide metabolites for the TCA cycle and thus for an enhancement of ATP production. Due to this fact, another, albeit indirect parameter to be tested, would be the ATP concentration during the re-oxygenation period to uncover possible differences in enzymatic activities caused by different Mn translocation.

Another important factor that may lead to a decreased capacity to recover from oxygen deficiency is a reduced ability to overcome damages mediated by the phytohormone ethylene. Ethylene plays an important role in signalling pathways during hypoxia conditions and the following period of re-oxygenation. The two Arabidopsis transcription factors hypoxia responsive erfs1 (HRE1) and related to AP2.2 (RAP2.2) are under the control of ethylene and essential for hypoxic signalling (Hinz *et al.*, 2010, Yang *et al.*, 2011). Furthermore, the alcohol dehydrogenase 1 (ADH1) is known to serve as a marker enzyme for oxygen-deficient conditions (Mustroph *et al.*, 2010). RAP2.2 promotes *ADH1* expression following a hypoxic signal. This transcription factor belongs to the same family as the submergence tolerance gene *SUB1A* from rice. It is also induced by darkness and its overexpression leads to an increased tolerance to low-oxygen stress. Only a part of the low-oxygen- and ethylene-associated genes involved in sugar metabolism,

I Discussion

fermentation pathway, and ethylene biosynthesis showed to be affected by RAP2.2 (Hinz *et al.*, 2010). Furthermore, mutants of genes that play an essential role in ethylene signalling [*ethylene insensitive 2;3 (EIN2;3)* and *EIN3-like1 (EIL1)*] showed a decreased tolerance to re-oxygenation, and the activity of ethylene biosynthetic enzymes like *aminocyclopropane-1-carboxylic acid (ACC) synthases (ACS)* and ACC oxidases were found to be enhanced during re-oxygenation (Tsai *et al.*, 2014). *ACS6*, *ACS7*, and *ACS11* were induced in the early stages of re-supply of oxygen, whereas *ACS2*, *ACS4*, and *ACS8* were so in the later stages. Ethylene is perceived by the ethylene receptor 1 (ETR1), which shows a histidine kinase activity (Gamble *et al.*, 1998). The role of ETR1 in ethylene binding was also confirmed in yeast studies (Schaller & Bleecker, 1995). Interestingly, this receptor is known to be Mn-dependent: its auto-phosphorylation was promoted by Mn, but also, with a lower affinity, by Mg (Gamble *et al.*, 1998). The ethylene response sensor 1 (ERS1), that belongs to the same subfamily of ethylene receptors as ETR1, is auto-phosphorylated at a histidine and a serine residue in the presence of Mn *in vitro*, but His phosphorylation was lost in the additional presence of Mg, which lead to the assumption that this does not occur *in vivo* because both cations are present (Moussatche & Klee, 2004). The auto-phosphorylation could potentially be important for the interaction with other proteins that are involved in ethylene signalling like *constitutive triple response 1 (CTR1)*, a serine/threonine protein kinase (Gamble *et al.*, 1998). In *Rumex palustris*, a homolog of the Arabidopsis ethylene response sensor ERS1 was described to be up-regulated under submergence as also under high CO₂. It was concluded that this regulation is necessary to overcome those conditions (Vriezen *et al.*, 1997). In Arabidopsis, ETR1 is involved in the signal transduction of ethylene, and *etr1-1* mutants showed that the increase in expression of *AtERF73/HRE1* transcription factors was less compared to the wild type under hypoxia treatment (Yang *et al.*, 2011). RNAi lines of *AtERF73/HRE1* transcription factors showed a reduced induction of genes involved in glycolysis and fermentation and an increased induction of peroxidase and cytochrome P450 genes under hypoxia.

Due to the dependence of ethylene perception on Mn, the additional Mn that is translocated in Col-0 plants during re-oxygenation may increase the kinase activity of ETR1/ERS1, and thus different proteins may be activated which then would not occur in *mtp10* mutant plants. One example is CTR1 which acts downstream of ETR1 and thus is

involved in ethylene signalling (Chang *et al.*, 1993). The CTR1 protein kinase fills the gap between the ethylene receptor complex in the membrane of the ER and the transcription factors in the nucleus by directly interacting with EIN2 (Ju *et al.*, 2012): Ethylene binds to ETR1, and kinase activity of CTR1 decreases. In turn the phosphorylation of EIN2, also decreases, which results in a cleavage of the C-terminus of EIN2 from the nucleus. This again allows the ethylene signal to reach downstream transcription factors (Ju *et al.*, 2012, Bakshi *et al.*, 2015). The hypothesis, that Mn translocated by AtMTP10 under post-hypoxic stress is important for ethylene signalling may be tested indirectly by determining the response of *mtp10* mutants to ethylene under normoxia. Alternatively, a more direct approach may be the analysis of the ETR1/ERS1-dependent phosphoproteome during re-oxygenation.

4.5 AtMTP10 - a novel factor of Mn homeostasis in plants

AtMTP10 is a transporter for manganese that is located in the ER and in vesicles of the *trans*-Golgi network (TGN). Studies with an iron-sensitive yeast deletion strain also showed an ability of AtMTP10 for Fe transport for which there is currently no evidence to be physiologically relevant *in planta*. Promoter-GUS studies showed promoter activity of *AtMTP10* in the vasculature of the whole plant, which in roots is clearly defined to cells of the pericycle. Mutant lines defective in *AtMTP10*, which were grown under sufficient Mn concentrations, showed decreased shoot Mn concentrations, which led to the assumption that AtMTP10 is involved in xylem loading. This notion was confirmed by analysis of xylem exudates which showed decreased Mn translocation rates in *mtp10-1* in the dark period of the day. Both, enhanced growth of the mutant under Mn toxicity and decreased growth of those plants under Mn deficiency support the assumption of an involvement of AtMTP10 in xylem loading. A putative model of the function of AtMTP10 *in planta* is drafted in the following sketch (Fig. 37): AtMTP10 may be responsible for the transport of Mn into vesicles of the *trans*-Golgi network. These vesicles may be predetermined for exocytosis or for the transport of cations to other organelles with a demand for those cations. Due to the presence of AtMTP10 in cells of the pericycle and in case of an involvement of the *trans*-Golgi vesicles in exocytosis, AtMTP10 may be

I Discussion

involved in the movement of Mn towards the stele apoplast where it is then translocated in the xylem stream that is driven by transpiration or root pressure.

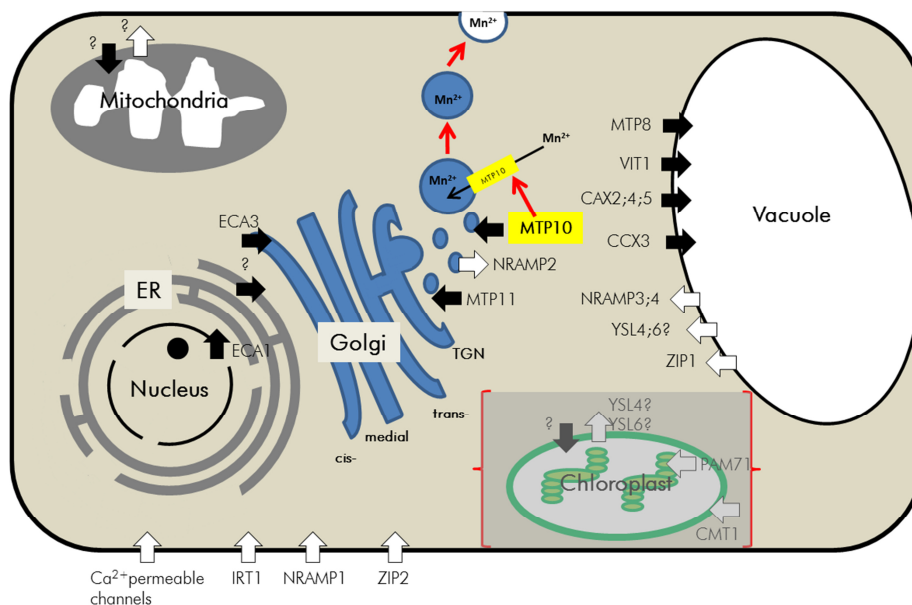


Fig. 37: Schematic representation of a hypothetical Arabidopsis cell including previously described Mn transporters and a working model for AtMTP10. White arrows: importers (transport direction into the cytosol). Black arrows: exporters (transport direction out of the cytosol).

Another evidence for the involvement of AtMTP10 in xylem loading mechanisms is the absence of the additional Mn translocation after oxygen deprivation of the root zone in *mtp10* mutant plants. This additional Mn was potentially relevant to overcome the conditions of re-oxygenation which was reflected in an increased growth of the wild type during recovering from oxygen-deprived conditions. There are various genes encoding for enzymes with a dependency on Mn in the post-anoxic/hypoxic metabolic pathways that were shown to be up-regulated during re-oxygenation. The breakdown of alanine to provide carbon and nitrogen depends on the activity of the alanine aminotransferase (AlaAT). Albeit it has not been described if AlaAT depends on Mn activation, the formation of the substrate, α -ketoglutarate, is mediated by enzymes that were shown to be Mn-dependent: isocitrate dehydrogenases and glutamate dehydrogenases. Furthermore, NAD malic enzymes, metabolizing pyruvate, were also shown to be Mn-dependent. Not only the readjustment of the C/N cycle, but also the defence of reactive oxygen species is a challenge that plants have to cope with during re-oxygenation. Low-

I Discussion

mass ROS scavengers like ascorbate and glutathione were shown to be important in this respect. Until now, only the glutathione reductase of the yeast *Cyberlindnera mraki* has been shown to depend on Mn activation.

Ethylene is known to have a profound influence on the regeneration of plants during re-oxygenation. Transcription factors that are under the control of ethylene were shown to be up-regulated under hypoxia and responsible for controlling genes important to overcome such stresses. They operate downstream of the ethylene receptor ETR1, which was shown to depend on Mn via promoting its autophosphorylation.

A number of proteins have been identified that may present potential targets for Mn translocated by AtMTP10 during re-oxygenation. The elucidation of the ones that critically depend on the activity of this transporter and thus determine Mn-dependent plant survival under those conditions represents a challenge for future work.

5 Summary

The goal of this thesis was the functional characterization of AtMTP10 in *Arabidopsis thaliana*. By employing a spectrum of molecular methods, function and roles of this protein were to be uncovered. Studies on *AtMTP10*-expressing mutants of the baker's yeast *Saccharomyces cerevisiae* showed that AtMTP10 is able to transport Mn. This is in agreement with phylogenetic data indicating that AtMTP10 is a member of the subgroup of Mn transporters of the Cation Diffusion Facilitator (CDF) family. In addition, AtMTP10 complemented a Fe-hypersensitive yeast mutant, which indicated that the protein also transports Fe, which has previously been shown for another member of the Mn subgroup of CDFs, AtMTP8. Other divalent metal cations (Cu, Co, Zn) were no substrates for AtMTP10. Expression of *AtMTP10*, examined by promoter-GUS studies, was observed in the vasculature of the whole plant, which was restricted to cells of the pericycle in roots. This provoked the hypothesis that AtMTP10 may play a role in xylem loading of Mn. This idea was supported by a partial co-localization with AtMTP11, for which an involvement in Mn secretion out of the cell has been shown before. Further co-localization experiments revealed a subcellular localization of AtMTP10 to the ER and to vesicles of the *trans*-Golgi Network. Loss-of-function mutants were employed to analyse the role of AtMTP10 *in planta*. Homozygous *mtp10* knock-out mutants showed a higher tolerance to Mn toxicity and a hypersensitivity to Mn deficiency. Shoot Mn concentrations were significantly decreased in *mtp10* mutants, while Fe and Zn concentrations were not altered. This pointed to a defect in root-to-shoot translocation of Mn. Interestingly, the Mn translocation rate in the xylem exudates differed only in the dark period between an *mtp10* mutant and the wild type. Furthermore, *mtp10* mutants were sensitive to re-oxygenation after oxygen deprivation, either triggered by submergence (hypoxia) or N₂ aeration (anoxia), in soil-, agar-, and nutrient solution-based cultivation systems. The relationship of this phenotype with AtMTP10 was confirmed by complementation lines transformed with the genomic DNA of *AtMTP10*. All experimental set-ups showed an increase in *AtMTP10* expression in the early phase of re-oxygenation. Interestingly, anoxia in the root zone was sufficient to provoke the diminished regeneration ability of *mtp10* mutants. Since an effect of AtMTP10 on Mn translocation in the xylem had been observed before, metal contents of xylem exudates immediately after re-oxygenation were

I Summary

examined. It was found that under those conditions, plants translocated increased amounts of Mn to the shoot. This response was absent in an *mtp10* mutant, suggesting that this may be the reason for its poorer regeneration ability. The physiological role of the Mn translocated by AtMTP10 after re-oxygenation remains to be elucidated, whereby initial data point to a defect of *mtp10* mutants in the utilization of alanine, which serves as C and N source in the re-oxygenation phase.

Zusammenfassung

Ziel dieser Arbeit war die funktionelle Charakterisierung von AtMTP10 in *Arabidopsis thaliana*. Mit Hilfe eines Spektrums molekularbiologischer Methoden sollten die Funktionen und die Rolle dieses Transportproteins aufgedeckt werden. Studien mit AtMTP10-exprimierenden Mutanten der Hefe *Saccharomyces cerevisiae* zeigten, dass AtMTP10 in der Lage ist, Mn zu transportieren. Dies stimmt mit der phylogenetischen Einordnung von AtMTP10 in die Mn-Untergruppe der Cation Diffusion Facilitator (CDF)-Familie überein. Daneben komplementierte AtMTP10 eine Fe-hypersensitive Hefemutante, was darauf hinweist, dass AtMTP10 auch Eisen transportiert. Dies wurde zuvor für ein anderes Mitglied der Mn-Untergruppe der CDFs, AtMTP8, gefunden. Andere divalente Metallkationen (Cu, Co, Zn) waren keine Substrate für AtMTP10. Aufgrund der in Promoter-GUS-Studien ermittelten Expression von AtMTP10 im Leitgewebe der gesamten Pflanze, die in Wurzeln lediglich auf Zellen des Perizykels beschränkt war, wurde vermutet, dass AtMTP10 eine Rolle in der Xylembeladung mit Mn spielen könnte. Diese Vermutung wurde durch die teilweise Kolokalisation mit AtMTP11 unterstützt, für das zuvor eine Beteiligung an der Mn-Sekretion aus der Zelle gezeigt wurde. Weitere Kolokalisationsexperimente zeigten die subzelluläre Lokalisation von AtMTP10 im ER und in Vesikeln des *Trans*-Golgi-Netzwerks. Durch die Verwendung von Funktionsverlustmutanten wurde die Rolle von AtMTP10 *in planta* untersucht. Homozygote *mtp10*-Knockoutmutanten zeigten eine erhöhte Toleranz gegenüber Mn-Toxizität und eine Hypersensitivität gegenüber Mn-Mangel. Mn-Konzentrationen im Spross waren in *mtp10*-Mutanten signifikant niedriger als im Wildtyp, während Fe und Zn Konzentrationen nicht verändert waren. Dies wies auf einen Defekt in der Wurzel-zu-Spross-Translokation von Mn hin. Interessanterweise unterschieden sich die Raten der Mn-Translokation im Xylem zwischen einer *mtp10*-Mutante und dem Wildtyp nur in der Dunkelperiode. Daneben waren *mtp10*-Mutanten überempfindlich gegenüber der Wiederbelüftung nach Sauerstoffmangel. Dieser Phänotyp konnte bei Wasserüberstau (Hypoxie) oder N₂-Begasung in boden-, agar- und nährlösungs-basierten Kultursystemen (Anoxie) beobachtet werden. Die Verbindung dieses Phänotyps zu AtMTP10 wurde durch Komplementationslinien, die mit genomischer DNA von AtMTP10 transformiert waren, bestätigt. Alle Versuchsansätze zeigten einen Anstieg der Expression von AtMTP10 in der

I Summary

frühen Phase der Wiederbelüftung. Um die verminderte Regenerationsfähigkeit der *mtp10*-Mutanten hervorzurufen, reichte es interessanterweise aus, lediglich die Wurzeln einem Sauerstoffmangel auszusetzen. Da im Vorfeld ein Einfluss von AtMTP10 auf die Mn-Translokation im Xylem gefunden wurde, wurden die Metallgehalte von Xylemexsudaten direkt nach der Wiederbelüftung untersucht. Hier zeigte sich, dass es unter solchen Bedingungen zu einer Erhöhung der Mn-Verlagerung in den Spross kam. Diese Reaktion blieb in der *mtp10*-Mutante aus, was darauf schließen lässt, dass dies der Grund für ihr schlechteres Regenerationsvermögen ist. Die physiologische Rolle des durch AtMTP10 nach Wiederbelüftung verlagerten Mn bleibt noch zu klären, wobei erste Untersuchungen auf einen Defekt von *mtp10*-Mutanten in der Nutzung von Alanin hinweisen, welches als C- und N-Quelle in der Wiederbelüftungsphase dient.

6 Appendix

6.1 List of primers

All primers were obtained from Eurofins Genomics, Ebersberg, Germany. The design of the primers was performed with the help of the online tools primer3 (bioinfo.ut.ee/primer3/) and NetPrimer (premierbiosoft.com/netprimer/).

Tab. 5: List of primers used in this study

name	sequence 5'→3'	restriction side
T-DNA mtp10-1_F	TCAGCGACCATGACTTGTGA	---
T-DNA mtp10-1_R	GGCATTAGCTGTAACCAGAGG	---
T-DNA mtp10-2_F	AGGGCCTATGCTCAAGATCAC	---
T-DNA mtp10-2_R	ATAAACAGAGACGGCACAACG	---
T-DNA mtp10-3_F	AGGTAGTTTTTGTACATTGGGG	---
T-DNA mtp10-3_R	TAGGGGAAGTTGTGAGAAAGAGA	---
T-DNA mtp10-4/5_F	GAGAGACTTGCGGTTCACATA	---
T-DNA mtp10-4/5_R	ATAAACAGAGACGGCACAACG	---
SALK_Lb (A)	TGGTTCACGTAGTGGGCCATCG	---
SALK_Rb (A)	TAAAACGGCTTGCCCGCTCATC	---
FLAG_Lb (4a)	CCAGGTGCCACGGAATAG	---
FLAG_Rb (4a)	GGGTTGGGGTTTCTACAGGAC	---
Ds5-2a_G-edge	TCCGTTCCGTTTTTCGTTTTTAC	---
Ds3-2a_H-edge	CCGGATCGTATCGGTTTTTCG	---
qrT_MTP10_F	TCTTTCTTTTCTCACAACTTCCC	---
qrT_MTP10_R	GCGCATCGTCTCACTAGGT	---
Random Hexamer (dN) ₆	NNNNN	---
Poly T (dT) ₃₇	TT	---
gMTP10_F	TCTGGCAGGTGGTGATGAG	SmaI
gMTP10_R	TGCTTATCTTGCGAACTGTGTCTTG	SmaI
PrMTP10_R	ATACGACTCACACAAACTCTTCG	SmaI
C-terminal YFP_F	ATGCCGCTTAACTCCTATATTTTCT	XmaI
C-terminal YFP_R	TGCGTTACACTTGTGTTCAGGACGAT	XmaI
N-terminal YFP_F	ATGCCGCTTAACTCCTATATTTTCT	BamHI
N-terminal YFP_R	CTAGTTACACTTGTGTTCAGGACGAT	BamHI
MTP10_F-NotI	ATGCCGCTTAACTCCTATATTTTCT	NotI
MTP10_R-NotI	CTAGTTACACTTGTGTTCAGGACGAT	NotI
pFL61_F2	TCAAGTTCTTAGATGCTTTCTTTT	---
pFL61_R2	GCGTAAAGGATGGGGAAAGAG	---
pART7-MCS_F	CAATCCCACTATCCTTCGCAAGA	---
mGFP5-front_R	TTGTGCCCATTAACATACCA	---
ocs-3'_R	ATGCGATCATAGGCGTCTCG	---
T3 (pGreen)	AATTAACCCTCACTAAAGGG	---
T7 (pGreen)	TAATACGACTCACTATAGGG	---

6.2 List of chemicals

Tab. 6: List of chemicals used in this study

Substance	Structure	Company	Cat. No.
2-mercaptoethanol	C ₂ H ₆ SO	Merck	15433
2-propanol	C ₃ H ₈ O	Carl Roth	T910.1
3,3'-Diaminobenzidine Tetrahydrochlorid (DAB)	C ₁₂ H ₁₄ N ₄ x 4HCl	Carl Roth	CN75.1
(3,4-Dihydroxybenzylidene) malononitrile (TYR A23)	C ₁₀ H ₆ N ₂ O ₂	Santa Cruz Biotechnology	sc-3554
3',5'-Dimethoxy-4'-hydroxyaceto- phenon (Acetosyringon)	C ₁₀ H ₁₂ O ₄	Sigma-Aldrich	D134406
5-Brom-4-chlor-3-indolyl-β-D- glucuronic acid (x-Gluc)	C ₁₄ H ₁₃ BrClNO ₇	xGluc direct	P5264044
Acridine Orange	C ₁₇ H ₁₉ N ₃	Sigma-Aldrich	235474
Agar-Agar, Kobe I	---	Carl Roth	5210.2
Ammonium sulfate	(NH ₄) ₂ SO ₄	Fluka	09980
Ampicillin sodium	C ₁₆ H ₁₈ N ₃ O ₄ SNa	Duchefa	A0104.0005
Aniline blue WS	C ₃₂ H ₂₅ N ₃ Ma ₂ O ₉ S ₃	VWR ProLab	21999.183
BASTA	---	Bayer Crop science	
Beaf extract	---	Carl Roth	X975.1
Berberine hemisulfate	C ₂₀ H ₁₈ NO ₄ x 0,5 SO ₄	Sigma-Aldrich	B3412
Biozym LE Agarose	---	Biozym Scientific	840004
Biozym Plaque agarose	---	Biozym Scientific	840101
BIS-Tris-Propane (BTP)	C ₁₁ H ₂₆ N ₂ O ₆	Sigma-Aldrich	B6755
Boric acid	H ₃ BO ₃	Carl Roth	6943.1
Bovine serum albumin (BSA)	---	Carl Roth	T844.2
Calcium chloride dihydrate	CaCl ₂ x 2H ₂ O	Sigma-Aldrich	31307
Casein hydrolysate	---	Carl Roth	AE41.1
Cobalt chloride	CoCl ₂ x 6H ₂ O	Riedel deHaen	12914
Complete Supplement Mixture (CSM) Drop-Out: -URA	---	Formedium™	DCS0169
Copper sulfate pentahydrate	CuSO ₄ x 5H ₂ O	Riedel deHaen	31293
Dimethylsulfoxide (DMSO)	C ₂ H ₆ OS	Carl Roth	7029.1
Dithiothreitol (DTT)	C ₄ H ₁₀ O ₂ S ₂	Carl Roth	6908.3
DL-Phosphinothricin	C ₅ H ₁₅ N ₂ O ₄ P	Duchefa	P0159.0250
D-Sorbit	C ₆ H ₁₄ O ₆	Carl Roth	6213.1
Ethanol	C ₂ H ₆ O	Carl Roth	9065.2
Ethylene glycol tetraacetic acid (EGTA)	C ₁₄ H ₂₄ N ₂ O ₁₀	Carl Roth	3054.2
Ethylenediaminetetraacetic acid (EDTA)	C ₁₀ H ₁₆ N ₂ O ₈	Fluka	03680
Ferric chloride	FeCl ₃ x 6H ₂ O	Merck	3943
Gentamycin sulphate	---	Duchefa	G0124.0001
Glucose	C ₆ H ₁₂ O ₆	Carl Roth	HN06.2
Glycerol	C ₃ H ₈ O ₃	Carl Roth	3783.2
hydrochloric acid	HCl	Merck	K34997717
Hydrogen peroxide	H ₂ O ₂	Carl Roth	8070.1
Iron-sodium EDTA	FeNaEDTA	Duchefa	E0509.1000
Iva-Val-Val-Sta-Ala-Sta (Pepstatin A)	C ₃₄ H ₆₃ N ₅ O ₉	Carl Roth	2936.1
Kanamycin monosulfate	C ₁₈ H ₃₆ N ₄ O ₁₁ x H ₂ SO ₄	Carl Roth	T832.1
Magnesium ATP	C ₁₀ H ₁₆ N ₅ O ₁₃ P ₃ · xMg ²⁺	Sigma-Aldrich	20-113
Magnesium chloride	MgCl ₂	Merck	5833.1000
Magnesium sulfate heptahydrate	MgSO ₄ x 7H ₂ O	Sigma-Aldrich	63140
Manganese sulfate	MnSO ₄ x H ₂ O	Fluka	M7634
Mannitol	C ₆ H ₁₄ O ₆	Sigma-Aldrich	M1902
MES	C ₆ H ₁₃ NO ₄ S	Sigma-Aldrich	M2933

I Appendix

Murashige & Skoog salts + vitamins (MS+Vit)	---	Duchefa	M0231.0025
N-acetyl-L-Leucyl-L-leucyl-arginal (Leupeptin Hemisulfate)	$C_{20}H_{38}N_6O_4 \times 0,5H_2SO_4$	Carl Roth	CN33.1
Natriummolybdat dihydrate	$NaMoO_4 \times 2H_2O$	Carl Roth	0274.1
Nitric acid	HNO_3	Carl Roth	X943.1
Nitro blue tetrazolium chloride (NBT)	$C_{40}H_{30}Cl_2N_{10}O_6$	Carl Roth	4421.3
Octoxinol 9 (Triton X-100)	$C_{14}H_{22}O(C_2H_4O)_n$ (n=9-10)	Fluka	93426
Phenylmethylsulfonyl fluoride (PMSF)	$C_7H_7FO_2S$	Sigma-Aldrich	78830
Phyto-agar	---	Duchefa	P1003.1000
Poly(ethylene glycol)4000 (PEG4000)	$H(OCH_2CH_2)_nOH$	Sigma-Aldrich	95904
Polyvinylpyrrolidone (40kDa) (PVP40)	$(C_6H_9NO)_n$	Sigma -Aldrich	EC201-800-4
Potassium chloride	KCl	Duchefa	P0515.1000
Potassium dihydrogen phosphate	KH_2PO_4	Fluka	60220
Potassium hexacyanoferrate	$K_3[Fe_2(CN)_6]$ (III)	Fluka	60300
Potassium hexacyanoferrate-II-Trihydrat	$K_4[Fe_2(CN)_6]$ (II) $\times 3 H_2O$	neoLab	9570.0500
Potassium hydroxide	KOH	Fluka	60375
Potassium nitrate	KNO_3	Sigma-Aldrich	P8291
Roti Quant	---	Carl Roth	K015.3
Silwet L-77	---	Lehle Seeds	Vis-O2
Sodium chloride	NaCl	Carl Roth	3957.1
Sodium Dodecyl sulfate (SDS)	$NaC_{12}H_{25}SO_4$	Carl Roth	CN30.2
Sodium Hypo chlorite	NaClO	Carl Roth	9062.4
Spectinomycin dihydrochloride Pentahydrate	$C_{14}H_{24}N_2O_7 \times 2HCl \times 5H_2O$	Duchefa	S0188:0005
Sucrose	$C_{12}H_{22}O_{11}$	Carl Roth	4621.1
Tris(hydroxymethyl)aminomethane (Tris)	$C_4H_{11}NO_3$	Carl Roth	AE15.2
Triton™ X-100	t-Oct- C_6H_4- (OCH_2CH_2) _x OH, x= 9-10	Fluka	93426
Tryptone	---	Formedium™	TRP02
YeastExtract	---	Formedium™	YEM02
Yeast Nitrogen Base without Amino Acids & Calcium Chloride	---	Formedium™	CYN2501
Zinc sulfate heptahydrate	$ZnSO_4 \times 7H_2O$	Riedel deHaen	31665

6.3 List of enzymes

Tab. 7: List of enzymes used in this study

Enzymes	Cut side	overhangs	Company	Cat. No.
BamHI	GGATCC	5' - GATC	New England Biolabs	R0136S
Cellulase Onozuka R-10	---	---	Duchefa Biochemie	C8001.0010
DNase I	---	---	Omega bio-tek, USA	E1091-02
GoTaq G2 DNA Polymerase	---	---	Promega	M784B
Macerozyme R-10	---	---	Duchefa Biochemie	M8002.0010
M-MuLV reverse Transcriptase	---	---	New England Biolabs	M0253S
NotI	GCGGCCGC	5' - GGCC	New England Biolabs	R0189S
Pectolyase Y-23	---	---	Duchefa Biochemie	P8004.0001
Phusion HF DNA Polymerase	---	---	New England Biolabs	M0530S
Protoscript II	---	---	New England Biolabs	M0368
SmaI	CCCGGG	blunt	New England Biolabs	R0141S
SuperScript [®] II reverse Transcriptase	---	---	Life Technologies	18064014
T4 DNA Ligase	---	---	New England Biolabs	M02025
Shrimp alkaline phosphatase (SAP)	---	---	NEB	M0371S
XmaI	CCCGGG	5' - CCGG	New England Biolabs	R0180S
Zymolyase 20T	---	---	amsbio	120491-1

6.4 List of figures and tables

- Fig. 1: Schematic representation of known Mn transporter in Arabidopsis cells.
- Fig. 2: Schematic representation of metabolic pathways of plant species with a different tolerance to submergence.
- Fig. 3: Structure of AtMTP10.
- Fig. 4: Absence/presence of *AtMTP10* transcript shown by reverse transcriptase-PCR (rT-PCR).
- Fig. 5: Expression of *AtMTP10* in four different overexpressor lines determined by quantitative real time PCR (qRT PCR).
- Fig. 6: Expression of *AtMTP10* in four different complementation lines determined by quantitative real time PCR (qRT PCR).
- Fig. 7: Ten-fold dilution series of *Saccharomyces cerevisiae* wild type and deletion strains.
- Fig. 8: *pmr1Δ* cells expressing *AtMTP10-YFP*.
- Fig. 9: Mn contents in *pmr1Δ* cells expressing *AtMTP10* or carrying the empty vector.
- Fig. 10: ⁵⁴Mn transport assay with endosomal membrane vesicles.
- Fig. 11: Acridin orange test of endosomal membrane vesicles.
- Fig. 12: Cotyledons of five independent PrMTP10-GUS lines stained for GUS activity.
- Fig. 13: Promoter GUS studies.
- Fig. 14: Subcellular Localization of MTP10 in Arabidopsis mesophyll protoplasts.
- Fig. 15: Co-localization of MTP10-EYFP with ER-mCherry in tobacco.
- Fig. 16: Co-localization of MTP10-EYFP with SYP61-mCherry in tobacco.
- Fig. 17: Localization studies with Tyrphostin A23 or Mn in tobacco protoplasts transformed with pBART-MTP10-EYFP.
- Fig. 18: Growth of *mtp10-1* under Mn toxicity.
- Fig. 19: Growth of *mtp10-4* under Mn toxicity.
- Fig. 20: Growth of *mtp10-1::gMTP10.1* under Mn toxicity.
- Fig. 21: Growth *mtp10-1* under Mn deficiency.
- Fig. 22: Analysis of xylem exudates.

I Appendix

- Fig. 23: Analysis of xylem exudates in the course of the day.
- Fig. 24: Analysis of xylem exudates in the course of the day (II).
- Fig. 25: Analysis of the metal composition of shoots from plants analysed for xylem exudates.
- Fig. 26: Expression of *AtMTP10* in the course of the day determined by quantitative real time PCR (qRT PCR).
- Fig. 27: Microarray data of *AtMTP10* during and after oxygen deprivation from GEO repository (<https://www.ncbi.nlm.nih.gov/geo/>).
- Fig. 28: T-DNA insertion lines of *AtMTP* genes under submergence.
- Fig. 29: Promoter GUS studies of *PrMTP10* during re-aeration.
- Fig. 30: Growth of *mtp10-1* under re-oxygenation after anoxia conditions on agar plates.
- Fig. 31: Growth of *mtp10-1* under anoxia conditions on liquid culture media.
- Fig. 32: Analysis of xylem exudates of plants transiently exposed to oxygen deprivation under anoxia conditions.
- Fig. 33: Analysis of xylem exudates of plants transiently exposed to oxygen deprivation under anoxia conditions (II).
- Fig. 34: Analysis of xylem exudates of *AtMTP10* complementation line transiently exposed to oxygen deprivation under anoxia conditions (II).
- Fig. 35: Growth of *mtp10-1* and *mtp10-gMTP10.2* on different nitrogen sources.
- Fig. 36: Proposed pathways of metabolisms under hypoxia and during re-oxygenation
- Fig. 37: Schematic representation of a hypothetical Arabidopsis cell including previously described Mn transporter and a putative working model of AtMTP10.
- Tab. 1: Growth media for *E.coli* cells
- Tab. 2: Constructs used in this study
- Tab. 3: Growth media for *Agrobacterium tumefaciens* cells
- Tab. 4: Growth media for *Saccharomyces cerevisiae* cells
- Tab. 5: List of primers used in this study
- Tab. 6: List of chemicals used in this study

I Appendix

Tab. 7: List of enzymes used in this study

6.5 Reference list

Abreu I. A., Cabelli D. E. (2010). Superoxide dismutases-a review of the metal-associated mechanistic variations. *Biochimica et Biophysica Acta* **1804**: 263-274.

Alejandro S., Cailliatte R., Alcon C., Dirick L., Domergue F., Correia D., Castaings L., Briat J. F., Mari S., Curie C. (2017). Intracellular Distribution of Manganese by the Trans-Golgi Network Transporter NRAMP2 Is Critical for Photosynthesis and Cellular Redox Homeostasis. *Plant Cell* **29**: 3068-3084.

Allen M. D., Kropat J., Tottey S., Del Campo J. A., Merchant S. S. (2007). Manganese deficiency in *Chlamydomonas* results in loss of photosystem II and MnSOD function, sensitivity to peroxides, and secondary phosphorus and iron deficiency. *Plant Physiology* **143**: 263-277.

Alscher R. G., Erturk N., Heath L. S. (2002). Role of superoxide dismutases (SODs) in controlling oxidative stress in plants. *Journal of Experimental Botany* **53**: 1331-1341.

Arpat A. B., Magliano P., Wege S., Rouached H., Stefanovic A., Poirier Y. (2012). Functional expression of PHO1 to the Golgi and trans-Golgi network and its role in export of inorganic phosphate. *The Plant Journal* **71**: 479-491.

Arrivault S., Senger T., Kramer U. (2006). The Arabidopsis metal tolerance protein AtMTP3 maintains metal homeostasis by mediating Zn exclusion from the shoot under Fe deficiency and Zn oversupply. *The Plant Journal* **46**: 861-879.

Arteca R. N., Arteca J. M. (2000). A novel method for growing *Arabidopsis thaliana* plants hydroponically. *Physiologia Plantarum* **108**: 188-193.

Bailey-Serres J., Fukao T., Gibbs D. J., Holdsworth M. J., Lee S. C., Licausi F., Perata P., Voeselek L. A., Van Dongen J. T. (2012). Making sense of low oxygen sensing. *Trends in Plant Science* **17**: 129-138.

Bailey-Serres J., Voeselek L. a. C. J. (2008). Flooding stress: Acclimations and genetic diversity. *Annual Review of Plant Biology* **59**: 313-339.

Bakshi A., Wilson R. L., Lacey R. F., Kim H., Wupalapapati S. K., Binder B. (2015). Identification of regions in the receiver domain of the ETHYLENE RESPONSE1 ethylene receptor of Arabidopsis important for functional divergence. *Plant Physiology* **169**: 219-232.

I Reference list

Banbury D. N., Oakley J. D., Sessions R. B., Banting G. (2003). Tyrphostin A23 inhibits internalization of the transferrin receptor by perturbing the interaction between tyrosine motifs and the medium chain subunit of the AP-2 adaptor complex. *Journal of Biological Chemistry* **278**: 12022-12028.

Barber D. A., Lee R. B. (1974). The effect of micro-organisms on the absorption of manganese by plants. *New Phytologist* **73**: 97-106.

Barberon M., Zelazny E., Robert S., Conejero G., Curie C., Friml J., Vert G. (2011). Monoubiquitin-dependent endocytosis of the iron-regulated transporter 1 (IRT1) transporter controls iron uptake in plants. *Proceedings of the National Academy of Sciences of the United States of America* **108**: E450-E458.

Biemelt S., Keetman U., Albrecht G. (1998). Re-aeration following hypoxia or anoxia leads to activation of the antioxidative defense system in roots of wheat seedlings. *Plant Physiology* **116**: 651-658.

Blasing O. E., Gibon Y., Gunther M., Hohne M., Morcuende R., Osuna D., Thimm O., Usadel B., Scheible W. R., Stitt M. (2005). Sugars and circadian regulation make major contributions to the global regulation of diurnal gene expression in *Arabidopsis*. *Plant Cell* **17**: 3257-3281.

Blaudez D., Kohler A., Martin F., Sanders D., Chalot M. (2003). Poplar metal tolerance protein 1 confers zinc tolerance and is an oligomeric vacuolar zinc transporter with an essential leucine zipper motif. *Plant Cell* **15**: 2911-2928.

Blokhina O., Virolainen E., Fagerstedt K. V. (2003). Antioxidants, oxidative damage and oxygen deprivation stress: a review. *Annals of Botany* **91**: 179-194.

Blom C. W. P. M., Voeselek L. a. C. J. (1996). Flooding: The survival strategies of plants. *Trends in Ecology & Evolution* **11**: 290-295.

Bowler C., Montagu M. V., Inzé D. (1992). Superoxide dismutase and stress tolerance. *Annual Review of Plant Biology* **43**: 83-116.

Bradl H. B. (2004). Adsorption of heavy metal ions on soils and soils constituents. *Journal of Colloid and Interface Science* **277**: 1-18.

Branco-Price C., Kaiser K. A., Jang C. J. H., Larive C. K., Bailey-Serres J. (2008). Selective mRNA translation coordinates energetic and metabolic adjustments to cellular oxygen deprivation and reoxygenation in *Arabidopsis thaliana*. *The Plant Journal* **56**: 743-755.

Brundrett M. C., Enstone D. E., Peterson C. A. (1988). A berberine-aniline blue fluorescent staining procedure for suberin, lignin, and callose in plant-tissue. *Protoplasma* **146**: 133-142.

Bueno P., Varela J., Gimenez-Gallego G., Del Rio L. A. (1995). Peroxisomal copper, zinc superoxide dismutase. Characterization of the isoenzyme from watermelon cotyledons. *Plant Physiology* **108**: 1151-1160.

Burnell J. N., 1988. The biochemistry of manganese in plants. In: **Graham RD**, ed. *Manganese in Soils and Plants*. Dordrecht, NL: Kluwer Academic Publishers, 125-137.

Cailliatte R., Lapeyre B., Briat J. F., Mari S., Curie C. (2009). The NRAMP6 metal transporter contributes to cadmium toxicity. *Biochemical Journal* **422**: 217-228.

Cailliatte R., Schikora A., Briat J. F., Mari S., Curie C. (2010). High-affinity manganese uptake by the metal transporter NRAMP1 is essential for Arabidopsis growth in low manganese conditions. *Plant Cell* **22**: 904-917.

Castaigns L., Caquot A., Loubet S., Curie C. (2016). The high-affinity metal Transporters NRAMP1 and IRT1 Team up to Take up Iron under Sufficient Metal Provision. *Scientific Reports* **6**: 37222.

Chang C., Kwok S. F., Bleecker A. B., Meyerowitz E. M. (1993). Arabidopsis ethylene-response gene ETR1: similarity of product to two-component regulators. *Science* **262**: 539-544.

Chang R., Jang C. J. H., Branco-Price C., Nghiem P., Bailey-Serres J. (2012). Transient MPK6 activation in response to oxygen deprivation and reoxygenation is mediated by mitochondria and aids seedling survival in Arabidopsis. *Plant Molecular Biology* **78**: 109-122.

Chen Z., Fujii Y., Yamaji N., Masuda S., Takemoto Y., Kamiya T., Yusuyin Y., Iwasaki K., Kato S., Maeshima M., Ma J. F., Ueno D. (2013). Mn tolerance in rice is mediated by MTP8.1, a member of the cation diffusion facilitator family. *Journal of Experimental Botany* **64**: 4375-4387.

I Reference list

Cheng N. H., Pittman J. K., Shigaki T., Hirschi K. D. (2002). Characterization of CAX4, an Arabidopsis H⁺/cation antiporter. *Plant Physiology* **128**: 1245-1254.

Christianson J. A., Wilson I. W., Llewellyn D. J., Dennis E. S. (2009). The low-oxygen-induced NAC domain transcription factor ANAC102 affects viability of Arabidopsis seeds following low-oxygen treatment. *Plant Physiology* **149**: 1724-1738.

Chu H. H., Car S., Socha A. L., Hindt M. N., Punshon T., Guerinot M. L. (2017). The Arabidopsis MTP8 transporter determines the localization of manganese and iron in seeds. *Scientific Reports* **7**: 11024.

Clarkson D. T., Carvajal M., Henzler T., Waterhouse R. N., Smyth A. J., Cooke D. T., Steudle E. (2000). Root hydraulic conductance: diurnal aquaporin expression and the effects of nutrient stress. *Journal of Experimental Botany* **51**: 61-70.

Clough S. J., Bent A. F. (1998). Floral dip: a simplified method for *Agrobacterium*-mediated transformation of *Arabidopsis thaliana*. *The Plant Journal* **16**: 735-743.

Colmer T. D., Greenway H. (2011). Ion transport in seminal and adventitious roots of cereals during O₂ deficiency. *Journal of Experimental Botany* **62**: 39-57.

Conklin D. S., McMaster J. A., Culbertson M. R., Kung C. (1992). COT1, a gene involved in cobalt accumulation in *Saccharomyces cerevisiae*. *Molecular and Cellular Biology* **12**: 3678-3688.

Culotta V. C., Yang M., Hall M. D. (2005). Manganese transport and trafficking: Lessons learned from *Saccharomyces cerevisiae*. *Eukaryotic Cell* **4**: 1159-1165.

Curie C., Alonso J. M., Le J. M., Ecker J. R., Briat J. F. (2000). Involvement of NRAMP1 from *Arabidopsis thaliana* in iron transport. *Biochemical Journal* **347 Pt 3**: 749-755.

Curie C., Cassin G., Couch D., Divol F., Higuchi K., Jean M., Misson J., Schikora A., Czernic P., Mari S. (2009). Metal movement within the plant: contribution of nicotianamine and yellow stripe 1-like transporters. *Annals of Botany* **103**: 1-11.

Curie C., Panaviene Z., Loulergue C., Dellaporta S. L., Briat J. F., Walker E. L. (2001). Maize yellow stripe1 encodes a membrane protein directly involved in Fe(III) uptake. *Nature* **409**: 346-349.

I Reference list

Delhaize E., Gruber B. D., Pittman J. K., White R. G., Leung H., Miao Y., Jiang L., Ryan P. R., Richardson A. E. (2007). A role for the *AtMTP11* gene of Arabidopsis in manganese transport and tolerance. *The Plant Journal* **51**: 198-210.

Delhaize E., Kataoka T., Hebb D. M., White R. G., Ryan P. R. (2003). Genes encoding proteins of the cation diffusion facilitator family that confer manganese tolerance. *Plant Cell* **15**: 1131-1142.

Diab H., Limami A. M. (2016). Reconfiguration of N Metabolism upon Hypoxia Stress and Recovery: Roles of Alanine Aminotransferase (AlaAT) and Glutamate Dehydrogenase (GDH). *Plants (Basel)* **5**: 25.

Dodd A. N., Salathia N., Hall A., Kevei E., Toth R., Nagy F., Hibberd J. M., Millar A. J., Webb A. a. R. (2005). Plant circadian clocks increase photosynthesis, growth, survival, and competitive advantage. *Science* **309**: 630-633.

Drew M. C. (1992). Soil aeration and plant-root metabolism. *Soil Science* **154**: 259-268.

Drew M. C. (1997). Oxygen deficiency and root metabolism: Injury and acclimation under hypoxia and anoxia. *Annual Review of Plant Physiology and Plant Molecular Biology* **48**: 223-250.

Ducic T., Leinemann L., Finkeldey R., Polle A. (2006). Uptake and translocation of manganese in seedlings of two varieties of Douglas fir (*Pseudotsuga menziesii* var. *viridis* and *glauca*). *New Phytologist* **170**: 11-20.

Ducic T., Polle A. (2005). Transport and detoxification of manganese and copper in plants. *Brazilian Journal of Plant Physiology* **17**: 103-112.

Durr G., Strayle J., Plemper R., Elbs S., Klee S. K., Catty P., Wolf D. H., Rudolph H. K. (1998). The medial-Golgi ion pump Pmr1 supplies the yeast secretory pathway with Ca²⁺ and Mn²⁺ required for glycosylation, sorting, and endoplasmic reticulum-associated protein degradation. *Molecular Biology of the Cell* **9**: 1149-1162.

Edmond C., Shigaki T., Ewert S., Nelson M. D., Connorton J. M., Chalova V., Noordally Z., Pittman J. K. (2009). Comparative analysis of CAX2-like cation transporters indicates functional and regulatory diversity. *Biochemical Journal* **418**: 145-154.

I Reference list

Eide D., Broderius M., Fett J., Guerinot M. L. (1996). A novel iron-regulated metal transporter from plants identified by functional expression in yeast. *Proceedings of the National Academy of Sciences of the United States of America* **93**: 5624-5628.

Eisenhut M., Hoecker N., Schmidt S. B., Basgaran R. M., Flachbart S., Jahns P., Eser T., Geimer S., Husted S., Weber A. P. M., Leister D., Schneider A. (2018). The plastid envelope CHLOROPLAST MANGANESE TRANSPORTER1 is essential for manganese homeostasis in Arabidopsis. *Molecular Plant* **11**: 955-969.

Elble R. (1992). A simple and efficient procedure for transformation of yeasts. *Biotechniques* **13**: 18-20.

Ellis M. H., Dennis E. S., Peacock W. J. (1999). Arabidopsis roots and shoots have different mechanisms for hypoxic stress tolerance. *Plant Physiology* **119**: 57-64.

Erbasol I., Bozdogan G. O., Koc A., Pedas P., Karakaya H. C. (2013). Characterization of two genes encoding metal tolerance proteins from *Beta vulgaris* subspecies *maritima* that confers manganese tolerance in yeast. *Biometals* **26**: 795-804.

Eroglu S., Giehl R. F. H., Meier B., Takahashi M., Terada Y., Ignatyev K., Andresen E., Kupper H., Peiter E., Von Wiren N. (2017). Metal Tolerance Protein 8 Mediates Manganese Homeostasis and Iron Reallocation during Seed Development and Germination. *Plant Physiology* **174**: 1633-1647.

Eroglu S., Meier B., Von Wiren N., Peiter E. (2016). The vacuolar manganese transporter MTP8 determines tolerance to iron deficiency-induced chlorosis in Arabidopsis. *Plant Physiology* **170**: 1030-1045.

Fageria N. K., Baligar V. C., Clark R. B. (2002). Micronutrients in crop production. *Advances in Agronomy* **77**: 185-268.

Fan S. C., Lin C. S., Hsu P. K., Lin S. H., Tsay Y. F. (2009). The Arabidopsis nitrate transporter NRT1.7, expressed in phloem, is responsible for source-to-sink remobilization of nitrate. *Plant Cell* **21**: 2750-2761.

Fecht-Christoffers M. M., Braun H. P., Lemaitre-Guillier C., Vandorselaer A., Horst W. J. (2003a). Effect of Manganese toxicity on the proteome of the leaf apoplast in cowpea. *Plant Physiology* **133**: 1935-1946.

Fecht-Christoffers M. M., Maier P., Horst W. J. (2003b). Apoplastic peroxidases and ascorbate are involved in manganese toxicity and tolerance of *Vigna unguiculata*. *Physiologia Plantarum* **117**: 237-244.

Fontaine J. X., Terce-Laforgue T., Armengaud P., Clement G., Renou J. P., Pelletier S., Catterou M., Azzopardi M., Gibon Y., Lea P. J., Hirel B., Dubois F. (2012). Characterization of a NADH-dependent glutamate dehydrogenase mutant of *Arabidopsis* demonstrates the key role of this enzyme in root carbon and nitrogen metabolism. *Plant Cell* **24**: 4044-4065.

Frank J., Happeck R., Meier B., Hoang M. T. T., Stribny J., Hause G., Ding H., Morsomme P., Baginsky S., Peiter E. (2018). Chloroplast-localized BICAT proteins shape stromal calcium signals and are required for efficient photosynthesis. *New Phytologist*.

Gamble R. L., Coonfield M. L., Schaller G. E. (1998). Histidine kinase activity of the ETR1 ethylene receptor from *Arabidopsis*. *Proceedings of the National Academy of Sciences of the United States of America* **95**: 7825-7829.

Gao H., Xie W., Yang C., Xu J., Li J., Wang H., Chen X., Huang C. F. (2018). NRAMP2, a trans-Golgi network-localized manganese transporter, is required for *Arabidopsis* root growth under manganese deficiency. *New Phytologist* **217**: 179-193.

Garland W. J., Dennis D. T. (1977). Steady-state kinetics of glutamate dehydrogenase from *Pisum sativum* L. mitochondria. *Archives of biochemistry and biophysics* **182**: 614-625.

Gazzarrini S., Lejay L., Gojon A., Ninnemann O., Frommer W. B., Von Wiren N. (1999). Three functional transporters for constitutive, diurnally regulated, and starvation-induced uptake of ammonium into *Arabidopsis* roots. *Plant Cell* **11**: 937-948.

Geigenberger P. (2003). Response of plant metabolism to too little oxygen. *Current Opinion in Plant Biology* **6**: 247-256.

George T. S., French A. S., Brown L. K., Karley A. J., White P. J., Ramsay L., Daniell T. J. (2014). Genotypic variation in the ability of landraces and commercial cereal varieties to avoid manganese deficiency in soils with limited manganese availability: is there a role for root-exuded phytases? *Physiologia Plantarum* **151**: 243-256.

Ghiorse W. C., (1988). The biology of manganese transforming microorganisms in soil. In. *Manganese in Soils and Plants*. Springer, 75-85.

I Reference list

Gibbs J., Greenway H. (2003). Mechanisms of anoxia tolerance in plants. I. Growth, survival and anaerobic catabolism. *Functional Plant Biology* **30**: 1-47.

Gleave A. P. (1992). A Versatile Binary Vector System with A T-Dna Organizational-Structure Conducive to Efficient Integration of Cloned Dna Into the Plant Genome. *Plant Molecular Biology* **20**: 1203-1207.

Gonzalez-Carranza Z. H., Shahid A. A., Zhang L., Liu Y., Ninsuwan U., Roberts J. A. (2012). A novel approach to dissect the abscission process in Arabidopsis. *Plant Physiology* **160**: 1342-1356.

Groen A. J., Sancho-Andres G., Breckels L. M., Gatto L., Aniento F., Lilley K. S. (2014). Identification of trans-golgi network proteins in *Arabidopsis thaliana* root tissue. *Journal of Proteome Research* **13**: 763-776.

Guerinot M. L. (2000). The ZIP family of metal transporters. *Biochimica et Biophysica Acta-Biomembranes* **1465**: 190-198.

Hamburger D., Rezzonico E., Petetot J. M. C., Somerville C., Poirier Y. (2002). Identification and characterization of the Arabidopsis PHO1 gene involved in phosphate loading to the xylem. *Plant Cell* **14**: 889-902.

Haney C. J., Grass G., Franke S., Rensing C. (2005). New developments in the understanding of the cation diffusion facilitator family. *Journal of Industrial Microbiology and Biotechnology* **32**: 215-226.

Hattori Y., Nagai K., Furukawa S., Song X. J., Kawano R., Sakakibara H., Wu J., Matsumoto T., Yoshimura A., Kitano H., Matsuoka M., Mori H., Ashikari M. (2009). The ethylene response factors SNORKEL1 and SNORKEL2 allow rice to adapt to deep water. *Nature* **460**: 1026-1030.

Hauck M., Paul A., Gross S., Raubuch M. (2003). Manganese toxicity in epiphytic lichens: chlorophyll degradation and interaction with iron and phosphorus. *Environmental and Experimental Botany* **49**: 181-191.

Hawes C., Satiat-Jeunemaitre B. (2005). The plant Golgi apparatus - Going with the flow. *Biochimica et Biophysica Acta-Molecular Cell Research* **1744**: 93-107.

Haydon M. J., Bell L. J., Webb A. A. (2011). Interactions between plant circadian clocks and solute transport. *Journal of Experimental Botany* **62**: 2333-2348.

Haydon M. J., Cobbett C. S. (2007). Transporters of ligands for essential metal ions in plants. *New Phytologist* **174**: 499-506.

Haydon M. J., Roman A., Arshad W. (2015). Nutrient homeostasis within the plant circadian network. *Frontiers in Plant Science* **6**: 299.

He Z. L. L., Yang X. E., Stoffella P. J. (2005). Trace elements in agroecosystems and impacts on the environment. *Journal of Trace Elements in Medicine and Biology* **19**: 125-140.

Hebbern C. A., Laursen K. H., Ladegaard A. H., Schmidt S. B., Pedas P., Bruhn D., Schjoerring J. K., Wulfsohn D., Husted S. (2009). Latent manganese deficiency increases transpiration in barley (*Hordeum vulgare*). *Physiologia Plantarum* **135**: 307-316.

Hellens R. P., Edwards E. A., Leyland N. R., Bean S., Mullineaux P. M. (2000). pGreen: a versatile and flexible binary Ti vector for *Agrobacterium*-mediated plant transformation. *Plant Molecular Biology* **42**: 819-832.

Hinz M., Wilson I. W., Yang J., Buerstenbinder K., Llewellyn D., Dennis E. S., Sauter M., Dolferus R. (2010). Arabidopsis RAP2.2: an ethylene response transcription factor that is important for hypoxia survival. *Plant Physiology* **153**: 757-772.

Hodges M., Flesch V., Galvez S., Bismuth E. (2003). Higher plant NADP⁺-dependent isocitrate dehydrogenases, ammonium assimilation and NADPH production. *Plant Physiology and Biochemistry* **41**: 577-585.

Ishimaru Y., Masuda H., Bashir K., Inoue H., Tsukamoto T., Takahashi M., Nakanishi H., Aoki N., Hirose T., Ohsugi R., Nishizawa N. K. (2010). Rice metal-nicotianamine transporter, OsYSL2, is required for the long-distance transport of iron and manganese. *The Plant Journal* **62**: 379-390.

Ishimaru Y., Takahashi R., Bashir K., Shimo H., Senoura T., Sugimoto K., Ono K., Yano M., Ishikawa S., Arai T., Nakanishi H., Nishizawa N. K. (2012). Characterizing the role of rice NRAMP5 in Manganese, Iron and Cadmium Transport. *Scientific Reports* **2**: 286.

Ismond K. P., Dolferus R., De Pauw M., Dennis E. S., Good A. G. (2003). Enhanced low oxygen survival in *Arabidopsis* through increased metabolic flux in the fermentative pathway. *Plant Physiology* **132**: 1292-1302.

Jefferson R. A., Kavanagh T. A., Bevan M. W. (1987). Gus Fusions - β -Glucuronidase as a sensitive and versatile gene fusion marker in higher-plants. *EMBO Journal* **6**: 3901-3907.

Ju C., Yoon G. M., Shemansky J. M., Lin D. Y., Ying Z. I., Chang J., Garrett W. M., Kessenbrock M., Groth G., Tucker M. L. (2012). CTR1 phosphorylates the central regulator EIN2 to control ethylene hormone signaling from the ER membrane to the nucleus in *Arabidopsis*. *Proceedings of the National Academy of Sciences of the United States of America* **109**: 19486-19491.

Kasai K., Takano J., Miwa K., Toyoda A., Fujiwara T. (2011). High boron-induced ubiquitination regulates vacuolar sorting of the BOR1 borate transporter in *Arabidopsis thaliana*. *Journal of Biological Chemistry* **286**: 6175-6183.

Kim S. A., Punshon T., Lanzirotti A., Li L. T., Alonso J. M., Ecker J. R., Kaplan J., Guerinot M. L. (2006). Localization of iron in *Arabidopsis* seed requires the vacuolar membrane transporter VIT1. *Science* **314**: 1295-1298.

Kirch H. H., Schlingensiepen S., Kotchoni S., Sunkar R., Bartels D. (2005). Detailed expression analysis of selected genes of the aldehyde dehydrogenase (ALDH) gene superfamily in *Arabidopsis thaliana*. *Plant Molecular Biology* **57**: 315-332.

Klok E. J., Wilson I. W., Wilson D., Chapman S. C., Ewing R. M., Somerville S. C., Peacock W. J., Dolferus R., Dennis E. S. (2002). Expression profile analysis of the low-oxygen response in *Arabidopsis* root cultures. *Plant Cell* **14**: 2481-2494.

Kobae Y., Uemura T., Sato M. H., Ohnishi M., Mimura T., Nakagawa T., Maeshima M. (2004). Zinc transporter of *Arabidopsis thaliana* AtMTP1 is localized to vacuolar membranes and implicated in zinc homeostasis. *Plant Cell Physiology* **45**: 1749-1758.

Korshunova Y. O., Eide D., Clark W. G., Guerinot M. L., Pakrasi H. B. (1999). The IRT1 protein from *Arabidopsis thaliana* is a metal transporter with a broad substrate range. *Plant Molecular Biology* **40**: 37-44.

Kotchoni S. O., Kuhns C., Ditzer A., Kirch H. H., Bartels D. (2006). Over-expression of different aldehyde dehydrogenase genes in *Arabidopsis thaliana* confers tolerance to abiotic stress and protects plants against lipid peroxidation and oxidative stress. *Plant Cell and Environment* **29**: 1033-1048.

Kothari S. K., Marschner H., Römheld V. (1991). Effect of a vesicular-arbuscular mycorrhizal fungus and rhizosphere micro-organisms on manganese reduction in the rhizosphere and manganese concentrations in maize (*Zea mays L.*). *New Phytologist* **117**: 649-655.

Kreuzwieser J., Harren F. J. M., Laarhoven L. J. J., Boamfa I., Te Lintel-Hekkert S., Scheerer U., Huglin C., Rennenberg H. (2001). Acetaldehyde emission by the leaves of trees - correlation with physiological and environmental parameters. *Physiologia Plantarum* **113**: 41-49.

Lanquar V., Lelievre F., Bolte S., Hames C., Alcon C., Neumann D., Vansuyt G., Curie C., Schroder A., Kramer U., Barbier-Brygoo H., Thomine S. (2005). Mobilization of vacuolar iron by AtNRAMP3 and AtNRAMP4 is essential for seed germination on low iron. *EMBO Journal* **24**: 4041-4051.

Lapinskas P. J., Cunningham K. W., Liu X. F., Fink G. R., Culotta V. C. (1995). Mutations in PMR1 suppress oxidative damage in yeast cells lacking superoxide dismutase. *Molecular and Cellular Biology* **15**: 1382-1388.

Lee C. P., Eubel H., Millar A. H. (2010). Diurnal changes in mitochondrial function reveal daily optimization of light and dark respiratory metabolism in *Arabidopsis*. *Molecular & Cellular Proteomics* **9**: 2125-2139.

Lee S. C., Mustroph A., Sasidharan R., Vashisht D., Pedersen O., Oosumi T., Voeselek L. a. C. J., Bailey-Serres J. (2011). Molecular characterization of the submergence response of the *Arabidopsis thaliana* ecotype Columbia. *New Phytologist* **190**: 457-471.

Lemaitre T., Hodges M. (2006). Expression analysis of *Arabidopsis thaliana* NAD-dependent isocitrate dehydrogenase genes shows the presence of a functional subunit that is mainly expressed in the pollen and absent from vegetative organs. *Plant and Cell Physiology* **47**: 634-643.

Leskova A., Giehl R. F. H., Hartmann A., Fargasova A., Von Wiren N. (2017). Heavy Metals Induce Iron Deficiency Responses at Different Hierarchic and Regulatory Levels. *Plant Physiology* **174**: 1648-1668.

Leterrier M., Barroso J. B., Palma J. M., Corpas F. J. (2012). Cytosolic NADP-isocitrate dehydrogenase in *Arabidopsis* leaves and roots. *Biologia Plantarum* **56**: 705-710.

I Reference list

Li L., Chen O. S., Mcvey W. D., Kaplan J. (2001). CCC1 is a transporter that mediates vacuolar iron storage in yeast. *Journal of Biological Chemistry* **276**: 29515-29519.

Li X. Y., Chanroj S., Wu Z. Y., Romanowsky S. M., Harper J. F., Sze H. (2008). A distinct endosomal Ca²⁺/Mn²⁺ pump affects root growth through the secretory process. *Plant Physiology* **147**: 1675-1689.

Licausi F., Kosmacz M., Weits D. A., Giuntoli B., Giorgi F. M., Voeselek L. A., Perata P., Van Dongen J. T. (2011). Oxygen sensing in plants is mediated by an N-end rule pathway for protein destabilization. *Nature* **479**: 419-422.

Licausi F., Van Dongen J. T., Giuntoli B., Novi G., Santaniello A., Geigenberger P., Perata P. (2010). HRE1 and HRE2, two hypoxia-inducible ethylene response factors, affect anaerobic responses in *Arabidopsis thaliana*. *The Plant Journal* **62**: 302-315.

Lidon F. C., Barreiro M. G., Ramalho J. C. (2004). Manganese accumulation in rice: implications for photosynthetic functioning. *Plant Physiology* **161**: 1235-1244.

Liepman A. H., Olsen L. J. (2003). Alanine aminotransferase homologs catalyze the glutamate : glyoxylate aminotransferase reaction in peroxisomes of *Arabidopsis*. *Plant Physiology* **131**: 215-227.

Limami A. M., Glevarec G., Ricoult C., Cliquet J. B., Planchet E. (2008). Concerted modulation of alanine and glutamate metabolism in young *Medicago truncatula* seedlings under hypoxic stress. *Journal of Experimental Botany* **59**: 2325-2335.

Logan D. C., Leaver C. J. (2000). Mitochondria-targeted GFP highlights the heterogeneity of mitochondrial shape, size and movement within living plant cells. *Journal of Experimental Botany* **51**: 865-871.

Lopez F., Bousser A., Sissoeff I., Gaspar M., Lachaise B., Hoarau J., Mahe A. (2003). Diurnal regulation of water transport and aquaporin gene expression in maize roots: contribution of PIP2 proteins. *Plant Cell Physiology* **44**: 1384-1395.

Loreti E., Poggi A., Novi G., Alpi A., Perata P. (2005). A genome-wide analysis of the effects of sucrose on gene expression in *Arabidopsis* seedlings under anoxia. *Plant Physiology* **137**: 1130-1138.

I Reference list

Luis A., Lyon D. S., Olah I., Glick B., Salin M. L. (1983). Immunocytochemical evidence for a peroxisomal localization of manganese superoxide dismutase in leaf protoplasts from a higher plant. *Planta* **158**: 216-224.

Luk E., Culotta V. C. (2001). Manganese superoxide dismutase in *Saccharomyces cerevisiae* acquires its metal co-factor through a pathway involving the Nramp metal transporter, Smf2p. *Journal of Biological Chemistry* **276**: 47556-47562.

Luk E., Jensen L. T., Culotta V. C. (2003). The many highways for intracellular trafficking of metals. *Journal of Biological Inorganic Chemistry Society* **8**: 803-809.

Maeda T., Sugiura R., Kita A., Saito M., Deng L., He Y., Yabin L., Fujita Y., Takegawa K., Shuntoh H., Kuno T. (2004). Pmr1, a P-type ATPase, and Pdt1, an Nramp homologue, cooperatively regulate cell morphogenesis in fission yeast: The importance of Mn²⁺ homeostasis. *Genes to Cells* **9**: 71-82.

Marschner H., 1995. *Mineral Nutrition of Higher Plants*. London, UK: Academic Press.

Maser P., Thomine S., Schroeder J. I., Ward J. M., Hirschi K., Sze H., Talke I. N., Amtmann A., Maathuis F. J., Sanders D., Harper J. F., Tchieu J., Gribskov M., Persans M. W., Salt D. E., Kim S. A., Guerinot M. L. (2001). Phylogenetic relationships within cation transporter families of Arabidopsis. *Plant Physiology* **126**: 1646-1667.

Meguro N., Tsuji H., Suzuki Y., Tsutsumi N., Hirai A., Nakazono M. (2006). Analysis of expression of genes for mitochondrial aldehyde dehydrogenase in maize during submergence and following re-aeration. *Breeding Science* **56**: 365-370.

Merchant S., Sawaya M. R. (2005). The light reactions: a guide to recent acquisitions for the picture gallery. *Plant Cell* **17**: 648-663.

Migocka M., Papierniak A., Kosieradzka A., Posyniak E., Maciaszczyk-Dziubinska E., Biskup R., Garbiec A., Marchewka T. (2015). Cucumber metal tolerance protein CsMTP9 is a plasma membrane H⁺-coupled antiporter involved in the Mn²⁺ and Cd²⁺ efflux from root cells. *The Plant Journal* **84**: 1045-1058.

Migocka M., Papierniak A., Maciaszczyk-Dziubinska E., Pozdzik P., Posyniak E., Garbiec A., Filleur S. (2014). Cucumber metal transport protein MTP8 confers increased tolerance to manganese when expressed in yeast and *Arabidopsis thaliana*. *Journal of Experimental Botany* **65**: 5367-5384.

Miki T., Tsujimoto Y., Miyabe S., Sugiyama K., Izawa S., Inoue Y., Kimura A. (1996). Oxidative stress response in yeast: purification and characterization of glutathione reductase from *Hansenula mrakii*. *Bioscience, Biotechnology, and Biochemistry* **60**: 1207-1209.

Millaleo R., Reyes-Diaz M., Ivanov A. G., Mora M. L., Alberdi M. (2010). Manganese as essential and toxic element for plants: transport, accumulation and resistance mechanisms. *Journal of Soil Science and Plant Nutrition* **10**: 476-494.

Mills R. F., Doherty M. L., López-Marqués R. L., Weimar T., Dupree P., Palmgren M. G., Pittman J. K., Williams L. E. (2008). ECA3, a Golgi-localized P₂A-type ATPase, plays a crucial role in manganese nutrition in *Arabidopsis*. *Plant Physiology* **146**: 116-128.

Milner M. J., Seamon J., Craft E., Kochian L. V. (2013). Transport properties of members of the ZIP family in plants and their role in Zn and Mn homeostasis. *Journal of Experimental Botany* **64**: 369-381.

Minet M., Dufour M. E., Lacroute F. (1992). Complementation of *Saccharomyces cerevisiae* auxotrophic mutants by *Arabidopsis thaliana* cDNAs. *The Plant Journal* **2**: 417-422.

Miyashita Y., Dolferus R., Ismond K. P., Good A. G. (2007). Alanine aminotransferase catalyses the breakdown of alanine after hypoxia in *Arabidopsis thaliana*. *The Plant Journal* **49**: 1108-1121.

Monk L. S., Braendle R., Crawford R. M. M. (1987a). Catalase activity and postanoxic injury in monocotyledonous Species. *Journal of Experimental Botany* **38**: 233-246.

Monk L. S., Fagerstedt K. V., Crawford R. M. M. (1987b). Superoxide-dismutase as an anaerobic polypeptide - a key factor in recovery from oxygen deprivation in *Iris-Pseudacorus*. *Plant Physiology* **85**: 1016-1020.

Monk L. S., Fagerstedt K. V., Crawford R. M. M. (1989). Oxygen-toxicity and superoxide-dismutase as an antioxidant in physiological stress. *Physiologia Plantarum* **76**: 456-459.

Montanini B., Blaudez D., Jeandroz S., Sanders D., Chalot M. (2007). Phylogenetic and functional analysis of the Cation Diffusion Facilitator (CDF) family: improved signature and prediction of substrate specificity. *BMC Genomics* **8**: 1-16.

Mora M. L., Alfaro M. A., Jarvis S. C., Demanet R., Cartes P. (2006). Soil aluminium availability in Andisols of southern Chile and its effect on forage production and animal metabolism. *Soil Use and Management* **22**: 95-101.

Morgan M. J., Lehmann M., Schwarzlander M., Baxter C. J., Sienkiewicz-Porzucek A., Williams T. C. R., Schauer N., Fernie A. R., Fricker M. D., Ratcliffe R. G., Sweetlove L. J., Finkemeier I. (2008). Decrease in manganese superoxide dismutase leads to reduced root growth and affects tricarboxylic acid cycle flux and mitochondrial redox homeostasis. *Plant Physiology* **147**: 101-114.

Morris J., Tian H., Park S., Sreevidya C. S., Ward J. M., Hirschi K. D. (2008). AtCCX3 is an Arabidopsis endomembrane H⁺-dependent K⁺ transporter. *Plant Physiology* **148**: 1474-1486.

Moussatche P., Klee H. J. (2004). Autophosphorylation activity of the Arabidopsis ethylene receptor multigene family. *Journal of Biological Chemistry* **279**: 48734-48741.

Mustroph A., Barding G. A., Jr., Kaiser K. A., Larive C. K., Bailey-Serres J. (2014). Characterization of distinct root and shoot responses to low-oxygen stress in Arabidopsis with a focus on primary C- and N-metabolism. *Plant, Cell and Environment* **37**: 2366-2380.

Mustroph A., Lee S. C., Oosumi T., Zanetti M. E., Yang H., Ma K., Yaghoubi-Masihi A., Fukao T., Bailey-Serres J. (2010). Cross-kingdom comparison of transcriptomic adjustments to low-oxygen stress highlights conserved and plant-specific responses. *Plant Physiology* **152**: 1484-1500.

Mustroph A., Zanetti M. E., Jang C. J., Holtan H. E., Repetti P. P., Galbraith D. W., Girke T., Bailey-Serres J. (2009). Profiling transcriptomes of discrete cell populations resolves altered cellular priorities during hypoxia in Arabidopsis. *Proceedings of the National Academy of Sciences of the United States of America* **106**: 18843-18848.

Nelson B. K., Cai X., Nebenfuhr A. (2007). A multicolored set of in vivo organelle markers for co-localization studies in Arabidopsis and other plants. *The Plant Journal* **51**: 1126-1136.

Nevo Y., Nelson N. (2006). The NRAMP family of metal-ion transporters. *Biochimica et Biophysica Acta* **1763**: 609-620.

I Reference list

Ni L., Zhou J., Hurley T. D., Weiner H. (1999). Human liver mitochondrial aldehyde dehydrogenase: three-dimensional structure and the restoration of solubility and activity of chimeric forms. *Protein Science* **8**: 2784-2790.

Ni W., Robertson E. F., Reeves H. C. (1986). Purification and characterization of cytosolic NADP specific isocitric dehydrogenase from *Pisum sativum*. *Federation Proceedings* **45**: 1891-1891.

Nies D. H., Silver S. (1995). Ion efflux systems involved in bacterial metal resistances. *Journal of Industrial Microbiology and Biotechnology* **14**: 186-199.

Noordally Z. B., Ishii K., Atkins K. A., Wetherill S. J., Kusakina J., Walton E. J., Kato M., Azuma M., Tanaka K., Hanaoka M., Dodd A. N. (2013). Circadian control of chloroplast transcription by a nuclear-encoded timing signal. *Science* **339**: 1316-1319.

O'neal D., Joy K. W. (1974). Glutamine synthetase of pea leaves: divalent cation effects, substrate specificity, and other properties. *Plant Physiology* **54**: 773-779.

Oomen R. J., Wu J., Lelievre F., Blanchet S., Richaud P., Barbier-Brygoo H., Aarts M. G., Thomine S. (2009). Functional characterization of NRAMP3 and NRAMP4 from the metal hyperaccumulator *Thlaspi caerulescens*. *New Phytologist* **181**: 637-650.

Palmiter R. D., Findley S. D. (1995). Cloning and functional characterization of a mammalian zinc transporter that confers resistance to zinc. *EMBO Journal* **14**: 639-649.

Pantazis D. A., Ames W., Cox N., Lubitz W., Neese F. (2012). Two interconvertible structures that explain the spectroscopic properties of the oxygen-evolving complex of photosystem II in the S2 state. *Angewandte Chemie International Edition* **51**: 9935-9940.

Papadakis I. E., Giannakoula A., Therios I. N., Bosabalidis A. M., Moustakas M., Nastou A. (2007). Mn-induced changes in leaf structure and chloroplast ultrastructure of *Citrus volkameriana* (L.) plants. *Plant Physiology* **164**: 100-103.

Pedas P., Schiller S. M., Hegelund J. N., Ladegard A. H., Schjoerring J. K., Husted S. (2014). Golgi localized barley MTP8 proteins facilitate Mn transport. *PLoS One* **9**: e113759.

Pedas P., Ytting C. K., Fuglsang A. T., Jahn T. P., Schjoerring J. K., Husted S. (2008). Manganese efficiency in barley: identification and characterization of the metal ion transporter HvIRT1. *Plant Physiology* **148**: 455-466.

Peiter E., Montanini B., Gobert A., Pedas P., Husted S., Maathuis F. J., Blaudez D., Chalot M., Sanders D. (2007). A secretory pathway-localized cation diffusion facilitator confers plant manganese tolerance. *Proceedings of the National Academy of Sciences of the United States of America* **104**: 8532-8537.

Pittman J. K. (2005). Managing the manganese: molecular mechanisms of manganese transport and homeostasis. *New Phytologist* **167**: 733-742.

Pittman J. K., Shigaki T., Marshall J. L., Morris J. L., Cheng N.-H., Hirschi K. D. (2004). Functional and regulatory analysis of the *Arabidopsis thaliana* CAX2 cation transporter. *Plant Molecular Biology* **56**: 959-971.

Podar D., Scherer J., Noordally Z., Herzyk P., Nies D., Sanders D. (2012). Metal selectivity determinants in a family of transition metal transporters. *Journal of Biological Chemistry* **287**: 3185-3196.

Poirier Y., Thoma S., Somerville C., Schiefelbein J. (1991). Mutant of *Arabidopsis* deficient in xylem loading of phosphate. *Plant Physiology* **97**: 1087-1093.

Rawlyer A., Arpagaus S., Braendle R. (2002). Impact of oxygen stress and energy availability on membrane stability of plant cells. *Annals of Botany* **90**: 499-507.

Rengel Z., Marschner P. (2005). Nutrient availability and management in the rhizosphere: exploiting genotypic differences. *New Phytologist* **168**: 305-312.

Ricard B., Couee I., Raymond P., Saglio P. H., Saintges V., Pradet A. (1994). Plant-metabolism under hypoxia and anoxia. *Plant Physiology and Biochemistry* **32**: 1-10.

Rutherford A. W. (1989). Photosystem II, the water-splitting enzyme. *Trends in Biochemical Sciences* **14**: 227-232.

Sakamoto M., Munemura I., Tomita R., Kobayashi K. (2008). Reactive oxygen species in leaf abscission signaling. *Plant Signaling & Behaviour* **3**: 1014-1015.

Sauter M. (2013). Root responses to flooding. *Current Opinion in Plant Biology* **16**: 282-286.

Schaaf G., Catoni E., Fitz M., Schwacke R., Schneider A., Von Wiren N., Frommer W. B. (2002). A putative role for the vacuolar calcium/manganese proton antiporter AtCAX2 in heavy metal detoxification. *Plant Biology* **4**: 612-618.

Schaaf G., Ludewig U., Erenoglu B. E., Mori S., Kitahara T., Von Wiren N. (2004). ZmYS1 functions as a proton-coupled symporter for phytosiderophore- and nicotianamine-chelated metals. *Journal of Biological Chemistry* **279**: 9091-9096.

Schaller G. E., Bleecker A. B. (1995). Ethylene-binding sites generated in yeast expressing the Arabidopsis ETR1 gene. *Science* **270**: 1809-1811.

Schmidt S. B., Jensen P. E., Husted S. (2016). Manganese deficiency in plants: the impact on photosystem II. *Trends in Plant Science* **21**: 622-632.

Schneider A., Steinberger I., Herdean A., Gandini C., Eisenhut M., Kurz S., Morper A., Hoecker N., Ruhle T., Labs M., Flugge U. I., Geimer S., Schmidt S. B., Husted S., Weber A. P., Spetea C., Leister D. (2016). The Evolutionarily Conserved Protein PHOTOSYNTHESIS AFFECTED MUTANT71 Is Required for Efficient Manganese Uptake at the Thylakoid Membrane in Arabidopsis. *Plant Cell* **28**: 892-910.

Schrader M., Fahimi H. D. (2006). Peroxisomes and oxidative stress. *Biochimica et Biophysica Acta* **1763**: 1755-1766.

Shingaki-Wells R., Millar A. H., Whelan J., Narsai R. (2014). What happens to plant mitochondria under low oxygen? An omics review of the responses to low oxygen and reoxygenation. *Plant, Cell and Environment* **37**: 2260-2277.

Simpson D. J., Robinson S. P. (1984). Freeze-fracture ultrastructure of thylakoid membranes in chloroplasts from manganese-deficient plants. *Plant Physiology* **74**: 735-741.

Skutnik M., Rychter A. M. (2009). Differential response of antioxidant systems in leaves and roots of barley subjected to anoxia and post-anoxia. *Plant Physiology* **166**: 926-937.

Socha A. L., Guerinot M. L. (2014). Mn-euvering manganese: the role of transporter gene family members in manganese uptake and mobilization in plants. *Frontiers in Plant Science* **5**: 106.

Steffens B., Steffen-Heins A., Sauter M. (2013). Reactive oxygen species mediate growth and death in submerged plants. *Frontiers in Plant Science* **4**: 179.

I Reference list

Stevenson F. J., 1994. *Humus chemistry: genesis, composition, reactions*. John Wiley & Sons.

Sugiura Y., Kawabe H., Tanaka H., Fujimoto S., Ohara A. (1981). Purification, enzymatic properties, and active site environment of a novel manganese(III)-containing acid phosphatase. *Journal of Biology and Chemistry* **256**: 10664-10670.

Sweetlove L. J., Beard K. F. M., Nunes-Nesi A., Fernie A. R., Ratcliffe R. G. (2010). Not just a circle: flux modes in the plant TCA cycle. *Trends in Plant Science* **15**: 462-470.

Takagi S. I., Nomoto K., Takemoto T. (1984). Physiological aspect of mugineic acid, a possible phytosiderophore of graminaceous plants. *Journal of Plant Nutrition* **7**: 469-477.

Takano J., Noguchi K., Yasumori M., Kobayashi M., Gajdos Z., Miwa K., Hayashi H., Yoneyama T., Fujiwara T. (2002). Arabidopsis boron transporter for xylem loading. *Nature* **420**: 337-340.

Takase T., Ishikawa H., Murakami H., Kikuchi J., Sato-Nara K., Suzuki H. (2011). The circadian clock modulates water dynamics and aquaporin expression in Arabidopsis roots. *Plant Cell Physiology* **52**: 373-383.

Thomine S., Lelievre F., Debarbieux E., Schroeder J. I., Barbier-Brygoo H. (2003). AtNRAMP3, a multispecific vacuolar metal transporter involved in plant responses to iron deficiency. *The Plant Journal* **34**: 685-695.

Thomine S., Wang R., Ward J. M., Crawford N. M., Schroeder J. I. (2000). Cadmium and iron transport by members of a plant metal transporter family in Arabidopsis with homology to Nramp genes. *Proceedings of the National Academy of Sciences of the United States of America* **97**: 4991-4996.

Tronconi M. A., Fahnenstich H., Weehler M. C. G., Andreo C. S., Flugge U. I., Drincovich M. F., Maurino V. G. (2008). Arabidopsis NAD-malic enzyme functions as a homodimer and heterodimer and has a major impact on nocturnal metabolism. *Plant Physiology* **146**: 1540-1552.

Tronconi M. A., Maurino V. G., Andreo C. S., Drincovich M. F. (2010). Three different and tissue-specific NAD-malic enzymes generated by alternative subunit association in Arabidopsis thaliana. *Journal of Biological Chemistry* **285**: 11870-11879.

- Tronconi M. A., Wheeler M. C. G., Drincovich M. E., Andreo C. S.** (2012). Differential fumarate binding to Arabidopsis NAD⁺-malic enzymes 1 and-2 produces an opposite activity modulation. *Biochimie* **94**: 1421-1430.
- Tsai K. J., Chou S. J., Shih M. C.** (2014). Ethylene plays an essential role in the recovery of Arabidopsis during post-anaerobiosis reoxygenation. *Plant Cell and Environment* **37**: 2391-2405.
- Tsuji H., Meguro N., Suzuki Y., Tsutsumi N., Hirai A., Nakazono M.** (2003). Induction of mitochondrial aldehyde dehydrogenase by submergence facilitates oxidation of acetaldehyde during re-aeration in rice. *Febs Letters* **546**: 369-373.
- Tsukamoto T., Nakanishi H., Kiyomiya S., Watanabe S., Matsuhashi S., Nishizawa N. K., Mori S.** (2006). ⁵²Mn translocation in barley monitored using a positron-emitting tracer imaging system. *Journal of Soil Science and Plant Nutrition* **52**: 717-725.
- Tsunemitsu Y., Yamaji N., Ma J. F., Kato S. I., Iwasaki K., Ueno D.** (2018). Rice reduces Mn uptake in response to Mn stress. *Plant Signaling & Behaviour* **13**: e1422466.
- Ueno D., Sasaki A., Yamaji N., Miyaji T., Fujii Y., Takemoto Y., Moriyama S., Che J., Moriyama Y., Iwasaki K., Ma J. F.** (2015). A polarly localized transporter for efficient manganese uptake in rice. *Nature Plants* **1**: 15170.
- Ueoka-Nakanishi H., Tsuchiya T., Sasaki M., Nakanishi Y., Cunningham K. W., Maeshima M.** (2000). Functional expression of mung bean Ca²⁺/H⁺ antiporter in yeast and its intracellular localization in the hypocotyl and tobacco cells. *European Journal of Biochemistry* **267**: 3090-3098.
- Ushimaru T., Kanematsu S., Katayama M., Tsuji H.** (2001). Antioxidative enzymes in seedlings of *Nelumbo nucifera* germinated under water. *Physiologia Plantarum* **112**: 39-46.
- Ushimaru T., Shibasaka M., Tsuji H.** (1992). Development of the O₂⁻-detoxification system during adaptation to air of submerged rice seedlings. *Plant and Cell Physiology* **33**: 1065-1071.
- Van Dongen J. T., Frohlich A., Ramirez-Aguilar S. J., Schauer N., Fernie A. R., Erban A., Kopka J., Clark J., Langer A., Geigenberger P.** (2009). Transcript and metabolite profiling of the adaptive response to mild decreases in oxygen concentration in the roots of Arabidopsis plants. *Annals of Botany* **103**: 269-280.

Vantoai T. T., Bolles C. S. (1991). Postanoxic injury in soybean (*Glycine-Max*) seedlings. *Plant Physiology* **97**: 588-592.

Vert G. A., Briat J. F., Curie C. (2003). Dual regulation of the Arabidopsis high-affinity root iron uptake system by local and long-distance signals. *Plant Physiology* **132**: 796-804.

Vervuren P. J. A., Blom C. W. P. M., De Kroon H. (2003). Extreme flooding events on the Rhine and the survival and distribution of riparian plant species. *Journal of Ecology* **91**: 135-146.

Von Wiren N., Mori S., Marschner H., Romheld V. (1994). Iron inefficiency in maize mutant Ys1 (*Zea-Mays* l Cv Yellow-Stripe) is caused by a defect in uptake of iron phytosiderophores. *Plant Physiology* **106**: 71-77.

Vriezen W. H., Van Rijn C. P., Voeselek L. A., Mariani C. (1997). A homolog of the Arabidopsis thaliana ERS gene is actively regulated in Rumex palustris upon flooding. *The Plant Journal* **11**: 1265-1271.

Waters B. M., Chu H. H., Didonato R. J., Roberts L. A., Easley R. B., Lahner B., Salt D. E., Walker E. L. (2006). Mutations in Arabidopsis yellow stripe-like1 and yellow stripe-like3 reveal their roles in metal ion homeostasis and loading of metal ions in seeds. *Plant Physiology* **141**: 1446-1458.

White P. J., Bowen H. C., Demidchik V., Nichols C., Davies J. A. (2002). Genes for calcium-permeable channels in the plasma membrane of plant root cells. *Biochimica et Biophysica Acta-Biomembranes* **1564**: 299-309.

Wilkinson R. E., Ohki K. (1988). Influence of manganese deficiency and toxicity on isoprenoid syntheses. *Plant Physiology* **87**: 841-846.

Winter D., Vinegar B., Nahal H., Ammar R., Wilson G. V., Provart N. J. (2007). An "Electronic Fluorescent Pictograph" browser for exploring and analyzing large-scale biological data sets. *PLoS One* **2**: e718.

Winzeler E. A., Shoemaker D. D., Astromoff A., Liang H., Anderson K., Andre B., Bangham R., Benito R., Boeke J. D., Bussey H., Chu A. M., Connelly C., Davis K., Dietrich F., Dow S. W., El Bakkoury M., Foury F., Friend S. H., Gentalen E., Giaever G., Hegemann J. H., Jones T., Laub M., Liao H., Liebundguth N., Lockhart D. J., Lucau-Danila A., Lussier M., M'rabet N., Menard P., Mittmann M., Pai C., Rebischung C., Revuelta J. L., Riles L., Roberts C. J., Ross-Macdonald P., Scherens B., Snyder M., Sookhai-Mahadeo S., Storms R. K., Veronneau S., Voet M., Volckaert G., Ward T. R., Wysocki R., Yen G. S., Yu K. X., Zimmermann K., Philippsen P., Johnston M., Davis R. W. (1999). Functional characterization of the *S-cerevisiae* genome by gene deletion and parallel analysis. *Science* **285**: 901-906.

Wissemeyer A. H., Horst W. J. (1992). Effect of light-intensity on manganese toxicity symptoms and callose formation in cowpea (*Vigna-Unguiculata (L) Walp*). *Plant and Soil* **143**: 299-309.

Wu Z., Liang F., Hong B., Young J. C., Sussman M. R., Harper J. F., Sze H. (2002). An endoplasmic reticulum-bound $\text{Ca}^{2+}/\text{Mn}^{2+}$ pump, ECA1, supports plant growth and confers tolerance to Mn^{2+} stress. *Plant Physiology* **130**: 128-137.

Wymer C. L., Bibikova T. N., Gilroy S. (1997). Cytoplasmic free calcium distributions during the development of root hairs in *Arabidopsis thaliana*. *The Plant Journal* **12**: 427-439.

Yalovsky S., Trueblood C. E., Callan K. L., Narita J. O., Jenkins S. M., Rine J., Grissem W. (1997). Plant farnesyltransferase can restore yeast Ras signaling and mating. *Molecular and Cellular Biology* **17**: 1986-1994.

Yang C. Y., Hsu F. C., Li J. P., Wang N. N., Shih M. C. (2011). The AP2/ERF transcription factor AtERF73/HRE1 modulates ethylene responses during hypoxia in *Arabidopsis*. *Plant Physiology* **156**: 202-212.

Yang T. J., Perry P. J., Ciani S., Pandian S., Schmidt W. (2008). Manganese deficiency alters the patterning and development of root hairs in *Arabidopsis*. *Journal of Experimental Botany* **59**: 3453-3464.

Yen M. R., Tseng Y. H., Saier M. H. (2001). Maize Yellow Stripe1, an iron-phytosiderophore uptake transporter, is a member of the oligopeptide transporter (OPT) family. *Microbiology Society Journals* **147**: 2881-2883.

Yeung E., Van Veen H., Vashisht D., Sobral Paiva A. L., Hummel M., Rankenberg T., Steffens B., Steffen-Heins A., Sauter M., De Vries M., Schuurink R. C., Bazin J., Bailey-Serres J., Voeselek L., Sasidharan R. (2018). A stress recovery signaling network for enhanced flooding tolerance in *Arabidopsis thaliana*. *Proceedings of the National Academy of Sciences of the United States of America* **115**: E6085-E6094.

Yu Q., Osborne L. D., Rengel Z. (1999). Increased tolerance to Mn deficiency in transgenic tobacco overproducing superoxide dismutase. *Annals of Botany* **84**: 543-547.

Yuan L. B., Dai Y. S., Xie L. J., Yu L. J., Zhou Y., Lai Y. X., Yang Y. C., Xu L., Chen Q. F., Xiao S. (2017). Jasmonate Regulates Plant Responses to Postsubmergence Reoxygenation through Transcriptional Activation of Antioxidant Synthesis. *Plant Physiology* **173**: 1864-1880.

Zhang B., Zhang C., Liu C., Jing Y., Wang Y., Jin L., Yang L., Fu A., Shi J., Zhao F., Lan W., Luan S. (2018). Inner Envelope CHLOROPLAST MANGANESE TRANSPORTER 1 Supports Manganese Homeostasis and Phototrophic Growth in Arabidopsis. *Molecular Plant* **11**: 943-954.

Zhang M., Liu B. (2017). Identification of a rice metal tolerance protein OsMTP11 as a manganese transporter. *PLoS One* **12**: e0174987.

Zhang W., Gruszewski H. A., Chevone B. I., Nessler C. L. (2008). An Arabidopsis purple acid phosphatase with phytase activity increases foliar ascorbate. *Plant Physiology* **146**: 431-440.

Zhao H., Eide D. (1996). The ZRT2 gene encodes the low affinity zinc transporter in *Saccharomyces cerevisiae*. *Journal of Biological Chemistry* **271**: 23203-23210.

Zhao Y. F., Lei M. K., Wu Y. X., Wang C. W., Zhang Z. S., Deng F., Wang H. B. (2009). Molecular cloning and expression of the complete DNA sequence encoding NAD⁺-dependent acetaldehyde dehydrogenase from *Acinetobacter sp* strain HBS-2. *Annals of Microbiology* **59**: 97-104.

Zimmermann P., Hirsch-Hoffmann M., Hennig L., Gruissem W. (2004). GENEVESTIGATOR. Arabidopsis microarray database and analysis toolbox. *Plant Physiology* **136**: 2621-2632.

I Reference list

Zouni A., Witt H. T., Kern J., Fromme P., Krauss N., Saenger W., Orth P. (2001). Crystal structure of photosystem II from *Synechococcus elongatus* at 3.8 angstrom resolution. *Nature* **409**: 739-743.

7 Publications

7.1 Peer-reviewed papers

Eroglu, S., Meier, B., von Wiren, N., Peiter, E. (2016). The vacuolar manganese transporter MTP8 determines tolerance to iron deficiency-induced chlorosis in Arabidopsis. *Plant Physiology* **170**: 1030-1045

Eroglu, S., Giehl, R. F. H., Meier, B., Takahashi, M., Terada, Y., Ignatyev, K., Andresen, E., Kupper, H., Peiter, E., von Wiren, N. (2017). Metal Tolerance Protein 8 mediates manganese homeostasis and iron re-allocation during seed development and germination. *Plant Physiology* **174**: 1633-1647

Frank, J., Happeck, R., Meier, B., Hoang, M.T.T., Stribny, J., Hause, G., Ding, H., Morsomme, P., Baginsky, S., Peiter, E. (2018). Chloroplast-localized BICAT proteins shape stromal calcium signals and are required for efficient photosynthesis. *New Phytologist* **xx**: xx-xx. DOI: 10.1111/nph.15407.

7.2 Poster presentations

Höller S, **Meier B**, Mijovilovich A, Küpper H, Peiter E (2018). A CDF transporter determines metal translocation and redistribution in Arabidopsis thaliana under deficiency and resupply.

Presented at:

- Annual Meeting of the German Society of Plant Nutrition, 13 - 14 September 2018, Osnabrück, Germany.
1st prize at poster awards.

Meier B, Diercks I, Steudtel T, Peiter E (2018). Calcium signals in response to ammonium.

Presented at:

- Annual Meeting of the German Society of Plant Nutrition, 13 - 14 September 2018, Osnabrück, Germany.

Höller S, Eroglu S, Giehl RFH, **Meier B**, Andresen E, Ignatyev K, Garrevoet J, Falkenberg G, Küpper H, Peiter E, von Wirén N (2017). Impact of MTP8 on metal enrichment and localization in seeds of *Arabidopsis thaliana*.

Presented at:

- XVIII International Plant Nutrition Colloquium, 19-24 August 2017, Copenhagen, Denmark.

I Publications

Meier B, Diercks I, Peiter E (2017). Regulation of ammonium and nitrate uptake by calcium signalling.

Presented at:

- Plant Nutrition 2017: Annual Meeting of the German Society of Plant Nutrition (DGP), 05-06 May 2017, Gießen, Germany.
2st prize at poster awards.

Meier B, Fierlbeck L, Kirsten A, Nies D, Mustroph A, Peiter E (2015). Increasing manganese translocation after oxygen deficiency: a tool to manage resistance to waterlogging?

Presented at:

- Botanikertagung 2015, 30 August – 03 September, Freising, Germany.
- Plant Nutrition 2015: Annual Meeting of the German Society of Plant Nutrition (DGP), 17-18 September 2015, Göttingen, Germany.

Meier B, Fierlbeck L, Kirsten A, Nies D, Mustroph A, Peiter E (2014). Survival of Arabidopsis under post-anoxia conditions depends on a vascular manganese transporter.

Presented at:

- 17th International Symposium on Iron Nutrition and Interactions in Plants, 6 - 10 July 2014, Gatersleben, Germany.

Eroğlu S, **Meier B**, von Wirén N, Peiter E (2014). A manganese transporter essential for iron deficiency in Arabidopsis.

Presented at:

- 17th International Symposium on Iron Nutrition and Interactions in Plants, 6 - 10 July 2014, Gatersleben, Germany.
- Plant Nutrition 2014: International Conference of the German Society of Plant Nutrition, 10 - 12 September 2014, Halle (Saale), Germany.

Eroğlu S, **Meier B**, von Wirén N, Peiter E (2013). Characterization of a Mn transporter essential for Fe efficiency in *Arabidopsis thaliana*.

Presented at:

- XVII. International Plant Nutrition Colloquium, 19-22 August 2013, Istanbul, Turkey.
1st prize at poster awards.

Meier B, Kirsten A, Fierlbeck L, Nies D, Mustroph A, Peiter E (2013). A vascular manganese and iron transporter required for submergence tolerance of Arabidopsis.

Presented at:

- XVII. International Plant Nutrition Colloquium, 19-22 August 2013, Istanbul, Turkey.

I Publications

Meier B, Chen X, Peiter-Volk T, Peter K, Mustroph A, Peiter E (2012). An intracellular manganese transporter required for submergence tolerance of Arabidopsis.

Presented at:

- Challenges for Plant Nutrition in Changing Environments: International Workshop and Meeting of the German Society of Plant Nutrition, 05-08 September 2012, Bonn, Germany.
- Annual Meeting of the German Society of Plant Nutrition, 09-10 May 2013, Weißenstephan, Germany.

Meier B, Chen X, Gwinner A, Höroldt M, Peter K, Thor K, Peiter E (2011). Three Novel Transporters: Guiding manganese to the destined place.

Presented at:

- Annual Meeting of the German Society of Plant Nutrition, 27-29 September 2011, Kiel, Germany. **Published in:** *Mitteilungen der Gesellschaft für Pflanzenbauwissenschaften* **23**, 150, Verlag Liddy Halm (ISSN 0934-5116).

Meier B, Chen X, Gwinner A, Peiter-Volk T, Peter K, Peiter E (2010). Novel Manganese Transporters in Plants: Jacks of many trades.

Presented at:

- Genetics of Plant Mineral Nutrition, 30 September - 02 October 2010, Hannover, Germany.
1st prize at poster awards.

Chen X, Gwinner A, **Meier B**, Peiter-Volk T, Peiter E (2009). Identification and initial characterization of novel manganese transporters in plants.

Presented at:

- Annual Meeting of the German Society of Plant Nutrition, 11-12 June 2009, Osnabrück, Germany.

7.3 Oral presentations

The generation and specificity of calcium signals in response to ammonium. 16. Mitteldeutsche Pflanzenphysiologie-Tagung, 09-10 February 2018, Dresden, Germany

Survival of Arabidopsis under post-anoxia conditions depends on a vascular manganese transporter. Plant Nutrition 2014: International Conference of the German Society of Plant Nutrition, 10-12 September 2014, Halle (Saale), Germany

8 Curriculum vitae

Name: Dipl.Ing.-agr. Bastian Meier (m)
Marital Status: single
Date/Place of Birth: 26 January 1984, D-33100 Paderborn
Nationality: German
Corresponding address: Universitätsring 15
06108 Halle (Saale)
Mobile: +49 (0)160 1505671
eMail: Bastian.Meier@gmx.de

Community service

Sept. 2003 - Jun. 2004

Community service, foundation „Westphalenhof“, 33100 Paderborn

Jun. 2004 - Oct. 2004

Temporary employee, foundation „Westphalenhof“, 33100 Paderborn

Education

Oct. 2004 - Feb.2010

Studies of Agricultural Sciences, Martin Luther University Halle-Wittenberg,

Degree: Diploma (1.3)

Diploma thesis

Martin Luther University Halle-Wittenberg, Faculty of Natural Sciences III, Institute of Agricultural and Nutritional Sciences

Experience

Jan. 2010 - Feb. 2010

Scientific Assistant, Martin Luther University Halle-Wittenberg, Faculty of Natural Sciences III, Institute of Agricultural and Nutritional Sciences

I Curriculum vitae

Mar. 2010 - May 2016

Scientific Employee (PhD Student), Martin Luther University Halle-Wittenberg, Faculty of Natural Sciences III, Institute of Agricultural and Nutritional Sciences

Oct. 2016 - Dec. 2018

Scientific Employee, Agrochemisches Institut Piesteritz e. V. (AIP), Lutherstadt Wittenberg

Date

Signature

9 Acknowledgments

At first, I would like to thank all members of the plant nutrition group for the good cooperation. My excessive thank goes to Professor Dr. Edgar Peiter for the realization of this exciting project including the recruitment of the funding. This work was strongly influenced by his ideas, suggestions, and interpretations and therefore it could only be realized through his tireless scientific and friendly support. I really enjoyed our inspiring discussions and I thank him for his uninterrupted support. In addition, I would like to thank him for his trust delegating me some areas of the teaching, which was one of my favorite tasks. I would also like to express my special thanks to Annina Gwinner, who started the project with me and all the other colleges for the excellent working atmosphere and the inspiring discussions. Here I would like to highlight Dagmar Rissel, Mario Lange, Ricardo Happeck, Julia Frank, Nancy Nowak, Victoria Kiep, Jan-Peter Maas and Dr. Kathrin Thor. I have not only enjoyed the collective work in the laboratory, but also the get-together in the coffee breaks or even in the evening's after-work hours. Also noteworthy are Tina Peiter-Volk, Kristin Peter, Anja Janssen, Liane Freitag and Elvira Leibrich for their technical and emotional assistance. Worth mentioning are also Dr. Heidrun Beschow and Dr. Wolfgang Gans for sharing their offices and for the stimulating conversations. I also want to thank those students who supported the project within the scope of a master's and bachelor's thesis. This is especially true for Lukas Fierlbeck, Marie Hörold, Ines Voigt, Andrea Hecht and Katja Köhler. Next to the fantastic colleagues in our group, I also want to thank those people from other groups for the excellent cooperation. A special thank is addressed to Professor Dr. Angelika Mustroph from the university of Bayreuth for the submergence experiments which makes up a large part of this work. I am also very grateful for the great cooperation with Professor Dr. Nicolaus von Wirén and Seckin Eroğlu from the IPK Gatersleben concerning the research about MTP8. Furthermore, I want to thank Christine Krenkewitz and Alexandra Boritzki from the soil scientists group and Susanne Rainer from the IPK Gatersleben for the numerous ICP analysis and the resulting friendships. I also want to mention Professor Dr. Dietrich Nies, Andreas Kirsten and Christopher Schmidt from the department of microbiology for teaching me the handling with radioactive labeled manganese and providing the

I Acknowledgments

radionuclide laboratory. The confocal recordings were only made possible by the generous providing of the laser scanning microscope by Professor Dr. Behrens and thus I want to thank him and his group.

Thank you

10 Declaration under Oath

Eidesstattliche Erklärung / Declaration under Oath*

Ich erkläre an Eides statt, dass ich die Arbeit selbstständig und ohne fremde Hilfe verfasst, keine anderen als die von mir angegebenen Quellen und Hilfsmittel benutzt und die den benutzten Werken wörtlich oder inhaltlich entnommenen Stellen als solche kenntlich gemacht habe.

I declare under penalty of perjury that this thesis is my own work entirely and has been written without any help from other people. I used only the sources mentioned and included all the citations correctly both in word or content.

Datum / Date

Unterschrift des Antragstellers / *Signature of the applicant*

*Origin: [http://www.natfak3.uni-halle.de/ordnungen/ Eidesstattliche-Erklaerung.pdf](http://www.natfak3.uni-halle.de/ordnungen/Eidesstattliche-Erklaerung.pdf) vom 22.03.2013